UNIVERSITY OF HAWAII
LIBRARY

The PHILOSOPHICAL MAGAZINE

FIRST PUBLISHED IN 1798

l. 2 Eighth Series No. 13 January 1957

A Journal of Theoretical Experimental and Applied Physics

EDITOR
PROFESSOR N. F. MOTT, M.A., D.Sc., F.R.S.

EDITORIAL BOARD
SIR LAWRENCE BRAGG, O.B.E., M.C., M.A., D.Sc., F.R.S.
SIR GEORGE THOMSON, M.A., D.Sc., F.R.S.
PROFESSOR A. M. TYNDALL, C.B.E., D.Sc., F.R.S.

PRICE £1 0s. 0d.
Annual Subscription £10 10s. 0d. payable in advance

ALERE FLAMMAM.
Printed and Published by
TAYLOR & FRANCIS LTD.
RED LION COURT, FLEET STREET, LONDON, E.C.4

The Scientific Work of René Descartes

(1596–1650)

By

J. F. SCOTT, B.A., M.Sc., Ph.D.

With a foreword by H. W. TURNBULL, M.A., F.R.S.

This book puts the chief mathematical and physical discoveries of Descartes in an accessible form, and fills an outstanding gap upon the shelf devoted to the history of philosophy and science.

There is to be found in this volume the considerable contribution that Descartes made to the physical sciences, which involved much accurate work in geometrical optics and its bearing upon the practical problem of fashioning lenses, as also the deeper problems of light and sight and colour. The careful treatment that Dr. Scott has accorded to this work of Descartes is welcome, is well worth reading and will be an asset to all libraries. Publication is recommended and approved by the Publication Fund Committee of the University of London

212 *pages*, 7″ × 10″, *amply illustrated*

Price £1 - 0 - 0 net **First published July 1952**

Printed & Published by

TAYLOR & FRANCIS, LTD.

RED LION COURT, FLEET STREET, LONDON, E.C.4

THE
PHILOSOPHICAL MAGAZINE
A JOURNAL OF THEORETICAL EXPERIMENTAL
AND APPLIED PHYSICS
First Published in 1798
[EIGHTH SERIES—VOL. 2]

The Existence of Microcracks after Cold-Work[†]

By A. N. Stroh
Physics Department, University of Sheffield

[Received June 6, 1956]

Summary

It is suggested that changes in density and electrical resistance on cold-work may be due to the formation of microcracks. To fit the experimental values of Clarebrough *et al.* 8×10^4 cracks per cm^2 are needed, each $1{\cdot}3 \times 10^{-3}$ cm in length.

§ 1. Introduction

Recently Clarebrough *et al.* (1956) have measured the change in density occurring when cold-worked nickel is annealed; the density increases mainly in two stages correlating with two stages in the release of the stored energy. The change at the lower temperature, which is attributed to vacancies disappearing, will not be discussed here. The higher temperature changes in density and stored energy are accompanied by a softening of the material, which strongly suggests that dislocations are involved. However, they find that the number of dislocations needed to give the observed change in density is greatly in excess of the number deduced from the stored energy; and it is also larger, by an order of magnitude, than the dislocation densities deduced from x-ray measurements (Williamson and Smallman 1956). For their most severely deformed specimen Clarebrough *et al.* deduce from their stored energy measurements a dislocation density (assuming the dislocations are uniformly dispersed) of $3{\cdot}1\times10^{11}\,\mathrm{cm}^{-2}$; even if each edge dislocation produces the same dilatation as a row of vacancies—almost certainly an over-estimate—this number of dislocations gives a relative change in density of only $0{\cdot}7\times10^{-4}$ against an observed change of $4{\cdot}5\times10^{-4}$.

[†] Communicated by the Author.

A similar situation exists with regard to the increased electrical resistance due to cold work; Hunter and Nabarro (1953) have previously commented on this. The resistivity of a specimen of nickel, deformed the same amount as before, was found by Clarebrough *et al.* (1955) to decrease by 3×10^{-7} ohm cm in the stage of annealing we are considering. According to Hunter and Nabarro a dislocation in copper causes a change in resistance of about 4×10^{-21} ohms, and, assuming that the same value holds for nickel, the change in resistivity with the dislocation density used above is 10^{-9} ohm cm; even if a dislocation in nickel produces a rather larger effect than one in copper, it would still be difficult to account for more than a small fraction of the observed effect in this way.

The difficulty is not resolved, but rather made worse, if the dislocations are in piled-up groups rather than distributed more or less uniformly throughout the metal. For then, to give the same stored energy, fewer dislocations are needed (Stroh 1953); these then lead to even smaller changes in density and resistivity, for these latter are effects which depend largely on the dislocation cores, and so on the number but not the arrangement of the dislocations.

Thus it seems unlikely that dislocations can account for more than a small percentage of the observed changes in density and resistivity, while if vacancies are responsible for effects which anneal out at a lower temperature, they cannot also cause those we are now considering; there remains the possibility that microcracks may have been produced during the deformation. This we now consider.

§ 2. MICROCRACKS

We shall assume that the cracks are produced from piled-up groups of dislocations in the manner considered by Stroh (1954, 1955). Such cracks will have the remote stress field of the dislocations from which they were formed, and as the elastic energy of this stress field provides the driving force for recovery, the cracks should disappear at much the same rate as do the dislocations during annealing; this can be accomplished by dislocations of opposite sign to those from which the cracks were formed combining with them. If the cracks are responsible for the density and resistivity changes it is understandable, then, why these occur at the same temperature as the material softens. We shall use the experimental values to estimate the number and size of the cracks.

If a crack is formed from n dislocations each of Burgers vector $\mathbf{b}$ it will have a maximum width $n\mathbf{b}$, and a stable equilibrium length

$$c=n^2\mathbf{b}^2G/8\pi(1-\nu)\gamma, \qquad \ldots\ldots\ldots \quad (1)$$

where G is the rigidity modulus, ν Poisson's ratio, and γ the surface energy. The volume contained in the crack is

$$\Delta V=\tfrac{1}{2}n\mathbf{b}c=n^3\mathbf{b}^3G/16\pi(1-\nu)\gamma\;;$$

and so if there are N cracks crossing each unit area, the observed relative change in density will be

$$\Delta D/D=Nn^3\mathbf{b}^3G/16\pi(1-\nu)\gamma. \quad . \quad . \quad . \quad . \quad . \quad . \quad . \quad . \quad (2)$$

To find the change in the specific resistance ρ, consider a crack along the x-axis from $-\frac{1}{2}c$ to $\frac{1}{2}c$, and suppose a current flows which remote from the crack is of unit density and parallel to the y-axis. It is easily seen that the current everywhere can be obtained from the conformal mapping

$$u+iv=\{(x+iy)^2-\tfrac{1}{4}c^2\}^{1/2}\;; \quad . \quad . \quad . \quad . \quad . \quad . \quad . \quad (3)$$

u is the stream function and ρv the potential. Now consider a large rectangle bounded by $x=\pm X$, $y=\pm Y$. If the crack were absent, the potential difference across the sides $y=\pm Y$ would be $2\rho Y$ and the current flowing between $x=\pm X$, $2X$; hence the rectangle would have resistance

$$R=\rho Y/X. \quad . \quad . \quad . \quad . \quad . \quad . \quad . \quad . \quad . \quad . \quad . \quad (4)$$

With the crack, eqn. (3) gives the potential on the side $y=Y$ as

$$\rho v=\rho Y\{1+c^2/8(x^2+Y^2)\},$$

on neglecting terms of order c^4/Y^4 ; the mean potential difference between the sides $y=\pm Y$ is then

$$\frac{\rho}{X}\int_{-X}^{X} v\,dx=2\rho Y\left(1+\frac{c^2}{8XY}\tan^{-1}\frac{X}{Y}\right).$$

In the same way, the mean current flowing between $x=\pm X$ is

$$2X\{1+(c^2/8XY)\tan^{-1}(Y/X)\},$$

and so the resistance of the rectangle is now

$$R'=(\rho Y/X)(1+\pi c^2/16XY). \quad . \quad . \quad . \quad . \quad . \quad . \quad . \quad (5)$$

Comparing (4) and (5) we see that the crack produces an apparent change $\Delta\rho$ in the resistivity, where

$$\Delta\rho/\rho=\tfrac{1}{4}\pi c^2N,$$

if $N=1/4XY$. This equation holds if the undisturbed current is normal to the crack ; if it is parallel to the crack the current will be unaffected by the presence of the crack and so there will be no change in the apparent resistivity. Then averaging over all directions, we find the mean change in resistivity is given by

$$\Delta\rho/\rho=\tfrac{1}{12}\pi c^2N, \quad . \quad . \quad . \quad . \quad . \quad . \quad . \quad . \quad . \quad (6)$$

where c is given by eqn. (1).

The discussion of § 1 has indicated that almost all the change in density and resistivity is due to the cracks. Substituting the experimental values of Clarebrough *et al.* (1955, 1956) for heavily cold-worked nickel, i.e. $\Delta D/D = 4{\cdot}5\times10^{-4}$ and $\Delta\rho/\rho = 3{\cdot}8\times10^{-2}$, in eqns. (2) and (6) we obtain $n=330$, $N=8\times10^{4}$ cm^{-2}. Equation (1) then gives the length of the cracks to be $c=1{\cdot}3\times10^{-3}$ cm. These figures appear to be of a reasonable magnitude : the length of the cracks is not so large that there is any obvious objection to their being present, and indeed it would probably be difficult to detect such small cracks even if they were looked for ; also the value of n agrees roughly with the size of the piled-up group which, according to Stroh (1954), is needed to produce a crack.

Mott (1953) has suggested that in ductile fracture a number of microcracks are produced, and when these weaken the material sufficiently a visible crack is formed. In agreement with this idea, we find that, on the one hand, the distance between the cracks, $N^{-1/2}=3{\cdot}5\times10^{-3}$ cm, is only a small multiple of the length of the cracks, so that these must be beginning to weaken the material ; while, on the other hand, the specimens have been subjected to a large deformation, a torsional strain of 2·34, and so cannot be very far from fracture.

The energy of the cracks (Stroh 1954) is

$$W=\frac{Nn^2\mathbf{b}^2G}{4\pi(1-\nu)}\log\frac{32\pi e(1-\nu)\gamma R}{n^2\mathbf{b}^2G},$$

where R is the distance to which the stress field of the crack extends ; with the values of N and n we have obtained this is 7×10^{-3} cals/gm. As the measured value of the stored energy (Clarebrough *et al.* 1956) is 0·59 cals/gm, this must be due almost entirely to the dislocations ; accordingly dislocation densities determined from stored energy measurements will be independent of whether or not microcracks are formed. In the present case, there will still be $3{\cdot}1\times10^{11}$ dislocation lines per cm^2, as given by Clarebrough *et al.*, if the dislocations are dispersed ; or rather fewer if they are in piled-up groups, as they must be if the mechanism of crack formation we are considering is valid.

ACKNOWLEDGMENT

I acknowledge my indebtedness to Drs. Clarebrough, Hargreaves and West, whose work I was able to read in manuscript prior to its publication.

REFERENCES

CLAREBROUGH, L. M., HARGREAVES, M. E., and WEST, G. W., 1955, *Proc. Roy. Soc.* A, **232,** 252 ; 1956, *Phil. Mag.*, **1,** 528.

HUNTER, S. C., and NABARRO, F. R. N., 1953, *Proc. Roy. Soc.* A, **220,** 542.

MOTT, N. F., 1953, *Proc. Roy. Soc.* A, **220,** 1.

STROH, A. N., 1953, *Proc. Roy. Soc.* A, **218,** 391 ; 1954, *Ibid.*, **223,** 404 ; 1955, *Ibid.*, **232,** 548.

WILLIAMSON, G. K., and SMALLMAN, R. E., 1956, *Phil. Mag.*, **1,** 19.

The Effect of Isotopic Spin Impurity on (γ, p) and (γ, n) Cross Sections †

By F. C. Barker and A. K. Mann ‡
Research School of Physical Sciences,
The Australian National University, Canberra

[Received June 14, 1956]

Abstract

The presence of small isotopic spin impurity in an excited state of a self-conjugate nucleus can lead to large differences in the neutron and proton emissions from that state. This effect might be expected to be exhibited clearly in reactions involving a $T=1$ excited state produced by E1 absorption, e.g. in a giant resonance state of a photonuclear reaction. The photodisintegration data for ^{12}C do in fact suggest that the (γ, p) and (γ, n) cross sections are more dissimilar than can be explained by penetrability considerations. From calculations based on the shell model it is found that, for an excited state appropriate to the giant resonance in ^{12}C, an isotopic spin admixture of order 1% in intensity is required to fit the observed ratio of total cross sections. The angular distributions are sensitive to the details of the excited state wave function; however, if the calculated proton distribution is made to fit the observed distribution in the simplest way, a neutron distribution not very different from that for the protons is obtained. The photodisintegration of ^{16}O and the reactions $^{10}\mathrm{B}(\alpha, \mathrm{n})^{13}\mathrm{N}$ and $^{10}\mathrm{B}(\alpha, \mathrm{p})^{13}\mathrm{C}$ are also briefly considered.

§ 1. Introduction

The consequences of isotopic spin conservation for nuclear reactions and radiative transitions have recently received considerable attention. Adair (1952) has discussed the restrictions imposed on heavy particle reactions, in particular, those involving emission and absorption of particles with $T=0$, such as deuterons and α-particles, for which the selection rule is that target and residual nuclei must have the same isotopic spin. The existence of selection rules for the emission and absorption of electric dipole radiation was first pointed out by Trainor (1952); Radicati (1952) and Gell-Mann and Telegdi (1953) have since shown that for radiation of any multipolarity, electric or magnetic, the rule $\Delta T=0, \pm 1$ obtains, with the specialization that electric dipole transitions between states of the same isotopic spin in self-conjugate nuclei are forbidden except for very small contributions from higher order terms in the E 1 operator. These rules were used by the latter authors in the interpretation of gamma-ray absorption cross sections with emphasis on (γ, α) processes in ^{12}C and ^{16}O.

---

† Communicated by Professor E. W. Titterton.

‡ Fulbright Fellow, on leave from the University of Pennsylvania, Philadelphia, Pennsylvania.

Actually nuclear forces are not completely charge independent as is assumed in treating the total isotopic spin as a good quantum number, if only because of the Coulomb interaction ; this causes states of different isotopic spin to be mixed and will in effect result in a partial relaxation of the selection rules. Radicati (1953) and MacDonald (1955, 1956) have investigated theoretically the ability of the Coulomb interaction to mix states of different isotopic spin ; explicit calculations were carried out only for the ground states of certain light nuclei, for which small admixtures to the mainly $T=0$ states were found. These results are in agreement with experimental evidence on relatively low-lying states obtained from studies of radiative transitions by Wilkinson and his collaborators (Wilkinson and Jones 1953 a, b, Wilkinson and Clegg 1953 a, b). It is to be expected, however, that the degree of mixing will be greater for highly-excited states since, in part, mixing will depend on the proximity of states of different isotopic spin; in ^{16}O, for instance, for which the first $T=1$ state is at 12·5 MEV, Wilkinson (1953) has found an apparently large admixture ($>3\%$ intensity) of $T=1$ in the nominally $T=0$ state at 13·1 MEV.

As pointed out by Adair (1952), the amount of isotopic spin impurity in a given state is difficult to determine accurately from reactions involving $T=0$ particles or from radiative transitions ; the transition probabilities in both cases are proportional to the squares of the isotopic spin mixing coefficients. If, on the other hand, one observes the emission of protons and neutrons from a self-conjugate nucleus in an excited state of mixed isotopic spin, the mixing coefficients enter linearly into the expressions for the transition probabilities and small mixing can lead to large differences in the cross sections for neutron and proton emission. In order to distinguish this effect from that due to barrier penetration factors, the excited state must necessarily be well above the proton and neutron thresholds and hence well above the $T=1$ threshold.

Here we are concerned principally with proton and neutron emission from a self-conjugate nucleus in an excited state produced by photon absorption in the ground state. We are interested in the region where only E1 absorption is operative, resulting in excitation from a $T=0$ ground state to a $T=1$ excited state ; for all other multipoles both $T=0$ and $T=1$ excited states might be produced and, even if there were no isotopic spin mixing, interference between these states could cause different proton and neutron emissions. Now the giant resonances in photonuclear reactions are generally ascribed to E 1 absorption and occur at energies well above the proton and neutron thresholds. Thus it might be expected that the level or levels comprising the giant resonances will contain appreciable $T=0$ admixtures and so lead to different proton and neutron emission probabilities.†

It is, in fact, suggested by the available data that the (γ, p) and (γ, n) cross sections in ^{12}C are more dissimilar than can be explained by barrier penetrability and threshold considerations ; in the following section we present that evidence. In § 3 we calculate under certain simplifying assumptions the proton and neutron emissions from an excited state appropriate to ^{12}C to estimate the amount of isotopic spin mixing required to fit the experimental results. In § 4 we discuss other reactions of similar nature from which the magnitude of isotopic spin admixtures may be obtained.

§ 2. EXPERIMENTAL INFORMATION IN CARBON

The excitation functions for $^{12}C(\gamma, p)^{11}B$ and $^{12}C(\gamma, n)^{11}C$ exhibit giant resonances in the neighbourhood of 22 MeV photon energy. The resonances are approximately 6 and 3·5 MeV above the proton and neutron thresholds, respectively.

The most recent (γ, n) total cross section data are presented in the table, which shows fair agreement in the location of the giant resonance and its peak value. The detailed shapes of the cross section curves are different as is indicated by the different half-width values ; the measurements of Barber *et al.* (1955) show the existence of a large ' tail ' on the giant resonance beginning at about 25 MeV and extending well above the threshold for meson production.

Properties of the Giant Resonance in $^{12}C(\gamma, n)^{11}C$

Reference	E_{peak} (MeV)	$\sigma_{\max}$ (mb)	Half-width (MeV)
Montalbetti *et al.* (1953)	21·4	14·0	2·0
Nathans and Halpern (1954)	22·0	8·6	3·0
Barber *et al.* (1955)	22·5	8·3	(4)†

† This value is approximate due to the presence of the ' tail ' on the giant resonance.

Measurements of the differential cross section for the (γ, n) process have also been made by several investigators but the results are rather divergent : using 330 MeV bremsstrahlung, Terwilliger *et al.* (1951) have obtained a rough angular distribution for which the points at 38° and 142° are 10% lower than the value at 90° ; Fabricand *et al.* (1955), with 24 MeV bremsstrahlung, have obtained a provisional distribution which has a minimum at 90°†; finally, Dixon (1955) has measured an angular distribution of the form $\sigma(\theta)=\sigma(90)\ (1-0{\cdot}6\cos^2\theta)$, with 70 MeV bremsstrahlung as incident radiation. The total cross section measurements of Barber *et al.* indicate that at least half the neutrons arising from bombardment by 70 MeV bremsstrahlung are due to photon absorption in the vicinity of the giant resonance and hence the angular distributions from 24 and 70 MeV bremsstrahlung might be expected to be comparable.

---

† A suggestion that (γ, p) and (γ, n) cross sections in certain nuclei with $T=\frac{1}{2}$ ground states might differ due to different emission probabilities for protons and neutrons from excited $T=\frac{1}{2}$ and $T=\frac{3}{2}$ states has been made previously by Morinaga (1955).

A total cross section curve for the (γ, p) reaction was determined by Halpern and Mann (1951) who found from measurements at 90° the values: $E_{\mathrm{peak}}=21{\cdot}5$ MeV, a half-width of 1·7 MeV and $\sigma_{\mathrm{max}}=34$ mb assuming the angular distribution to be isotropic. The relatively thick targets required by their experimental arrangement introduced a large correction for target absorption; the energy distribution of the protons has since been measured (Cohen *et al.* 1956) and allows a more accurate correction to be made than was possible previously. When this correction is applied and account is taken of the known anisotropy of the proton angular distribution (Halpern *et al.* 1952) the value of σ_{max} becomes 18 mb. Haslam *et al.* (1953) have, from measurements of total nuclear absorption in carbon, obtained excitation functions for the (γ, p) process which depend on the nature of their detectors. Their data show a giant resonance of half-width about 2 MeV, located at 21·2 MeV, and with a peak value between 16 and 33 mb. From the nuclear emulsion data (Cohen *et al.*, 1956) on the proton energy distribution it is possible under certain assumptions to obtain an excitation function for transitions to the ground state of ^{11}B which gives the peak cross section of the main resonance between 22 and 23 MeV as 16 mb. The observed energy distribution also indicates that transitions to the first excited state of ^{11}B make an additional contribution of about 25% to the total peak cross section.

The angular distribution of the protons emitted under irradiation with 23 MeV bremsstrahlung has been determined (Halpern *et al.* 1952) to be of the form $\sigma(\theta)=\sigma(90)\ (1-0{\cdot}6\cos^2\theta)$, apart from a small contribution from electric quadrupole absorption.

In summarizing this information we note that within the experimental uncertainties the giant resonances of both the (γ, n) and (γ, p) processes occur at the same photon energy and are similar in half-width. Although the total cross section data for proton emission are inferior in accuracy to the neutron results, the weight of the former evidence suggests with some strength that the maximum (γ, p) cross section is about twice as large as the corresponding (γ, n) value. In what follows we make use only of the ratio of the maximum cross sections, for which we take $\sigma_{\mathrm{p}}/\sigma_{\mathrm{n}}=2$, and of the proton angular distribution. Since in the calculations of

---

† *Note added in proof.*—Further measurements by Fabricand *et al.* (1956) using 23 MeV bremsstrahlung indicate a (γ, n) angular distribution proportional to $(1-0{\cdot}6\cos^2\theta)$—strongly supporting the identity of the neutron and proton angular distributions.

§ 3 we do not consider the width of the resonance from which neutron and proton emission takes place, knowledge of the integrated cross sections is unnecessary. The lack of knowledge of the neutron angular distribution does, however, prevent us from making as thorough a test of our hypothesis as is desirable.

§ 3. CALCULATION OF CROSS SECTIONS

We use the shell model to provide wave functions of the various states and express transition probabilities in terms of reduced widths. The accuracy of the experimental results does not merit an attempt to fit them exactly and it appears sufficient to use for the ground states of ^{11}B, ^{11}C and ^{12}C the wave functions given by the shell model in the L–S coupling extreme, as these make up at least 60% of the actual ground state wave functions (Lane 1953, Kurath 1956). The single particle wave functions are taken as those for an oscillator potential well and only states of the lowest configuration are included. Thus

$$\Psi_{11}=\Psi_{11}\,(1\mathrm{s}^4\ 1\mathrm{p}^7\ [43]\ \tfrac{1}{2}M_T\ \tfrac{1}{2}\ 1\ \tfrac{3}{2}\ M):M_T=\pm\tfrac{1}{2}\ \text{for}\ \begin{matrix}^{11}\mathrm{B}\\ ^{11}\mathrm{C}\end{matrix}$$

$$\Psi_{12}=\Psi_{12}\,(1\mathrm{s}^4\ 1\mathrm{p}^8\ [44]\ 0\ 0\ 0\ 0\ 0\ 0\ )$$

where the last numbers specifying the states are $TM_T\ SLJM$.

Since the giant resonance exhausts much of the electric dipole oscillator strength, the matrix element of the E 1 operator between the ground state of ^{12}C and the giant resonance must be large; the wave function $\Psi_{12}{}^*$ describing the giant resonance state or states should then be approximated by the shell model wave function $\overline{\Psi}_{12}$ obtained by operating with the E 1 operator on the ground state wave function. This suggestion was originally put forth by Wilkinson (1955) who has attempted to explain the properties of giant resonances in terms of the excitation of such states.

In the usual notation, the E 1 operator is

$$D=\tfrac{1}{2}\sum_{i=1}^{n}(1-\tau_{zi})\,(\boldsymbol{\Gamma}_i-\mathbf{R}).\,\mathbf{e}$$

which, operating on Ψ_{12}, gives

$$\begin{aligned}\overline{\Psi}_{12}= &\sqrt{\left(\frac{20}{27}\right)}\,\Psi_{12}(\{1\mathrm{s}^4 1\mathrm{p}^7[43]\tfrac{1}{2}\tfrac{1}{2}1,1\mathrm{d}\tfrac{1}{2}\tfrac{1}{2}2\}10011M)\\ &-\sqrt{\left(\frac{4}{27}\right)}\,\Psi_{12}(\{1\mathrm{s}^4 1\mathrm{p}^7[43]\tfrac{1}{2}\tfrac{1}{2}1,2\mathrm{s}\tfrac{1}{2}\tfrac{1}{2}0\}10011M)\\ &-\sqrt{\left(\frac{3}{27}\right)}\,\Psi_{12}(\{1\mathrm{s}^3[3]\tfrac{1}{2}\tfrac{1}{2}0,1\mathrm{p}^9[441]\tfrac{1}{2}\tfrac{1}{2}1\}10011M)\\ \equiv &\sqrt{\left(\frac{20}{27}\right)}\,\Psi_{12}(C_1 1)-\sqrt{\left(\frac{4}{27}\right)}\,\Psi_{12}(C_2 1)-\sqrt{\left(\frac{3}{27}\right)}\,\Psi_{12}(C_3 1),\end{aligned}$$

where C_1, C_2 and C_3 refer to the three configurations and to all quantum numbers except T. As long as the wave function $\Psi_{12}{}^*$ contains mostly the state $\Psi_{12}(C_1 1)$, the giant resonance will contribute appreciably to the dipole sum, and as has been noted (Mann *et al.* 1955) the observed proton angular distribution may be explained. This latter arises from the fact that only d-wave protons may then be emitted in transitions to the ground state of ^{11}B and the angular distribution is uniquely $\sigma(\theta)=\sigma(90)\,(1-0{\cdot}6\cos^2\theta)$. For these reasons we take $\Psi_{12}{}^*$ as the state $\Psi_{12}(C_1 1)$, apart from $T=0$ admixtures introduced by the Coulomb interaction. The admixtures which cause different (γ, p) and (γ, n) total cross sections are the states $\Psi_{12}(\{1\mathrm{s}^4 1\mathrm{p}^7[43]\tfrac{1}{2}\tfrac{1}{2}1,\ \mathrm{nd}\tfrac{1}{2}\tfrac{1}{2}2\}00SL1M)$, as only these can emit d-wave nucleons in transitions to the ground states of ^{11}B and ^{11}C. The most important contribution is expected to come from $\Psi_{12}(\{1\mathrm{s}^4 1\mathrm{p}^7[43]\tfrac{1}{2}\tfrac{1}{2}1, 1\mathrm{d}\tfrac{1}{2}\tfrac{1}{2}2\}00011M)\equiv\Psi_{12}(C_1 0)$, which has the same zero order energy as $\Psi_{12}(C_1 1)$ and is directly coupled to it by the Coulomb interaction †. Thus we take initially

$$\Psi_{12}{}^*=\sum_{T=0,1}\alpha_T\Psi_{12}(C_1 T)$$

with $\alpha_0/\alpha_1<1$. The ground states of ^{11}B, ^{11}C and ^{12}C are assumed to remain pure T states.

The dimensionless reduced width amplitudes for the break up of the excited state of ^{12}C into the systems $^{11}\mathrm{B}+\mathrm{p}$ and $^{11}\mathrm{C}+\mathrm{n}$, designated by the M_T values $+\frac{1}{2}$ and $-\frac{1}{2}$ respectively, with channel spin s and relative orbital angular momentum l, are given by (Lane and Thomas 1956)

$$\theta_{M_T sl}=\text{const.}\,\delta(s,1)\,\delta(l,2)\sum_T\alpha_T(\tfrac{1}{2}\tfrac{1}{2}M_T-M_T|T0).$$

The differential cross sections for the reactions $^{12}\mathrm{C}(\gamma, \mathrm{p})^{11}\mathrm{B}$ and $^{12}\mathrm{C}(\gamma, \mathrm{n})^{11}\mathrm{C}$ are then

$$\sigma_{M_T}(\theta)=\text{const.}\sum_{sM\mu}\left|\sum_l(P_{M_T l})^{1/2}\theta_{M_T sl}(1lM0|1M)(11\mu M-\mu|1M)\,\Psi_{1\mu}(\theta\varphi)\right|^2$$

or

$$\sigma_{\pm\frac{1}{2}}(\theta)=\text{const.}\ \mathrm{P}_{\pm\frac{1}{2}2}|\alpha_1\pm\alpha_0|^2(1-0{\cdot}6\cos^2\theta),$$

where $P_{M_T l}$ is the penetration factor. On this basis, therefore, we obtain the observed proton angular distribution and require the neutron angular distribution to be the same. The ratio of the cross sections is

$$\frac{\sigma_\mathrm{p}}{\sigma_\mathrm{n}}=1{\cdot}3\left|\frac{\alpha_1+\alpha_0}{\alpha_1-\alpha_0}\right|^2,$$

where the factor 1·3 arises from the different proton and neutron penetrabilities and is not strongly dependent on the value of the channel radius. This ratio is 2 for $\alpha_0/\alpha_1=0{\cdot}11$, i.e. for about 1% intensity of the state $\Psi_{12}(C_1 0)$

---

† It should be noted that only wave functions which are orthogonal to

$$\sqrt{\left(\frac{20}{27}\right)}\,\Psi_{12}(C_1 0)-\sqrt{\left(\frac{4}{27}\right)}\,\Psi_{12}(C_2 0)-\sqrt{\left(\frac{3}{27}\right)}\,\Psi_{12}(C_3 0)$$

are admissible shell model wave functions, since all others contain in part excited states of the relative motion of the centre of mass and the well centre (Elliott and Skyrme 1955); thus $\Psi_{12}(C_1 0)$ can form at most $\frac{7}{27}$ of the total $T=0$ admixture intensity.

in Ψ_{12}^*. This result is not appreciably affected by replacing the 1d particle in $\Psi_{12}(\mathrm{C}_1 0)$ by a 2d, 3d, ... particle. $T=0$ admixtures with S, $L\neq 0$, 1 are less effective in producing different proton and neutron cross sections and can be neglected. The requirement of identical neutron and proton angular distributions is the result of our choice of wave functions. Different angular distributions can be obtained if Ψ_{12}^* contains states, such as $\Psi_{12}(C_2 T)$, which can emit s-wave nucleons. In order to fit the observed proton angular distribution, it must then be assumed either that Ψ_{12}^* contains very little of these states or that the phase relationship between s- and d-wave emission is such as to give the experimental distribution. This latter is possible for large amounts of s-wave emission, up to an s-wave contribution to the total cross section of 8 times the d-wave contribution, but it does not seem profitable to discuss this alternative in detail until forced to do so by the experimental results.

Difficulties with the procedure of calculating reduced widths from shell model wave functions have been pointed out by Lane and Thomas (1956) and a more realistic approach may be to replace the reduced widths in the formula for the cross section by matrix elements of the interaction between the emitted nucleon and the remaining nucleus. This allows both s- and d-wave nucleons to be emitted from the configuration C_1, and corresponds to some extent to the result of the reduced width calculation when configuration mixing is introduced.

We have calculated the matrix elements assuming that the interaction between the emitted nucleon and each of the remaining nucleons is a two-particle central interaction of Yukawa shape and Rosenfeld exchange character. The calculation is simplest using the Talmi method (Talmi 1952) with the radial wave functions for the emitted nucleon taken to be 2s or 1d for $l=0$, 2 respectively, and with the relative amplitudes given by the ratio of the Coulomb radial wave functions for s- and d-waves at the surface of the nucleus. For the same excited state wave function,

$$\Psi_{12}^* = \sum_T \alpha_T \Psi_{12}\,(C_1 T),$$

as before, the matrix elements are such that d-wave emission is still favoured, and the results for the angular distributions are much the same as those obtained from the reduced width calculations with an excited state containing a small admixture of the C_2 configuration. The main difference is that the matrix elements for $T=0$ states are larger, by factors of order 5, than those for $T=1$ states which increases the effect of the isotopic spin admixture coefficient on the cross sections so that $\sigma_\mathrm{p}/\sigma_\mathrm{n}=2$ is satisfied with $\alpha_0/\alpha_1=0{\cdot}03$.

The interesting feature of these calculations is that an isotopic spin admixture in the excited state of order 1% in intensity can cause the ratio of the proton and neutron total cross sections to be quite different from unity. As might be expected, the angular distributions are sensitive to the details of the excited state wave function; however, if the calculated proton distribution is made to fit the observed distribution in the simplest way, a neutron distribution not very different from the proton distribution is obtained.

It was assumed above that no isotopic spin impurities were present in the nuclear ground states. If, however, the ground state of ^{12}C contains $T=1$ impurities, E1 absorption can lead to the excitation of both $T=0$ and $T=1$ states which might then interfere to produce differences in neutron and proton emission. MacDonald (1956) has calculated an upper limit of 0·2% intensity for the $T=1$ admixture to the ground state of ^{12}C which appears to be too small to explain completely the observed difference in the (γ, p) and (γ, n) cross sections. $T=\frac{3}{2}$ impurities in the ground states of ^{11}B and ^{11}C will also contribute to different cross sections in the same manner as $T=0$ impurities in the excited state of ^{12}C. The presence of these impurities makes uncertain our estimate of the mixing in the excited state.

It is worth mentioning that the measured proton angular distribution (Halpern *et al.* 1952) shows that E 2 absorption is contributing to the cross section in the neighbourhood of the giant resonance. E 2 absorption will produce $T=0$ states, which can interfere with the $T=1$ states produced by E1 absorption to give different (γ, p) and γ, n) cross sections. The difference is, however, only in the angular distributions, because the interference term vanishes upon integration over all angles.

§ 4. OTHER REACTIONS

There are, unfortunately, few experimental results apart from those on the photodisintegration of carbon which permit a quantitative test of our hypothesis. The photodisintegration of ^{4}He apparently does not proceed through an excited state (Flowers and Mandl 1951, Gunn and Irving 1951) ; any difference between proton and neutron emissions must therefore be explained by a mechanism different from that described above. The data indicate that the proton total cross section (Fuller 1954, Perry and Bame 1955) is slightly larger than that for neutrons (Ferguson *et al.* 1954), but the difference could be due to penetrability factors and experimental uncertainties. The only other light self-conjugate nucleus for which photodisintegration cross section data are available is ^{16}O. At the peak of the giant resonance the (γ, p) cross section for transitions to the ground state of ^{15}N is about 10 mb (Stephens *et al.* 1955). Transitions to the first excited state of ^{15}N are observed to be about as frequent as those to the ground state which suggests, on the basis of penetrability considerations, that roughly $\frac{2}{3}$ of the observed (γ, n) transitions are to the ground state of ^{15}O. From these values the ratio of proton and neutron reduced widths is found to be close to unity.

Alternative methods of producing suitable highly excited states of self-conjugate nuclei would be by deuteron or α-particle bombardment. It seems, however, that even for low energy deuterons, the stripping contributions to the (d, p) and (d, n) cross sections will in general mask the compound nucleus features which are of interest here (see e.g. Bonner *et* *al.* 1956). The (α, p) and (α, n) reactions have suitable Q values for the target nucleus ^{10}B; these reactions have been studied and it has been suggested that the observed difference in proton and neutron emission from the 12·69 MeV state of ^{14}N leading to the ground states of ^{13}C and ^{13}N is possibly due to isotopic spin mixing in the excited states (Shire and Edge 1955). The angular distributions of the emitted protons and neutrons are consistent with the assumption that this state is 3^-, emitting only d-wave nucleons in the ground state transitions, which implies a definite channel spin of the final system. Under these conditions, the ratio of neutron and proton reduced widths may be obtained without specifying the states in detail and is

$$\frac{\gamma_n^2}{\gamma_p^2}=\left|\frac{\alpha_0-\alpha_1}{\alpha_0+\alpha_1}\right|^2,$$

where α_0 and α_1 are the coefficients of the relevant $T=0$ and $T=1$ parts of the excited state wave function, assumed to differ only in their T values. The observed ratio of 5·7 requires $\alpha_1/\alpha_0=-0{\cdot}41$, but in view of the small absolute magnitudes of these nucleon reduced widths this value cannot be taken to indicate the total $T=1$ impurity in the 12·69 MeV state of ^{14}N.

ACKNOWLEDGMENTS

One of us (A.K.M.) wishes to thank Professor E. W. Titterton for extending to him the hospitality of his laboratory, and the United States Educational Foundation for the Fulbright Award which made possible his visit to Canberra.

REFERENCES

ADAIR, R. K., 1952, *Phys. Rev.*, **87,** 1041.
BARBER, W. C., GEORGE, W. D., and REAGAN, D. D., 1955, *Phys. Rev.*, **98,** 73.
BONNER, T. W., EISINGER, J. T., KRAUS, A. A., and MARION, J. B., 1956, *Phys. Rev.*, **101,** 209.
COHEN, L., MANN, A. K., PATTON, B. J., REIBEL, K., STEPHENS, W. E., and WINHOLD, E. J., 1956, to be published.
DIXON, W. R., 1955, *Canad. J. Phys.*, **33,** 785.
ELLIOTT, J. P., and SKYRME, T. H. R., 1955, *Proc. Roy. Soc.* A, **232,** 561.
FABRICAND, B. P., ALLISON, B., and HALPERN, J., 1955, *Phys. Rev.*, **100,** 1249; 1956, **103,** *Ibid.*, 1755.
FERGUSON, G. A., HALPERN, J., NATHANS, R., and YERGIN, P. F., 1954, *Phys. Rev.*, **95,** 776.
FLOWERS, B. H., and MANDL, F., 1951, *Proc. Roy. Soc.* A, **206,** 131.
FULLER, E. G., 1954, *Phys. Rev.*, **96,** 1306.
GELL-MANN, M., and TELEGDI, V. L., 1953, *Phys. Rev.*, **91,** 169.
GUNN, J. C., and IRVING, J., 1951, *Phil. Mag.*, **42,** 1353.
HALPERN, J., and MANN, A. K., 1951, *Phys. Rev.*, **83,** 370.
HALPERN, J., MANN, A. K., and ROTHMAN, M., 1952, *Phys. Rev.*, **87,** 164.
HASLAM, R. N. H., HORSLEY, R. J., JOHNS, H. E., and ROBINSON, L. B., 1953, *Canad. J. Phys.*, **31,** 636.
KURATH, D., 1956, *Phys. Rev.*, **101,** 216.
LANE, A. M., 1953, *Proc. Phys. Soc.* A, **66,** 977.

Lane, A. M., and Thomas, R. G., 1956, to be published.
MacDonald, W. M., 1955, *Phys. Rev.*, **100,** 51 ; 1956, *Ibid.*, **101,** 271.
Mann, A. K., Stephens, W. E., and Wilkinson, D. H., 1955, *Phys. Rev.*, **97,** 1184.
Montalbetti, R., Katz, L., and Goldenberg, J., 1953, *Phys. Rev.*, **91,** 659.
Morinaga, H., 1955, *Phys. Rev.*, **97,** 444.
Nathans, R., and Halpern, J., 1954, *Phys. Rev.*, **93,** 437.
Perry, J. E., and Bame, S. J., 1955, *Phys. Rev.*, **99,** 1368.
Radicati, L. A., 1952, *Phys. Rev.*, **87,** 521 ; 1953, *Proc. Phys. Soc.* A, **66,** 139.
Shire, E. S., and Edge, R. D., 1955, *Phil. Mag.*, **46,** 640.
Stephens, W. E., Mann, A. K., Patton, B. J., and Winhold, E. J., 1955, *Phys. Rev.*, **98,** 839.
Talmi, I., 1952, *Helv. Phys. Acta*, **25,** 185.
Terwilliger, K. M., Jones, L. W., and Jarmie, W. N., 1951, *Phys. Rev.*, **82,** 820.
Trainor, L. E. H., 1952, *Phys. Rev.*, **85,** 962.
Wilkinson, D. H., 1953, *Phys. Rev.*, **90,** 721 ; 1955, *Proceedings of the* 1954 *Glasgow Conference on Nuclear and Meson Physics* (London and New York : Pergamon Press), p. 161.
Wilkinson, D. H., and Clegg, A. B., 1953 a, *Phil. Mag.*, **44,** 1269 ; 1953 b, *Ibid.*, **44,** 1322.
Wilkinson, D. H., and Jones, G. A., 1953 a, *Phys. Rev.*, **90,** 722 ; 1953 b, *Phil. Mag.*, **44,** 542.

Investigation of the Annealing of Deformed Nickel Powder by X-Ray and Stored Energy Measurements †

By D. MICHELL and F. D. HAIG
Division of Tribophysics, Commonwealth Scientific and Industrial Research Organization, University of Melbourne, Australia

[Received April 12, 1956]

ABSTRACT

The stored energy was measured by a calorimetric method. The measured value of 3·6 cal/g and the manner of its release suggests that a wide range of deformations is present, both the maximum and average deformations being considerably greater than those present in heavily deformed solid specimens of nickel.

The diffraction patterns, measured with a Geiger counter spectrometer, show that during annealing there is no change in the background intensity. The integrated intensities of the high angle lines remain constant and small changes in the low angle lines are attributed to changes in extinction. Only small changes occur in the tails of the lines at temperatures of annealing up to 400°c. No evidence has been found for stacking faults or changes in lattice parameter. The diffraction profiles are analysed by a number of methods, the broadening in each case being attributed partly to strain and partly to small particle size.

The results indicate two stages in the relief of strain. The first occurs mainly in the less severely deformed regions without increase in the 'apparent particle size' and is attributed to recovery. In the second, all the remaining strain is relieved by recrystallization with an increase in the 'apparent particle size'.

For the deformed powder the 'apparent particle size' is in the range 350–2300 Å and the energies derived from the analyses range from 0·02–1·5 cal/g. The discrepancy between the calculated values of energy and the value obtained experimentally is discussed in terms of the distribution of strain within the crystal.

§ 1. INTRODUCTION

RECENT work by Clarebrough *et al.* (1955, 1956) has shown that the energy stored in deformed nickel is released in at least two stages during annealing and that there are corresponding changes in electrical resistivity, density and hardness. Wilson and Thomassen (1934) investigated the x-ray line breadth, electrical resistivity, hardness and magnetic induction for a number of deformed metals after annealing at various temperatures. In particular, they found that, for nickel, the recovery of line breadth occurred in two stages.

---

† Communicated by Dr. W. Boas.

In view of the recent advances in the measurement (Warren and Averbach 1949, Hall and Williamson 1951) and interpretation (Hall 1949, Warren and Averbach 1950, 1952, Williamson and Smallman 1954) of x-ray diffraction patterns, it seemed desirable to correlate the measurements of Clarebrough *et al.* with changes in the x-ray diffraction pattern during annealing. As the first stage in this programme, the energy stored in deformed nickel powder has been measured and the X-ray diffraction patterns of the same powder determined with a Geiger counter spectrometer after various stages of annealing.

From the measured diffraction patterns the effect of annealing temperature on the integrated intensity of the lines, on the background level and on the position of the lines has been investigated. The line shapes have been analysed by a number of methods (Hall, 1949 Warren and Averbach 1950, 1952, Williamson and Smallman 1954), the broadening in each case being attributed partly to strain and partly to small particle size. Values of lattice strain and 'apparent particle size' have been calculated and these are considered in relation to the measured stored energy and the manner of its release during heating.

Some preliminary results of this work have already been published (Michell 1956).

§ 2. Preparation of Nickel Powder

The powder was prepared from a bar of nickel of commercial purity (99·6% Ni), taken from batch K as used by Clarebrough *et al.* (1955).

Since a considerable quantity of powder was required for the measurements of stored energy, this was prepared by surface grinding. Cuts of one-thousandth of an inch were taken from the nickel bar with an aluminium oxide wheel under a copious flow of coolant. The powder was collected, washed with water and then separated from the debris of the wheel by means of a magnet. This operation was repeated several times. The powder was then washed with acetone and again with benzene and, after drying and demagnetizing, sieved through a 350 mesh screen. A further magnetic separation was then carried out on the powder which had passed through the screen. After demagnetizing, the powder was stored on ice until required.

Microscopic examination of a number of samples of the powder revealed only a few fragments from the grinding wheel and these were attached to the individual chips of the nickel powder. In addition, chemical analysis showed that the total content of non-metallic inclusions was less than 0·1%.

§ 3. Stored Energy Measurements

The energy stored in the nickel powder during deformation was determined by measuring the difference between the power required to heat a container of deformed nickel powder and that to heat a contained of annealed nickel powder from room temperature to approximately 750°c at 6°c/min. The calorimeter used and the procedure adopted in making the measurements were as described by Clarebrough *et al.* (1952).

Cylindrical copper containers, as shown in fig. 1, were used to hold the powder in order to ensure good heat transfer between the central heating element, the nickel powder and the thermocouple block which is attached to the top of the container. The weights of the individual components of the containers were matched to within 2 mg and when assembled, the containers each weighed 65·2 g and held approximately 22 g of nickel powder. The containers were annealed *in vacuo* at 500°c before filling with powder. The powder was pressed into the containers with a mandrel under a pressure of 8000 lb/in². This pressure was the highest that could be used without causing appreciable changes in the outside diameters of the containers. The reference specimen for the measurment of stored energy was prepared by annealing a container of deformed powder *in vacuo* at 800°c.

Fig. 1

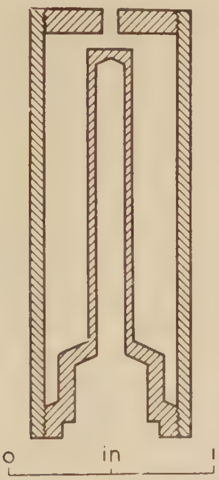

Section of a container used to hold the powder for the measurements of stored energy.

The results are shown in fig. 2 where curve (1) represents the measured power difference plotted against temperature (or time) and curve (2) represents the amount of stored energy remaining in the specimen at any temperature (or time) during the heating.

The following experiment was carried out to determine whether differences in the amounts of sintering in a freshly pressed container of powder and a container of powder annealed after pressing would effect significantly the measured power difference. A container was packed with annealed powder and a second container was packed with deformed powder and then annealed. No significant difference in power was required to heat these two specimens from room temperature to 750°c.

§ 4. Measurements of the x-ray Diffraction Pattern

4.1. *Experimental Method*

The x-ray diffraction patterns were measured with a Geiger counter spectrometer using monochromatic CuKα radiation obtained by reflection from a curved crystal of lithium fluoride. The source of radiation was a Norelco sealed-off x-ray tube operating with a full-wave rectified, unfiltered, high tension supply. Separate electronic stabilizers maintained the peak voltage input to the x-ray tube at 35 kv and the tube current at 20 mA throughout the measurements.

Fig. 2

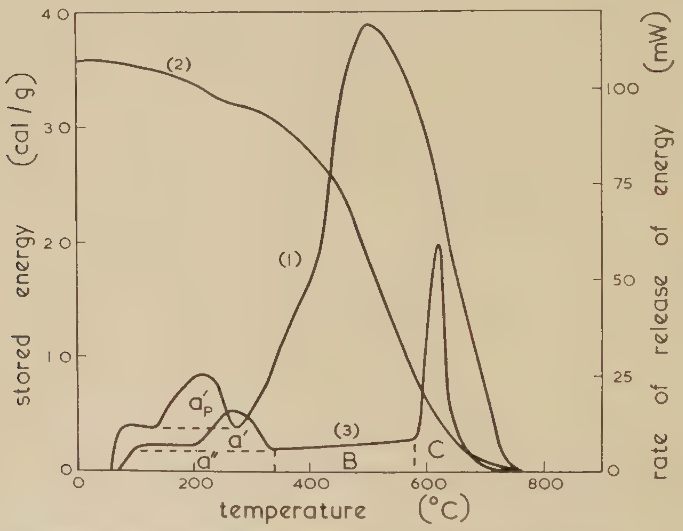

Release of energy from deformed nickel during annealing as a function of temperature.

(1) Rate of release of energy from 22·2 g of deformed nickel powder.
(2) Stored energy remaining in the powder.
(3) Rate of release of energy from solid nickel deformed almost to fracture in torsion. Scale adjusted to refer to 'a specimen' of 22·2 g.

The axis of the spectrometer was horizontal and the divergence of the x-ray beam from the focus of the monochromator was limited to 2° in the vertical direction. Soller slits were used to limit the divergence of the beam to 1° in the horizontal direction. All the measurements were made with a slit, 0·005 in. wide, in front of the Geiger counter. This slit subtended an angle of approximately 0·06° at the centre of the spectrometer.

To prepare the specimens of powder for the diffraction work, a holder was attached face downwards to a lapped steel plate and the powder was pressed into the holder from the back with a mandrel at the same pressure as that used in the preparation of the stored energy specimens, i.e. 8000 lb/in^2. This holder was then mounted on the spectrometer and adjusted, with the aid of a microscope, to lie on the axis of the spectrometer. During all the measurements the holder was rotated in its own plane by a small non-synchronous electric motor.

The diffraction patterns for the powder after heating to various temperatures were measured at room temperature over the angular range of 30° to 130° in 2θ on the side of the beam which increased the α_1, α_2 separation. The line shapes were recorded manually and measurements were made of the diffracted intensity, at intervals in 2θ varying from 0·5° in the background to 0·01° in the lines, using an electronic scaling unit and an electromechanical register. The total time spent on each pattern was approximately 45 hours spread over four days, all interruptions in the counting being made in the background region. Since the methods of analysis developed by Warren and Averbach (1950, 1952) require the measurement of more than one order of reflection from a given set of planes proportionally more time was spent on the measurement of the 111, 222, 200 and 400 lines than on the measurement of the 220 and 311 lines. The counting time was controlled by a monitor based on that described by Hargreaves *et al.* (1952). With this device, monitoring is carried out on the whole of the incident x-ray beam and counting of pulses from the Geiger counter occurs during the time taken for a predetermined number of x-ray quanta to fall on the specimen. In the present case the time of one counting interval was adjusted to be approximately one minute, while the number of intervals spent on individual points varied from five in the background regions to one on the more intense lines.

The diffraction pattern for the deformed powder was measured first. The powder and holder, with a thermocouple attached, were then placed in a silica tube and heated *in vacuo* at a rate of 6°c/min. On reaching 110°c the silica tube was quickly withdrawn from the furnace and cooled rapidly with water to room temperature. The diffraction pattern was then remeasured. The specimen was replaced in the silica tube and heated *in vacuo* as rapidly as possible to 110°c and then at 6°c/min to 190°c. It was then withdrawn, cooled as before and the diffraction pattern measured. This process was repeated for a number of temperatures up to 870°c. Finally, the specimen was heated to 870°c, held at this temperature for 45 minutes, cooled and the diffraction pattern measured. In this way eleven complete diffraction patterns were measured for the specimen heated to temperatures between 20°c and 870°c. X-ray photographs made of the specimen annealed at 870°c showed no sign of spottiness. Preliminary experiments indicated that there is no significant difference between the shape of a line obtained from a specimen annealed in stages as above to 370°c and that obtained from a specimen annealed at 6°c/min from room temperature to 370°c. Thus, no serious error should be introduced if the diffraction patterns obtained in this manner are correlated directly with the stored energy measurements.

Before and after each diffraction pattern was measured, the peaks of the 111 and 331 lines of an annealed nickel reference specimen were scanned so that corrections could be applied for changes in sensitivity of the spectrometer. However, no significant drift occurred over the eleven weeks required to make the measurements, although the standard deviation of the observed peaks was 1·5%. Therefore, no corrections have been made for this effect.

Frequent checks were made of the background level of the counter with a lead stop inserted in the monochromatic beam. This background remained constant at 45 counts/min and a correction for this has been applied to all measured intensities.

Fig. 3

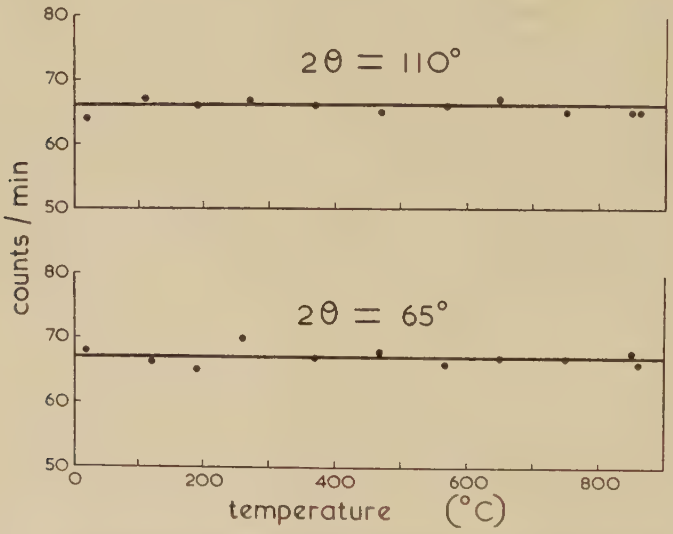

Corrected x-ray intensities at 65° and 110° in 2θ as functions of the temperature of annealing.

The time of counting for each interval of the monitor was recorded and corrections for the dead time of the counter (600 μ sec) and the wave shape of the x-ray output from the monochromator have been applied to all measurements.

4.2. *Results*

4.2.1. *Background level*

In order to determine the background levels of the x-ray diffraction patterns, the corrected intensities for each of the eleven diffraction patterns were plotted on an extended intensity scale and a compressed angular scale to accentuate any change in background level (Hall and Williamson 1951). These plots show that the tails of the lines obtained from the deformed powder extend for several degrees and in some cases overlap those from adjoining lines. However, at approximately 65° and 110° in 2θ there appeared to be no overlapping of the tails of adjoining lines. Furthermore, as shown in fig. 3, the intensity at each of these angles is equal within the experimental error and effectively independent of the temperature of annealing. Therefore the intensity at these angles has been taken as the background level.

4.2.2. *Shape of the diffracton lines*

The line shapes have been plotted from the corrected intensity figures with the background levels drawn in at the values given in fig. 3. Inspection of these line shapes shows that very little change occurs in the tails of the lines below 400°c, although the peak heights increase with increase in temperature. As the temperature of annealing is increased above 400°c there is a marked decrease in the tails of the lines accompanied by a further but more rapid increase in the peak heights. Detailed analyses of these changes are given in § 5.

Fig. 4

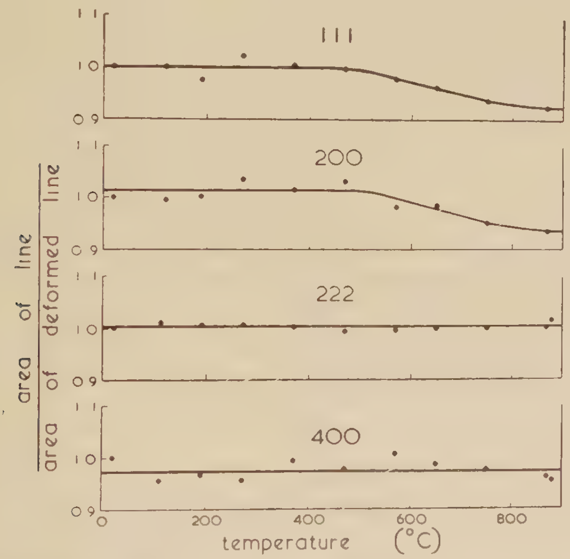

Integrated intensities of the 111, 200, 222, and 400 reflections, relative to the integrated intensities from the deformed powder, as functions of the temperature of annealing.

4.2.3. *Integrated intensities of the lines*

The areas of the lines above the background levels were computed using the trapezoidal rule. Where possible the measured values of intensity, after correction, were used directly in the calculations, but where overlapping of adjoining lines occurred the ordinates were determined by graphical separation. Figure 4 shows the variation, with temperature of annealing, of the integrated intensities of the 111, 200, 222 and 400 lines.

The 220 and 311 lines are not considered since the time spent on the measurement of these lines was insufficient to give an accuracy which would allow definite conclusions to be drawn regarding the integrated intensity.

4.2.4. *Positions of the maxima of the diffraction lines*

The α_1 and α_2 components of the measured line shapes were resolved graphically using the method of Rachinger (1948) and a mechanical aid, details of which will be published elsewhere.

Paterson (1952) has shown that the presence of stacking faults should decrease the separation between the 111 and 200 lines and increase the separation between the 222 and 400 lines. The changes in separation found in the present work were less than the experimental error of 0·01° and thus not significant.

During the annealing experiments changes of approximately 0·02° in 2θ were observed in the angular positions of the maxima of the resolved peaks. In order to see whether these changes were due to changes in lattice parameter during annealing the following experiments were carried out. Equal weights of deformed nickel powder and annealed aluminium powder were pressed into a holder at 1600 lb/in^2 and a few drops of a 5% solution of Canada balsam in xylol added to act as a binder. The 331 lines of the nickel and of the aluminium were measured with the spectrometer. Using the same holder a new specimen was then prepared from equal weights of annealed nickel powder and annealed aluminium powder and the two line shapes again measured. Three such experiments were made, new specimens being pressed for each measurement. Relative to the position of the 331 reflection for aluminium, the position of the resolved α_1 peaks for the annealed and deformed nickel powder agreed in all cases within the experimental error of 0·01° in 2θ. Thus, there is no significant change in lattice parameter during annealing and the small variations in line positions must be attributed to experimental errors resulting from removing, annealing and replacing the same specimen a number of times.

§ 5. Analysis of the Diffraction Patterns

The resolved α_1 lines were investigated by the method of Hall (1949) based on integral line breadths, the Fourier method of Warren and Averbach (1950, 1952) and its variant proposed by Williamson and Smallman (1954). In all cases the change in line shape has been attributed partly to lattice strain and partly to small 'apparent particle size'.

5.1. *Integral Line Breadths*

Hall (1949) has suggested that β, the integral line breadth corrected for instrumental broadening, is given by

$$\beta \cos \theta = \frac{\lambda}{t} + \frac{2\sigma_{\mathrm{av}} \sin \theta}{E_{hkl}},$$

where θ is the Bragg angle, λ is the wavelength of the x-rays, t is the particle size, E_{hkl} is Young's modulus in the $<hkl>$ direction and σ_{av} is a ' mean stress function '.

Integral breadths have been calculated for all the measured lines and, as the resolved line shapes were approximately Cauchy profiles, corrected for instrumental broadening by subtracting the breadth of the corresponding lines for the fully annealed specimen (Wood and Rachinger 1949). For each diffraction pattern, $\beta \cos \theta$ was plotted against $\sin \theta / E_{hkl}$ and straight lines fitted by the method of least squares. The results are shown in fig. 5 while the resulting values of ' apparent particle size ' and ' mean stress function ' are shown in fig. 6 as functions of annealing temperature.

Fig. 5

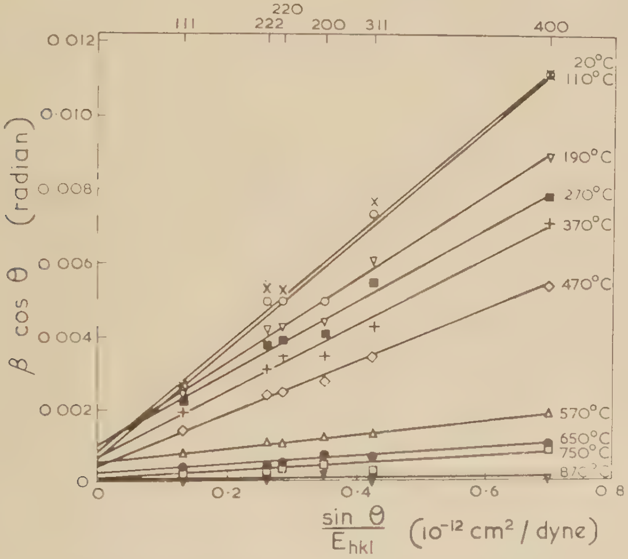

Plot of $\boldsymbol{\beta} \cos \boldsymbol{\theta}$ against $\sin \boldsymbol{\theta} / E_{hkl}$ for various temperatures of annealing.

If it is assumed that the stress distribution function is Gaussian, then $\sigma_{\text{r.m.s.}} = \sigma_{\text{av}} / \sqrt{2\pi}$ and approximate values of stored energy, V, can be computed from the equation

$$V = 3\sigma^2_{\text{r.m.s.}} / 2E$$

where E is the mean value of Young's modulus. Values of V are plotted as a function of temperature in fig. 6.

5.2. *Fourier Analysis of the Line Profiles*

Warren and Averbach (1950, 1952) have developed a method of investigating and separating the effects of lattice strain and ' apparent particle size ' by considering the Fourier components of the line profiles. For cubic crystals a set of orthogonal axes can be chosen to express any reflection in the form $(00l)$. In general, when the two effects are present simultaneously, the measured Fourier coefficients $A_n(l)$ for such a reflection are given by

$$A_n(l)=A_n^P \, . \, A_n^D(l),$$

where A_n^P is the particle size coefficient and $A_n^D(l)$ is the distortion

Fig. 6

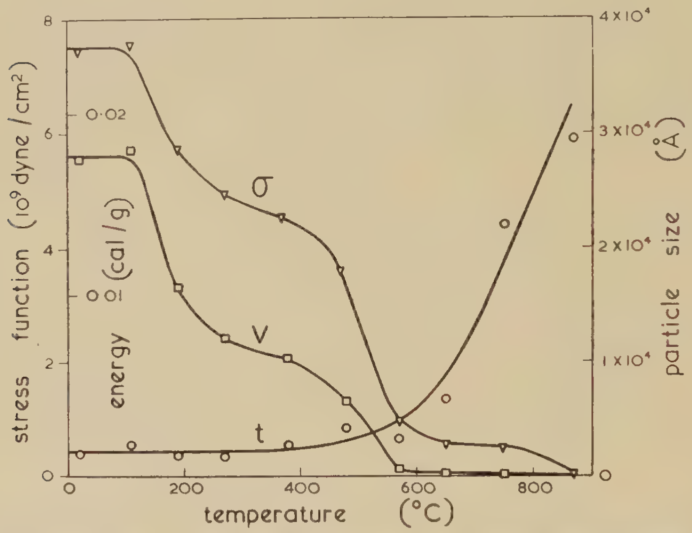

Results of the analysis of the line breadths. 'Apparent particle size', t, mean stress function, σ, and calculated stored energy, V, as functions of the temperature of annealing.

coefficient. The two effects can be separated by measuring several orders of reflection from the one set of planes, since the distortion coefficient depends on the order of the reflection while the particle size coefficient does not.

The Fourier coefficients for the low angle halves of the resolved α_1 components of the 111, 222, 200 and 400 line profiles have been computed, using Lipson–Beevers strips, and corrected for instrumental broadening by the method of Stokes (1948). The results are shown in fig. 7, where the abscissa is L, the distance in the crystal along a normal to the reflecting planes.

Warren and Averbach (1950) assume that the distribution of strain in the crystal is Gaussian, while Williamson and Smallman (1954) suggest that the distribution may equally well follow a Cauchy function. In the present experiments the derived coefficients have been interpreted for each of these distributions of strain.

5.2.1. *Gaussian strain distribution*

Using the method of Warren and Averbach the derived coefficients of the 111 and 222 and the 200 and 400 reflections were analysed to give

Fig. 7

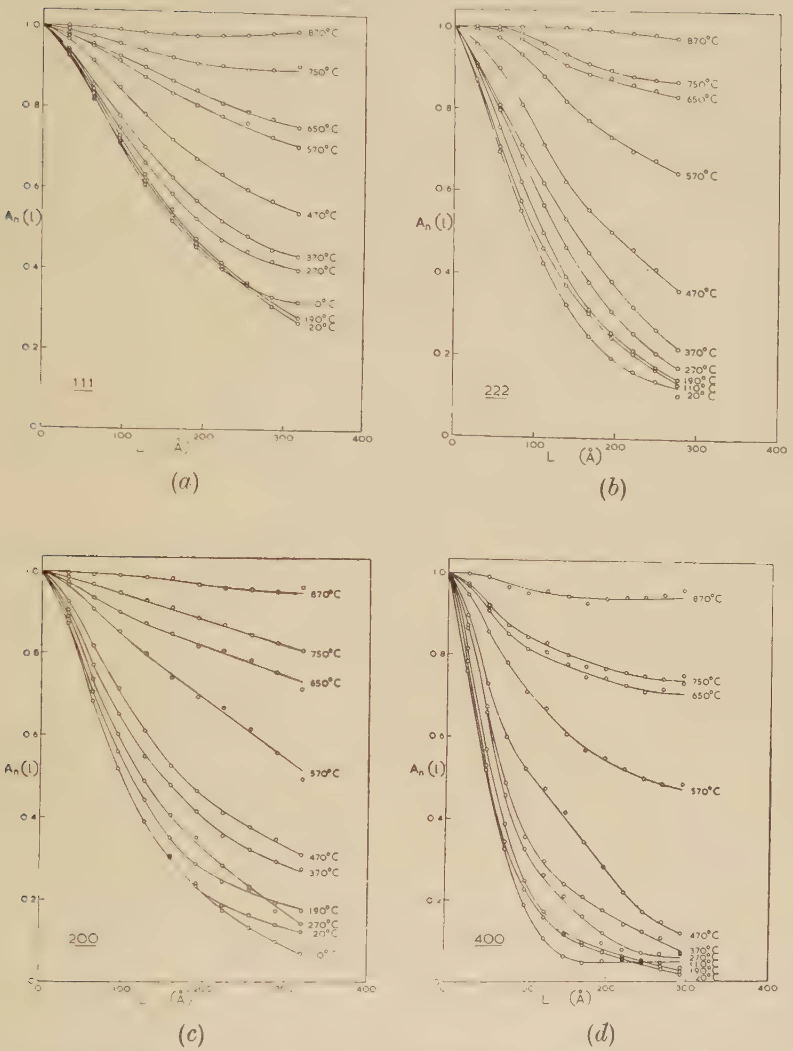

(*a*) (*b*)

(*c*) (*d*)

Fourier coefficients A_n (l) for a number of reflections from nickel powder after heating to various temperatures at 6°c/min. The coefficients are corrected for instrumental broadening and plotted against a distance, L, in the lattice. The reflections are (*a*) 111, (*b*) 222, (*c*) 200 and (*d*) 400.

values of 'apparent particle size' and root mean square strain for the nickel powder when annealed to various temperatures up to 870°c. Approximate values of stored energy, V, corresponding to these strains were calculated from the equation

$$V = 3E\epsilon^2/2(1+2\nu^2),$$

where ν is Poisson's ratio and ϵ is the root mean square strain. The results are shown in fig. 8.

5.2.2. *Cauchy strain distribution*

The method of Williamson and Smallman was applied to the derived coefficients of the 111 and 222 reflections and in all cases, except for the powder in the fully deformed state, real values of ‘ apparent particle size ’ and integral strain breadth ξ were obtained. Finite values of root mean square strain can be obtained only if the distribution is truncated at a finite value of strain, C say. In this case $\epsilon^2 = 2C\xi/\pi^2$. Williamson and Smallman suggest that the maximum reasonable value for C is the strain at which Hooke's law becomes invalid. Following these authors, this strain has been taken as 0·2 and values of root mean square strain calculated from the integral strain breadths.

Fig. 8

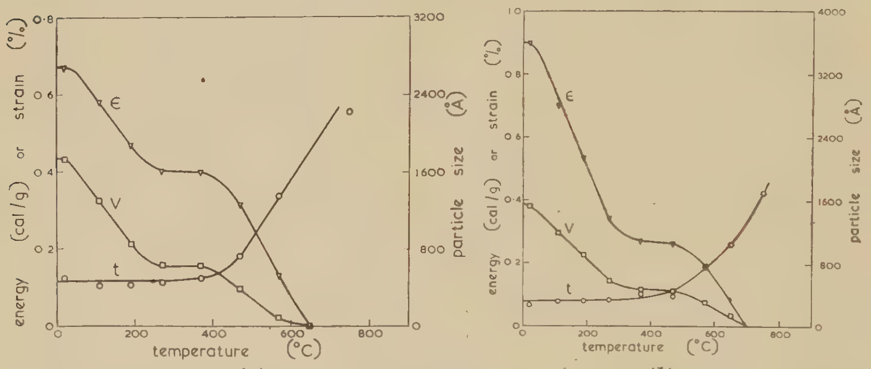

(*a*) (*b*)

Results of the Fourier analysis (Gaussian distribution of strain). ‘ Apparent particle size ’, t, root mean square strain, ϵ, and stored energy, V, as functions of the temperature of annealing (*a*) for the 111 and 222 reflections and (*b*) for the 200 and 400 reflections.

The values of ‘ apparent particle size ’, strain and the derived values of stored energy are plotted against temperature in fig. 9(*a*).

For the 200 and 400 reflections, real values of ‘ apparent particle size ’ could be obtained only at a few temperatures. These values, together with the strain and stored energy, are plotted against temperature in fig. 96(*b*). Also shown in fig. 9(*b*) are root mean square strains and energies derived from the coefficients of the 200 line without correction for the effect of small particle size.

§ 6. Discussion

6.1. *Stored Energy*

The stored energy results can be interpreted readily by reference to the results of Clarebrough *et al.* (1955) on the energy stored in solid specimens of nickel. A typical curve obtained by them for the release of energy from nickel, of identical composition to that used in the present work, after deformation almost to fracture in torsion is shown by curve

(3) in fig. 2. However, before comparing this curve with the corresponding results for the powder, curve (1), the effect of surface energy must be considered since the powder has a vastly greater surface area than the solid.

Fig. 9

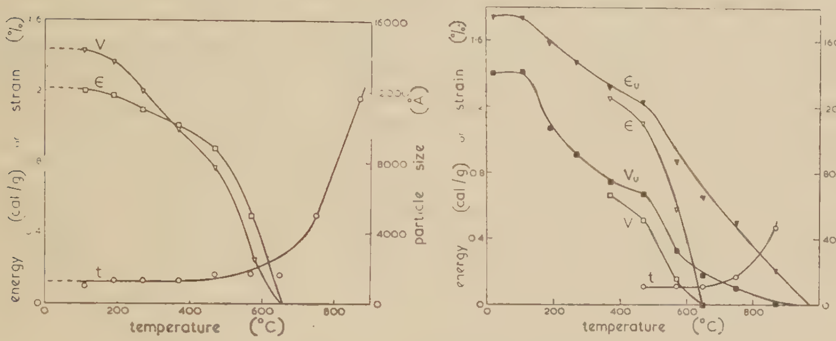

(*a*) (*b*)

Results of the Fourier analysis (Cauchy distribution of strain). 'Apparent particle size', *t*, root mean square strain, ϵ, and stored energy, V, as functions of the temperature (*a*) for the 111 and 222 reflections and (*b*) for the 200 and 400 reflections. Also shown in (*b*) are root mean square strain, ϵ_U, and stored energy, V_U, derived from the coefficients of the 200 line without correction for the effects of particle size.

The powder used had been passed through a sieve having apertures of about 35μ. If we assume that the surface energy is 1750 erg/cm^2 (Taylor (1954) and that the chips are spheres of diameter 35μ, the total surface energy is 0·004 cal/g. At best, this estimate will only be correct in order of magnitude since the chips are, in fact, long and fibrous rather than spherical and their dimensions vary over wide ranges. However, 0·1 cal/g should be a generous estimate for the total surface energy of the powder in the deformed state and only a part of this will be released during annealing. That the amount of surface energy released on annealing is, in fact, less than 0·1 cal/g is shown by the experimental result that the energy required to heat the container of powder pressed after annealing was effectively equal to that required to heat the container of powder annealed after pressing. This result shows also that no significant amount of stored energy is introduced into the powder by the pressing process. Since the total amount of energy released from the powder is 3·6 cal/g, a change in surface energy even as large as 0·1 cal/g can be neglected when comparing the shapes of curves (1) and (3). In comparing the total energy stored, after allowing for the surface energy, at least 3·5 cal/g is stored in the bulk of the powder by the deformation whereas only 0·8 cal/g is stored in a solid specimen deformed almost to fracture in torsion.

In the work on solid nickel, the curve showing the release of energy has been divided into various regions, as shown in fig. 2. The release of energy in the a' region is attributed to the disappearance of vacancies, that in the $a''+B$ region to recovery and that in region C to recrystallization. For the nickel powder, only two stages in the release of energy are apparent, the first stage extending up to about 270°c and the second stage from 270°c to 750°c. The second stage covers such a large range of temperature that it masks any intermediate stage, corresponding to region B, which may be present.

It seems reasonable to associate the region a'_p for the powder specimen with the region a' for the solid specimen, i.e. to attribute the energy represented by a'_p to the disappearance of vacancies. The value of 0·14 cal/g for this energy is very close to the values (approximately 0·1 cal/g) found for the region a' in the solid specimens and this confirms the observation of Clarebrough *et al.* that the stored energy associated with vacancies, and hence presumably the concentration of vacancies in heavily deformed metal, is not significantly affected by the amount of deformation.

The remainder of the energy, about 3·4 cal/g, must be stored as strains in the lattice caused chiefly by dislocations or arrays of dislocations and these strains must be relieved by recovery and recrystallization processes. The shapes of the curves in fig. 2 do not allow us to draw a sharp distinction between the recovery and recrystallization stages and the two stages presumably overlap considerably. However, by consideration of the results for solid specimens (Clarebrough *et al.* 1955), it seems reasonable to attribute most of the energy released below about 300°c to recovery and most of that released above about 400°c to recrystallization. The low temperature at which recrystallization appears to commence suggests that the maximum deformation present in the powder is greater than that present in solid specimens deformed almost to fracture, while the large range of temperature over which recrystallization occurs indicates that a wide range of deformations is present. Further, the release of 3·4 cal/g of energy by recovery and recrystallization processes in the powder, compared with the release of 0·7 cal/g by the same processes in solid specimens, shows that the average deformation in the powder is considerably higher than in solid specimens deformed almost to fracture.

6.2. *X-ray Measurements*

The most important features of the x-ray diffraction patterns and the analyses can now be summarized.

(1) The background intensity remains constant within ±1 count/min during annealing and no significant difference in the levels at 65° and 110° in 2θ is obtained.

(2) The integrated intensities of the 222 and 400 lines remain constant, within the experimental error, while those of the 111 and 200 decrease by about 7% over the temperature range 400°c to 870°c. These small decreases in intensity of the low angle lines are probably due to an increase in extinction resulting from an increase in both particle size and crystal

perfection. In the discussion which follows, it will be assumed that the integrated intensity of every line would remain constant if there were no change in extinction.

(3) The 'tails' of all the diffraction lines change only slightly below 400°C, although the peak intensities of the lines increase appreciably.

(4) The three methods of analysing the x-ray data give qualitatively similar results, i.e. the lattice strains decrease without change in 'apparent particle size' on annealing to 400°C, while a further decrease in lattice strain accompanied by an increase in 'apparent particle size' occurs on annealing to 870°C.

(5) The numerical values for 'apparent particle size', lattice strain and stored energy depend markedly on the method of analysis. For the 'apparent particle size' of the deformed powder, the line broadening analysis gives 2300 Å, while the Fourier methods give 350–1200 Å. The true value probably lies in the latter range since the Fourier analyses use more information and furthermore the line broadening analysis can overestimate the "apparent particle size' by a factor of up to π (Williamson and Hall 1953). For the lattice strains, too, the variation is considerable and this is particularly evident when comparing the calculated values of stored energy which range from 0·02 cal/g for the line broadening analysis to 0·4–1·4 cal/g for the Fourier analyses. However, in every case the calculated value of stored energy is less than the measured value of 3·6 cal/g.

(6) The measurements of line positions provide no evidence for the existence of stacking faults or for changes in lattice parameter on annealing.

6.3. *Interpretation*

It is possible to draw conclusions concerning the manner in which the strains of various magnitudes, present in the deformed metal, decrease during annealing. Observations (1) and (2) of §6.2 show that the same volume of material is diffracting into the lines in the deformed as in the annealed state. This means that, in the deformed state, even the most severely strained metal diffracts into the observed lines. Now the broadening due to particle size, even for particles of 400 Å, is insufficient to produce tails on diffraction lines as extensive as those measured in the present experiments for specimens annealed below 400°C. In fact, for the high angle lines at least, the broadening due to strain is comparable to or greater than that due to particle size. Therefore, the tails of the measured lines must be influenced mainly by strains corresponding to the tails of the strain distribution function and by the broadening due to particle size, since the diffraction profiles due to the two effects together are obtained by the use of a folding process on the profiles which would have been obtained if the effects had been present separately Stokes (1948). Consequently, as the 'apparent particle size' is constant and the tails are almost unchanged on annealing below 400°C, the tails of the strain distribution function can change only slightly below this temperature. Since these tails represent the most heavily distorted regions, it seems that the strain in these regions changes very little on annealing below 400°c. Conversely, the observed sharpening of the central portions of the lines indicates that there is a release of strain in the less severely distorted regions below 400°c. The measurements of stored energy, together with the detailed analyses of the line profiles, indicate that recovery occurs below 400°c with relief of strain but without appreciable recrystallization. Thus, this recovery appears to be due primarily to relief of strain in the less severely deformed regions, without increase in ‘ apparent particle size ’.

It is interesting to compare this interpretation with the model proposed by Gay *et al.* (1954). These authors suggest that a deformed metal consists of particles of comparatively low strain separated by boundary regions of greater distortion, the volumes occupied by the two regions being of comparable magnitude. Recovery is ascribed to a relief of the strain within the particles unaccompanied by any change in their size, while recrystallization corresponds to an increase in particle size and a relief of virtually all the remaining strain. On this basis the heavily distorted regions referred to here would correspond to the boundary regions of Gay *et al.* and the less heavily deformed regions to their particles.

The conclusions reached in the present work, for recovery below 400°c, are parallel to those of Gay *et al.* Further, the detailed analyses show that the more rapid, and eventually complete, relief of strain which takes place at higher temperatures is accompanied by an increase in ‘ apparent particle size ’ and is probably to be identified with recrystallization.

The disagreement between the measured and the calculated energies is disappointing but may well be ascribed to a lack of exact correspondence between the actual strain distribution and the function chosen. The importance of this choice is clearly demonstrated by the difference between the value of about 0·4 cal/g calculated on the basis of the Gaussian distribution and that of about 1·4 cal/g on the basis of a truncated Cauchy distribution. One inadequacy of both these distributions is that they involve only one parameter to specify the breadths of the distribution, whereas the experimental results show considerable changes in the central parts of the diffraction curves with only very small changes in the tails, indicating that more than one parameter is needed. Furthermore, the Gay *et al.* model implies that the boundary regions behave differently from the particles and it seems logical to postulate the existence of distinct strain distribution functions for each of these. The total distribution functions would then be a weighted sum of the individual functions. A simple case is illustrated in fig. 10 where curve (*a*) refers to strain within the particles, (*b*) to strain in the boundaries and (*c*) to the overall strain in the whole crystal. The effect of annealing at a low temperature is to decrease the breadth of (*a*) and leave (*b*) virtually unaltered. Thus, the tails of the strain distribution function and hence of the diffraction line remain virtually unaltered.

Fig. 10

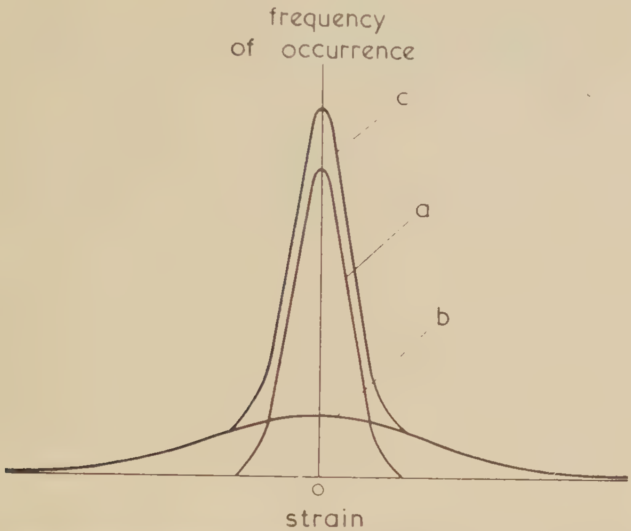

A possible distribution of strain for a deformed metal. Curve (*a*) represents the distribution of strain within the particles, (*b*) the distribution within the boundary regions and (*c*) is the overall distribution of strain in the whole crystal.

Such a case is not readily amenable to quantitative interpretation but it does seem reasonable to hope that if the true strain distribution function were known then the calculated stored energy would agree more closely with the measured value.

ACKNOWLEDGMENTS

We wish to thank Dr. W. Boas for proposing the outline of the investigation and for his continuous interest and encouragement. The stored energy measurements were made in conjunction with L. M. Clarebrough, M. E. Hargreaves and G. W. West, and the authors would particularly like to thank them for this cooperation. We would also like to thank our colleagues in the Division who have contributed in many ways to this work. In particular, thanks are due to J. F. Nicholas, L. M. Clarebrough and M. E. Hargreaves for many helpful discussions.

REFERENCES

CLAREBROUGH, L. M., HARGREAVES, M. E., MICHELL, D., and WEST, G. W., 1952, *Proc. Roy. Soc.* A, **215,** 507.

CLAREBROUGH, L. M., HARGEAVES, M. E., and WEST, G. W., 1955, *Proc. Roy. Soc.* A, **232,** 252 ; 1956, *Phil. Mag.*, **1,** 528.

GAY, P., HIRSCH, P. B., and KELLY, A., 1954, *Acta Cryst.*, **7,** 41.

HALL, W. H., 1949, *Proc. Phys. Soc.* A, **62,** 741.

HALL, W. H., and WILLIAMSON, G. K., 1951, *Proc. Phys. Soc.* B, **64,** 937, 946.

HARGREAVES, C. M., PRINCE, E., and WOOSTER, W. A., 1952, *J. Sci. Instr.*, **29,** 82.

Michell, D., 1956, *Phil. Mag.*, **1,** 584.
Paterson, M. S., 1952, *J. Appl. Phys.*, **23,** 805.
Rachinger, W. A., 1948, *J. Sci. Instr.*, **25,** 254.
Stokes, A. R., 1948, *Proc. Phys. Soc.*, **61,** 382.
Taylor, J. W., 1954, *Metallurgia*, **50,** 161.
Warren, B. E., and Averbach, B. L., 1949, *J. Appl. Phys.*, **20,** 1066 ; 1950, *Ibid.*, **21,** 595 ; 1952, *Ibid.*, **23,** 497.
Williamson, G. K., and Hall, W. H., 1953, *Acta Met.*, **1,** 22.
Williamson, G. K., and Smallman, R. E., 1954, *Acta Cryst.*, **7,** 574.
Wilson, J. E., and Thomassen, L., 1934, *Trans. Amer. Soc. Metals*, **22,** 769.
Wood, W. A., and Rachinger, W. A., 1949, *J. Inst. Met.*, **75,** 571.

A Note on Hydromagnetic Stability Problems†

By R. J. TAYLER
Atomic Energy Research Establishment, Harwell, Berks.

[Received June 29, 1956]

ABSTRACT

It is shown that care must be taken in the application of the principle of interchange of stabilities, particularly to problems in which the wave number-growth rate relation contains transcendental functions. Particular application is made to recently studied problems of hydromagnetic stability.

§ 1.

STABILITY problems in hydrodynamics are often reducible to the solution of a relation between a growth rate ($i\omega$) and a wave number (k), of the form

$$F(\omega k)=0.$$

In many such problems it is impossible to obtain or solve this relation exactly for all wave numbers. However it is often possible to solve the restricted problem of finding all wave numbers at which $\omega=0$ is a possible solution. In the simplest cases the wave numbers are then divided into regions of stability or instability, and the character of the equilibrium for wave numbers between two successive roots $\omega=0$ can be determined by the solution of the full equation for one particular wave number in the region. However in more complicated problems there may be several or even an infinite number of possible growth rates corresponding to one wave number, and then the solution $\omega=0$ will only determine states of marginal stability if it can be shown that there are no larger growth rates possible. To illustrate this we consider a particular case of a problem previously studied by Dungey and Loughhead (1954).

§ 2.

Dungey and Loughhead considered the instabilities of a twisted magnetic field confined within a cylindrical tube containing material of infinite electrical conductivity.

The field had the form

$$\mathbf{H}=\{0, H_\phi(r)H_Z(r)\} \quad . \quad . \quad . \quad . \quad . \quad . \quad . \quad . \quad (1)$$

and they considered perturbations proportional to

$$\exp\{i(\omega t+kz+m\phi)\}. \quad . \quad . \quad . \quad . \quad . \quad . \quad . \quad . \quad (2)$$

---

† Communicated by Dr. B. H. Flowers.

If the conducting fluid is compressible or has variable density they are unable to obtain a complete solution for the (ω, k) relation, but for the case of an incompressible fluid of constant density this can be found. They state and Loughhead (1955) claims to demonstrate that "the stability does not depend on the density or compressibility of the conducting fluid". However what is in fact shown is that the values of k, for which $\omega=0$ is a possible solution, are the same whether the fluid is compressible or not and do not depend on the density distribution. It is in neither case demonstrated that larger values of $(i\omega)$ are impossible.

§ 3.

We now show that for a particular case of the problem considered by Dungey and Loughhead larger values of $i\omega$ are possible. We consider the case of zero axial magnetic field, angular dependence of the disturbance given by $m=1$, and the plasma cylinder embedded in a vacuum. Then eqn. (24) of Dungey and Loughhead's paper becomes †

$$\left\{(4\pi\mu_1\omega^2-A^2)\frac{x}{I_1(x)}\frac{dI_1(x)}{dx}-2A^2\right\}\{(4\pi\mu_1\omega^2-A^2)^2-4A^4\}=\frac{1}{A^2} \quad . \quad (3)$$

where μ_1 is the density of the plasma, R is the radius of the cylinder, $x=k'R$, $H_\varphi=Ar$ and $k'^2=k^2\{1-[4A^4/(4\pi\mu_1\omega^2-A^2)^2]\}$.

We now write

$$-4\pi\mu_1\omega^2/A^2=Y^2 \quad . \quad . \quad . \quad (4)$$

$$kR=X \quad . \quad . \quad . \quad (5)$$

$$k'=ik\beta. \quad . \quad . \quad . \quad (6)$$

Then eqn. (3) becomes

$$\frac{\beta XJ_1'(\beta X)}{J_1(\beta X)}=\frac{2}{(1+Y^2)}-(1+Y^2) \quad . \quad . \quad . \quad (7)$$

and

$$\beta^2=\frac{4}{(1+Y^2)^2}-1 \quad . \quad . \quad . \quad (8)$$

and instability arises from real positive roots for Y^2.

In the particular case $\omega=Y=0$, eqn. (7) reduces to

$$\frac{\sqrt{3}XJ_1'(\sqrt{3}X)}{J_1(\sqrt{3}X)}=1$$

or

$$\frac{J_0(\sqrt{3}X)-J_2(\sqrt{3}X)}{J_0(\sqrt{3}X)+J_2(\sqrt{3}X)}=1. \quad . \quad . \quad . \quad (9)$$

The roots $\omega=0$ thus occur at zeros of $J_2(\sqrt{3}X)$. We will however show that to such a value of X there correspond also larger positive roots for Y^2. Let any such root for X be X_1, and consider the values of the expressions on the two sides of eqn. (7) for $X=X_1$ as Y varies between 0 and 1. As

---

† If eqn. (24) were taken as printed, the right-hand side of eqn. (3) above would appear as $-1/A^2$. However this term in A^2 occurs with the wrong sign in the original equation.

Y varies between 0 and 1, β varies monotonically between $\sqrt{3}$ and 0, and βX_1 between $\sqrt{3}X_1$ and 0. The right-hand side of eqn. (7) regarded as a function of βX_1 varies from -1 to 1 as βX_1 varies from 0 to $\sqrt{3}X_1$. This behaviour is shown in the figure. The exact behaviour of the left-hand side depends on which zero of $J_2(\sqrt{3}X)$, $\sqrt{3}X_1$ is. However when $\beta X_1=\sqrt{3}X_1$ and when $\beta X_1=0$ the value of the left-hand side is unity, and between these two values of βX_1 the function will take all real values between $\pm\infty$ at least once. Since for small βX_1 the function is decreasing towards $-\infty$ it is easy to see that there must be at least one value of βX_1 for which the left-hand side and right-hand side are equal. The case when $\sqrt{3}X_1$ is the first non-zero root of $J_2(\sqrt{3}X)$ is shown in the figure. Any intersection of the curves representing the two sides of eqn. (7) corresponds

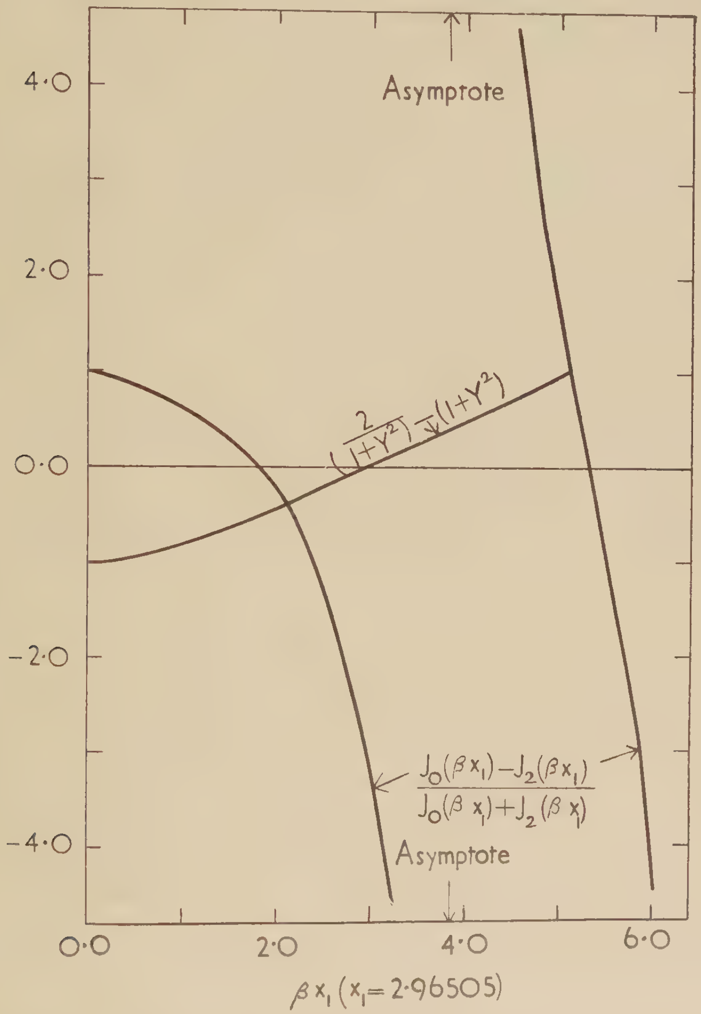

to a root Y^2 of eqn. (7) which is greater than zero. The largest value of Y^2 corresponding to each of the first six roots of $J_2(\sqrt{3X})$ is shown in the table below.

X	0·0000	2·9651	4·8597	6·7087	8·5424	10·3691	∞
Y^2	0·0000	0·6294	0·8116	0·8892	0·9279	0·9496	1·0000

Thus although at first it appears that the wave number $X=X_1$ corresponds to marginal stability, further investigation demonstrates that positive growth rates are also possible for disturbances of that wave number and it is thus really an unstable state. This one example shows that great care must be taken in applying the principle of the interchange of stabilities to problems involving transcendental functions.

ACKNOWLEDGMENT

I am grateful to Mr. E. B. Fossey and members of the computing group of A.E.R.E. Harwell for doing the calculations for the table.

REFERENCES

DUNGEY, J. W., and LOUGHHEAD, R. E., 1954, *Aust. J. Phys.*, **7**, 5.
LOUGHHEAD, R. E., 1955, *Aust. J. Phys.*, **8**, 319.

Interaction Lengths and Diffraction Scattering of 4·2 GeV π^--Mesons in G5 Emulsion†

By J. O. Clarke
The Physical Laboratories, The University, Manchester‡

and J. V. Major
Department of Physics, The Durham Colleges in the University of Durham, Durham

[Received June 8, 1956]

Abstract

A large block of G5 emulsion has been exposed to the 4·2 GeV π^--meson beam of the Berkeley Bevatron and 120 m of π^--meson track scanned. The total interaction length is found to be $(27{\cdot}1 \pm 2{\cdot}4)$ cm and the individual interaction lengths for the production of stars and scatters are $(38{\cdot}7 \pm 3{\cdot}5)$ cm and (90^{+23}_{-15}) cm respectively. The geometrical interaction length is 28·4 cm. Good agreement with diffraction scattering theory is found for the observed angular distribution of the secondaries in the elastic scattering events.

§ 1. Introduction

A large block of G5 emulsion has been exposed to the 4·2 GeV π^--meson beam of the Berkeley Bevatron. In this paper are described the results obtained from the scanning of 120 m of meson track. The aspects of the work considered here are the determination of the various interaction lengths and an examination of diffraction scattering. It is found that after correction for losses the total interaction length is closely geometrical. The elastic scattering of π^--mesons is adequately accounted for by diffraction theory and leads to a value for the cross section of the collision of a π^--meson with a proton in accordance with other recent determinations.

§ 2. Experimental

2.1. *General*

The block consisted of 120 emulsion strips each of size 25 cm × 10 cm × 400 μ and it was exposed to the π^--meson beam for two days. The flux of mesons incident to the end-face of the stack was $(2{\cdot}0 \pm 0{\cdot}2) \times 10^4$ cm^{-2} over a central area 5 cm × 5 cm.

Before processing by a temperature-cycle method, the emulsions were exposed to an x-ray beam to provide reference lines. The distortion level, as given by the curvature distortion vector $\mathbf{K}_2$ (Cosyns and Vanderhaege 1950, Major 1952) was about 20 μ, and less than 0·1% of the total area of emulsion was affected by bubbles. The plateau grain density was 11 grains/50 μ and its variation with depth was not larger than 10%. After processing, the plates were aligned by the x-ray marks and the glass cut to provide reference edges for tracing tracks between adjacent emulsions. Superposition to within 100 μ was possible.

---

† Communicated by Professor G. D. Rochester.

‡ Now at The Department of Physics, The Durham Colleges in the University of Durham, Durham.

2.2. *The π^--Meson Beam*

The collimation of the beam was found from a sample of 120 tracks selected in the course of scanning (see later); three-quarters of these tracks lay between $\pm 0{\cdot}2°$ of the mean direction of the beam.

The value of $p\beta$ for the beam was determined from scattering measurements on 100 tracks, each 2·5 cm long, 50 being chosen at random and 50 selected from the primaries of interactions. A large cell-length (1 mm) had to be used to keep the ratio of signal to noise high and this meant that a reliable estimate of $p\beta$ could not be obtained for any one track. Instead, the distribution of the second differences was found for both groups of tracks and the value of $p\beta$ was computed from the distributions. No significant difference was found between the two determinations of $p\beta$. The $4\bar{D}$ cut-off was adopted, and after allowing for noise, $p\beta$ for the 100 tracks was found to be $(4{\cdot}0 \pm 0{\cdot}1)$ Gev/c. Since β is close to unity, the value of $p\beta$ can be compared directly with the energy measured recently at Berkeley with a cloud chamber (Barkas, private communication), viz., $(4{\cdot}2 \pm 0{\cdot}3)$ Gev. The influence of emulsion dislocations (Biswas *et al.* 1955) on the value of $p\beta$ has not been considered in detail. Because of this, the Berkeley value has been used in all calculations.

The decay in flight of π^--mesons to fast μ^--mesons, and the production of secondary particles in interactions results in a small contamination of the beam. The main contamination is due to π–μ decays. For the assumed separation† of 3 m between target and emulsion block the contamination is estimated at about 2%. The contamination from secondaries lying within $\pm 0{\cdot}2°$ of the beam direction is negligible. Decays inside the emulsion would resemble π^--meson scatters. It is estimated that a decay will occur once in approximately 200 m of π^--meson track.

2.3. *Track Scanning*

The tracks were scanned, under a magnification of 45 × 1·5 × 15, chiefly on two Cooke M 4000 microscopes and also on one Beck microscope. Tracks were selected about 1 cm from the emulsion edge on which the beam had been incident and were then followed either out of the plate, or to an interaction. The general criterion for following a track was that it should be approximately parallel to the surface of the emulsion and to the traversing axis of the microscope. This would affect the observed collimation of the beam as it was determined from tracks accepted for following. The scanning rate was 1·5 m per man day.

---

† *Note added in proof.*—The separation is now known to be about 12 m leading to a contamination of about 5%. This increase does not affect the conclusions significantly.

An eyepiece hairline was aligned initially on each track to be followed and the direction of the track compared with that of the hairline every few fields of view.

The interactions were classified according to their size (Brown *et al.* 1949) and were separated into two groups. Those with $n_h=0$, and $n_s=1$ were grouped as 'scatters'. All other interactions including disappearances (n_h, $n_s=0$) were grouped as 'stars'. The star-size was estimated visually; no attempt was made to determine grain densities.

In the first group the spatial angle of scatter was determined in each case by measuring the horizontally and vertically projected angles of scatter. It was estimated that the combined effect of reading errors, uncertainty in the shrinkage factor and the depth of focus would result in an error of $\pm 15'$ on each spatial angle. Multiple scattering measurements were made on secondaries of length greater than 5 mm. The value of $p\beta$ was estimated from the distribution of second differences

§ 3. PRELIMINARY RESULTS AND SCANNING EFFICIENCIES

The total track length followed was 12 010 cm in which 377 interactions were found. Of these 100 were scatters and 277 were stars, the latter including 4 disappearances. The angular distributions of the horizontally and vertically projected angles of scatter are shown in figs. 1 and 2. The average value of $p\beta$ for the secondaries is (3·9 ± 0·1) GEV/c whilst the average for the primaries is (4·0 ± 0·1) GEV/c. Assuming the scanning was completely efficient the total interaction length is $\lambda_I=(31{\cdot}9\pm 1{\cdot}6)$ cm.

3.1. *Efficiency of Star Detection*

In fig. 3 are shown the frequency distributions of star-size for three observers, each normalized to a track length of 50 m. For $(n_h+n_s)\leqslant 4$ there are obvious differences between the different observers. In fig. 4 the three individual interaction lengths observed are compared with the corresponding value of the average star-size for each observer. The general trend of an increase in star-size with observed interaction length has been shown to be statistically significant and is presumably due to the loss of small stars. A correction for loss has been made relative to observer I. The star-size distributions have been arbitrarily divided at $(n_h+n_s)=6$ and the distributions of observers II and III increased with small size-stars until the ratio of stars of $(n_h+n_s)\leqslant 6$ to stars of $(n_h+n_s)>6$ is equal to that for I. The total number of stars is thus corrected from (277 ± 17) to (310 ± 28): this value will be uncertain by the inefficiency of I.

3.2. *Efficiency of Scatter Detection*

The majority of scatters were detected by the sudden change in direction of a track in the horizontal plane: few were detected by the change in

Fig. 1

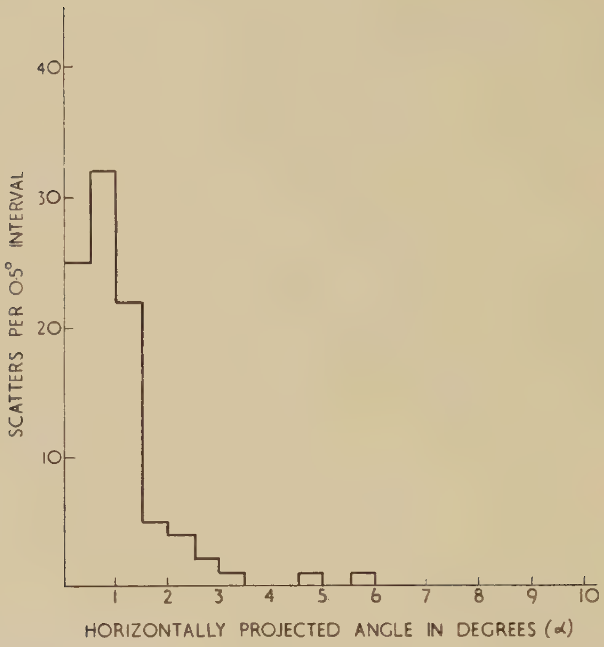

The distribution of the horizontally projected angles of scatter α.

Fig. 2

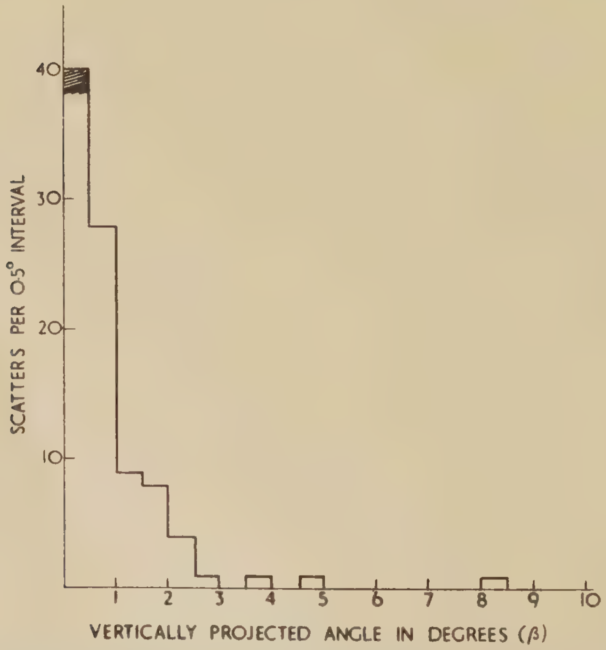

The distribution of the vertically projected angles of scatter β (possible Coulomb scatters shaded).

Fig. 3

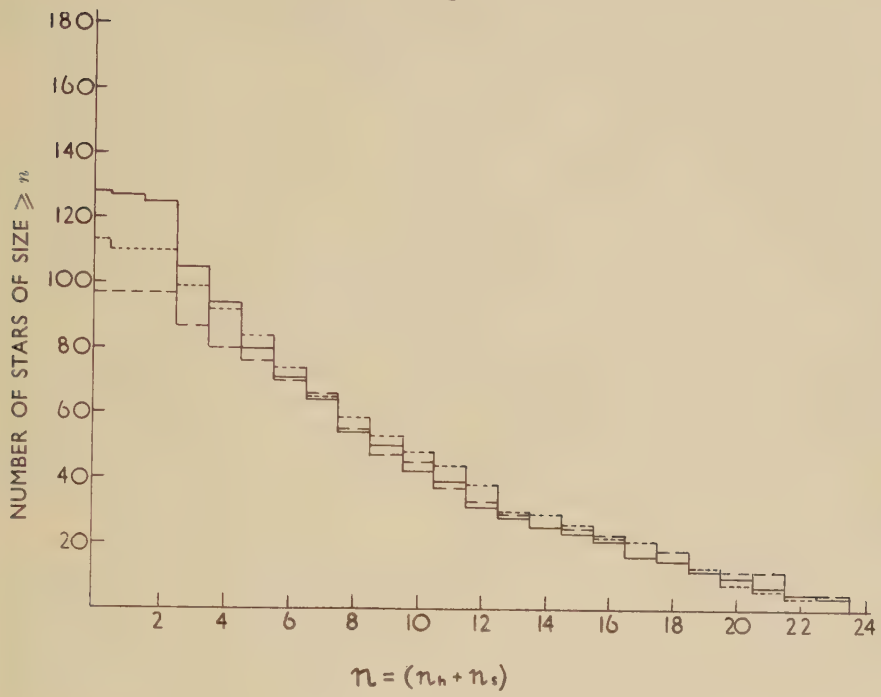

The integral star size distribution for three observers.

Fig. 4

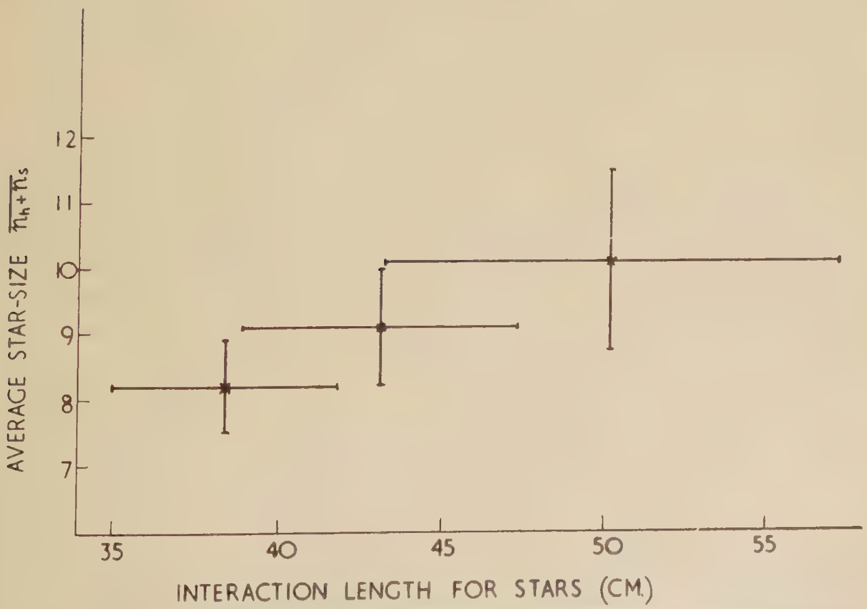

The variation of the observed star size with the apparent interaction length for three observers.

direction in the vertical plane. In the horizontal plane it is expected that small angles of scatter will be more difficult to detect than large angles, and that this will lead to values of the efficiency which will increase with increase in angle. In the vertical plane, efficiency is independent of angle (since detection was by the horizontally projected angle) but there is an overall efficiency of detection equal to the overall efficiency in the horizontal plane. Thus the distributions of the horizontally and vertically projected angles of scatter should differ considerably at the smaller angles. Since the number in each is the same, the peak of the horizontal distribution should be smaller and the breadth greater than those of the vertical distribution. Figures 1 and 2 show these differences. However since the horizontal angle is measured directly and the vertical angle involves the shrinkage factor, the errors in determining these angles may be quite different and their consequent effects on the broadening of the distributions have been calculated and shown to be small. It is estimated that the error in the horizontal angle is $\sim\pm 7'$ and $\sim\pm 15'$ in the vertical angle. These errors are not sufficient to explain the difference between the distributions.

An approximate value of the efficiency can be obtained in the following way. If the true distribution of projected angles of scatter is given by $T(\theta)$, the angular efficiency by $e(\theta)$ and the total efficiency by ϵ, then the horizontally projected distribution is given by $H(\theta)=e(\theta)T(\theta)$ and the vertically projected distribution by $V(\theta)=\epsilon T(\theta)$. For large values of θ, $e(\theta)$ is expected to reach the value 1, that is,

$$\underset{\theta\text{ large}}{\mathrm{Lt}}\frac{V(\theta)}{H(\theta)}=\underset{\theta\text{ large}}{\mathrm{Lt}}\frac{\epsilon}{e(\theta)}\longrightarrow\epsilon$$

Similarly,

$$\underset{\theta\text{ large}}{\mathrm{Lt}}\frac{\int_{\theta}^{\pi}V(\theta)\,d\theta}{\int_{\theta}^{\pi}H(\theta)\,d\theta}\longrightarrow\epsilon$$

The number of scatters is too small to permit an accurate estimate to be made. However, if full efficiency is reached at 1·0° (Walker and Crussard 1955), then the efficiency is $(69\pm 20)\%$. An independent estimate of an upper limit to the efficiency is $(82\pm 12)\%$. A final value of $\epsilon=(75\pm 15)\%$ is taken and the observed (100 ± 10) scatters corrected to (133 ± 27).

§ 4. THE CORRECTED INTERACTION LENGTHS AND CROSS SECTIONS

The corrected total interaction length found from (443 ± 39) stars and scatters is $\lambda_I=(27{\cdot}1\pm 2{\cdot}4)$ cm. The corresponding total area presented by the nuclei in 1 cm^3 of emulsion is $S_I=(0{\cdot}037\pm 0{\cdot}003)$ cm^2. The corresponding geometrical area, S_g, assuming the radius of the nucleus to be $1{\cdot}35\times 10^{-13}A^{1/3}$cm, has been calculated from the composition of the emulsion given in the table (Waller, private communication) and is 0·035 cm^2.

The interaction length for stars is $\lambda_A=(38{\cdot}7\pm3{\cdot}5)$ cm, the corresponding cross section per cm³ being $S_A=(0{\cdot}026\pm0{\cdot}002)$ cm², and for scatters, $\lambda_D=(90^{+23}_{-15})$ cm and $S_D=(0{\cdot}011\pm0{\cdot}002)$ cm².

Element	I	Ag	Br	S	C	N	O	H	Density
g/cm³ 58% r.h.	0·012	1·831 ±0·030	1·349 ±0·022	0·007	0·276 ± 0·005	0·073 ±0·001	0·249 ±0·004	0·0533 ±0·0009	3·850 ±0·041

(The limits quoted in the table are not experimental errors but represent extreme variations from batch to batch.)

§ 5. The Diffraction Scattering

In this section the 100 scatters are considered. It will be shown that diffraction scattering theory accounts for most of them. The measurements of $p\beta$ for the primaries and secondaries show that the scattering process is elastic.

5.1. *Theoretical Introduction*

The theory of diffraction scattering has been given by Fernbach *et al.* (1949). It is assumed that nuclear matter is characterized by a refractive index and an absorption coefficient both of which can be related to known nuclear parameters. Thus a matter wave incident on a nucleus will be attenuated and diffracted. The propagation constant k of the matter wave associated with the incident π^--meson is given by $k=p/\hbar$, where p is the momentum of the meson and $\hbar$ is the reduced value of Planck's constant. The wavelength λ of the meson is h/p, which is $\sim3\times10^{-14}$ cm in this experiment. Inside the nucleus, the value of the propagation constant becomes $(k+k_1)$ and is determined by the kinetic energy E of the π^--meson and the mean potential energy V of the meson inside the nucleus. Now $k_1=k\{(1+V/E)^{1/2}-1\}$, and since $V\sim30$ MeV and $E\sim4$ GeV, $V\ll E$ and $k_1=0$. This value of k_1 implies that there is no change of refractive index when the π^--meson enters the nucleus. Thus only the aspect of the theory for which $k_1=0$ need be considered. Again, in nuclear matter, the absorption coefficient K is given by the product of the nucleon density and the mean cross section for scattering of the π^--meson by a nucleon, $\sigma_{\pi\text{-}N}$,

$$K=\frac{3A}{4\pi R^3}\times\sigma_{\pi\text{-}N}$$

where

$$\sigma_{\pi\text{-}N}=\{Z\sigma_{\pi\text{-}p}+(A-Z)\sigma_{\pi\text{-}n}\}/A.$$

If the nuclear radius $R=r_0A^{1/3}$, then

$$K=\frac{3\sigma_{\pi\text{-}N}}{4\pi r_0^{\,3}} \qquad \text{. . . . . . (1)}$$

and is independent of A if $\sigma_{\pi\text{-}N}$ is not a function of A. This last point will be discussed more fully below since $\sigma_{\pi\text{-}N}$ is not known experimentally for incident π^--mesons of such great energies.

By considering the change of amplitude as a function of the length $2S$ of nuclear matter traversed by the π^--meson, it is found that the cross section for diffraction scattering σ_D is given by

$$\sigma_D=2\pi\int_0^R [1-\exp(-KS)]^2\rho\,d\rho.$$

The quantity $2S$ has the same value for all points on a spherical nucleus which are at an equal distance ρ from the line through the centre of the sphere. Thus $S=\surd(R^2-\rho^2)$ and, for $k_1=0$

$$\sigma_D=\pi R^2\{1+[1-2KR]\exp(-2KR)/2K^2R^2-4[1/K^2R^2-\exp(-KR)\\ \times(1/K^2R^2+1/KR)]\}$$

If the amplitude of the scattered wave as a function of the angle θ be written $f(\theta)$, it can be shown that,

$$f(\theta)=k\int_0^R\{1-\exp(-KS)\}J_0(k\rho\sin\theta)\rho\,d\rho$$

where J_0 is the Bessel function of zero order, and θ is the spatial angle of scatter. The differential scattering cross section

$$d\sigma_D(\theta)=\{f(\theta)\}^2 d\Omega=f^2(\theta)\times 2\pi\sin\theta\,d\theta.$$

Thus of those particles incident on nuclei of type i, a fraction

$$f_i(\theta)=\frac{d\sigma_{Di}(\theta)}{\sigma_{Di}}$$

are scattered between the angles θ and $(\theta+d\theta)$.

The absorption cross section, σ_A, is the product of the geometrical cross section, πR^2, and the probability that the π^--meson interacts with a nucleon in the nucleus. Assuming that there is no scattering at the nuclear surface,

$$\sigma_A=2\pi\int_0^R[1-\exp(-2KS)]\rho\,d\rho$$

whence

$$\sigma_A=\pi R^2\{1-[1-(1+2KR)\exp(-2KR)]/2K^2R^2\}$$

5.2. *Diffraction in a Composite Medium*

The probability of a meson being diffracted by a nucleus of type i is $N_i\sigma_{Di}$, where N_i is the number of these nuclei in 1 cm³ of emulsion, whence the final form of the angular distribution is obtained by weighting the angular distributions for the eight elements in the emulsion, according to the frequency with which they occur (see the table). Then

$$F(\theta)=\sum_i\left\{\frac{N_i\sigma_{Di}}{\sum_i N_i\sigma_{Di}}\cdot\frac{f_i^2(\theta)2\pi\sin\theta\,d\theta}{\sigma_{Di}}\right\}=\frac{2\pi\sin\theta\,d\theta}{\sum_i N_i\sigma_{Di}}\sum\{N_if_i^2(\theta)\}. \quad . \quad (2)$$

When an elastic diffraction scatter occurs, there is a momentum transfer P to the nucleus, which is independent of the type of nucleus, and is given by the approximate expression $P=70\theta$ MeV/c, where θ is the angle of scatter in degrees. For $A \geqslant 12$, the probability that the struck nucleus will have sufficient energy to sensitize the one grain necessary for it to appear as a recoil track is negligible. Hydrogen, however, has a recoil track of length 8 μ even when θ is 0·5° ; such diffraction scatters will be classified as $(1+1)\pi^-$-events.

The probability of diffraction on hydrogen is such that only about one such event would be expected. This would have no appreciable influence on the values of λ_A and λ_D.

5.3. *Determination of the Absorption Coefficient K and the Function $F(\theta)$*

Before it is possible to calculate $F(\theta)$, it is necessary to know the value of K. The expected values of both λ_D and λ_A are functions of K, but it is the total cross sections for diffraction and absorption, S_D and S_A respectively, that are found experimentally. Now, $S_D=\sum_i N_i\sigma_{Di}$ and $S_A=\sum_i N_i\sigma_{Ai}$, and their calculated values can be plotted as a function of K as shown in fig. 5. Since the experimental value of S_A is known more accurately than the value for S_D, it has been placed on the absorption curve giving a value of $K=(2{\cdot}75^{+1\cdot25}_{-0\cdot55})\times10^{12}$ cm^{-1}. The observed value of $S_D=(1{\cdot}1\pm0{\cdot}2)\times10^{-2}$ cm^2 is plotted for the same K value and is in reasonable agreement with the expected value of $S_D=(1{\cdot}25\pm0{\cdot}35)\times10^{-2}$ cm^2. This expected value of S_D corresponds to a detection efficiency of (62 ± 22)%, in reasonable agreement with the previous estimate.

Fig. 5

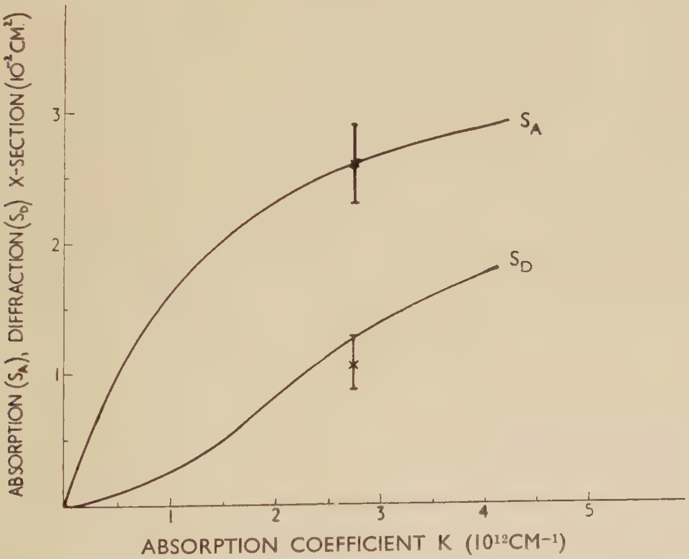

The total cross sections for diffraction and absorption S_D and S_A, as a function of the absorption coefficient K.

5.4. *The Angular Distributions (Spatial and Projected)*

The function $f(\theta)$ has been evaluated by numerical integration for values of ρ/R between zero and unity at 0·1 intervals and the values for different values of R have been combined to obtain $F(\theta)$ (see eqn. (2)) : θ was taken at 0·5° intervals.

Fig. 6

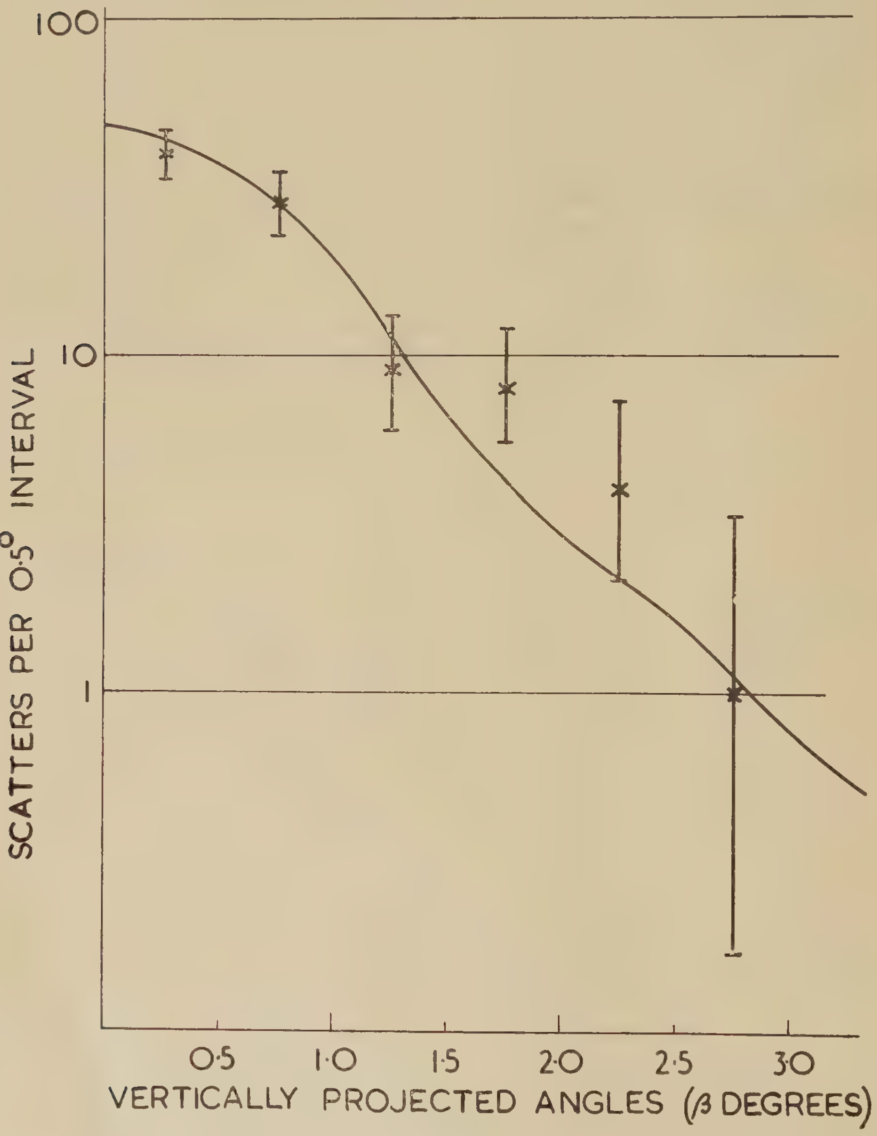

Logarithmic plot of the vertically projected angles of scatter.

Agreement between the theoretical and the corrected experimental distributions is reached at values of θ greater than $1\frac{1}{2}$° ; the discrepancy below this value is attributed to varying efficiency.

The projected distribution has been calculated from the spatial distribution. Since the distribution of the vertically projected angle β is free of selection bias, it can be compared directly with the theoretically expected distribution. This is shown in fig. 6 where the expected curve has been corrected (Lloyd and Wolfendale 1955) for the broadening effects of the errors of measurement. It is seen that good agreement is obtained with the vertical distribution. Coulomb scatters can only occur in the spatial angular range, $0<\theta<15'$: two events were found within this range.

§ 6. DISCUSSION

The optical model of the nucleus accounts well for the detailed experimental results. The scatters with large angles could possibly be inelastic events but the track lengths are too short for estimates of the energies of the secondaries. Even if the six events with $\theta>10^\circ$, are regarded as stars rather than elastic scatters the cross sections are not significantly altered. Since the absorption coefficient K has been determined experimentally, it is possible to determine the mean cross section for the interaction of π^--mesons with single nucleons from eqn. (1). If it is assumed that, at this energy, $\sigma_{\pi\text{-}p}=\sigma_{\pi\text{-}n}$, then $\sigma_{\pi\text{-}N}=\sigma_{\pi\text{-}p}$ and $\sigma_{\pi\text{-}N}$ can be compared with $\sigma_{\pi\text{-}p}$ determined directly from collisions in hydrogen. The value found is $\sigma_{\pi\text{-}N}=(30\pm11)$ mb. Maenchen *et al.* (1955) found $\sigma_{\pi\text{-}p}=(19\cdot7\pm3\cdot4)$ mb with 4·5 GeV π^--mesons in a hydrogen-filled cloud chamber; Bandtel *et al.* (1955) found $\sigma_{\pi\text{-}p}=(30\pm5)$ mb at 4·4 GeV by counter methods; Cool *et al.* (1954) found $\sigma_{\pi\text{-}p}=(34\pm3)$ mb at 1·5 GeV by counters using a difference method. All the results are in reasonable agreement.

For energies $\geqslant1$ GeV, $k_1=0$, and λ_A and λ_D become independent of energy (Sternheimer 1956). Thus the results presented here obtained at an energy of 4·2 GeV can be compared directly with those of Walker and Crussard (1955) obtained at 1·5 GeV. The value of λ_D is of the order of 100 cm and the value λ_A about 40 cm in both experiments.

The reciprocal of the absorption coefficient K gives the mean free path λ for the collision of the meson with a nucleon in the nucleus. From the observed value of K, $\lambda=(3\cdot64^{+1\cdot11}_{-1\cdot20})\times10^{-13}$ cm. Hence, on the average, a π^--meson will make about 2 collisions on traversing a nucleus of average size in the emulsion.

The average opacity of the nucleus, $S_A/S_g=0\cdot75$. If the partial transparency is explained by a nucleon consisting of a core of strongly interacting material surrounded by a region of weak interaction, then by considering the average opacity and the area of the nucleus, an approximate calculation yields a radius of $\sim0\cdot5\times10^{-13}$ cm for this core. This is in agreement with the estimate from π^--p scattering in emulsions (Walker and Crussard 1955).

ACKNOWLEDGMENTS

We wish to thank Professor G. D. Rochester for his constant advice and interest. We are indebted in particular to Professor E. O. Lawrence, Dr. W. K. Barkas, Dr E. J. Lofgren, Dr. Harry Heckman and Dr. Robert

Adair of the Radiation Laboratory, Berkeley, California, for permission to make an exposure and for making the preliminary and final exposures. Our thanks are due to Dr. A. Roberts and Lieutenant G. F. Cronin of the American Embassy for arranging the shipment of the emulsion, to the Holt Radium Institute, Manchester for the use of x-ray equipment. We are especially grateful to A. J. Apostolakis, Dr. L. Cohen, I. Macpherson and Dr. A. W. Wolfendale for many discussions. One of us (J.O.C.) wishes to thank the D.S.I.R. for a Maintenance Allowance.

REFERENCES

BANDTEL, K. C., BOSTICK, H. A., MOYER, B. J., WALLACE, R. W., and WIKNER, W. F., 1955, *Phys. Rev.*, **99,** 673.

BISWAS, S., PETERS, B., and RAMA, 1955, *Proc. Ind. Acad.* A, **41,** 154.

BROWN, R. H., CAMERINI, U., FOWLER, P. H., HEITLER, H., KING, D. T., and POWELL, C. F., 1949, *Phil. Mag.*, **40,** 862.

COOL, R. L., MADANSKY, L., and PICCIONI, O., 1954, *Phys. Rev.*, **93,** 249.

COSYNS, M., and VANDERHAEGE, G., 1950, *Bull. du Cen. de Phys. Nuc. de l'Université Libre de Bruxelles*, No. 15.

FERNBACH, S., SERBER, R., and TAYLOR, T. B., 1949, *Phys. Rev.*, **75,** 1352.

LLOYD, J. L., and WOLFENDALE, A. W., 1955, *Proc. Phys. Soc.* A, **68,** 1045.

MAENCHEN, G., POWELL, W. M., SAPHIR, G., and WRIGHT, R. W., 1955, *Phys. Rev.*, **99,** 1619.

MAJOR, J. V., 1952, *Brit. J. Appl. Phys.*, **3,** 309.

STERNHEIMER, R. M., 1956, *Phys. Rev.*, **101,** 384.

WALKER, W. D., and CRUSSARD, J., 1955, *Phys. Rev.*, **98,** 1416.

The Natural Radioactivity of Lanthanum †

By R. N. Glover and D. E. Watt
Department of Natural Philosophy, The University, Glasgow, W.2

[Received June 25, 1956]

ABSTRACT

The decay of ^{138}La, the middle member of a naturally occurring isobaric triplet, is studied by means of heavily shielded scintillation and proportional tube spectrometers. The existence of only two of three γ-rays reported by earlier investigators is confirmed, their energies being $(0{\cdot}81 \pm 0{\cdot}01)$ and $(1{\cdot}44 \pm 0{\cdot}02)$ MEV. No annihilation quanta were observed. Coincidence studies show that these γ-rays are not in cascade, and that the 1·44 MEV transition belongs to the electron capture branch. A previously unobserved β-ray spectrum with maximum energy (205 ± 10) kev is detected. The experimental log ft value of 19·0 and known spin change $\Delta I = 3$ indicate a 3rd forbidden transition. No evidence of a reported 1·0 MEV β-transition is found. A new decay scheme is proposed and agrees with the results of independent investigators on the β^- and β^+ activity of ^{138}Cs and ^{138}Pr respectively. The partial half-life of the electron capture branch is found to be $(1{\cdot}64 \pm 0{\cdot}06) \times 10^{11}$ yr, and of the β branch $(4{\cdot}1 \pm 0{\cdot}7) \times 10^{11}$ yr. and $(3{\cdot}5 \pm 0{\cdot}3) \times 10^{11}$ yr. measured by direct counting of the β-rays and by calculation of the total counts due to the 0·81 MEV γ-ray respectively. 70% of the total disintegrations are estimated to proceed by electron capture and 30% by β emission.

§ 1. INTRODUCTION

^{138}La is an odd–odd nucleus, and the middle member of the isobaric triplet (^{138}Ba$_{56}$, ^{138}La$_{57}$, ^{138}Ce$_{58}$). Throughout the nuclear table there exist only four naturally occurring isobaric triplets. Since, theoretically, no odd–odd nucleus above ^{14}N can be stable, ^{138}La may be expected to decay both by electron capture (and perhaps β^+ emission) and by β^- emission, the long half life being due to a large spin change involved in its decay.

Gamma activity was first observed by Pringle *et al.* (1950) and subsequently (1951) three γ-rays of energies 0·535, 0·807 and 1·39 MEV were reported, the latter being considered to be a crossover transition. From the intensity of the K x-rays it was suggested that the γ-rays followed electron capture. It was also proposed that the first and second excited states of ^{138}Ba were 0·807 and 1·39 MeV respectively above the ground state. However, the existence of a level at 0·807 MeV is not supported by subsequent investigations of the β^--decay of ^{138}Cs (Langer *et al.* 1953, Thulin 1955). The possibility of electron capture to both these excited states was indicated, and decay by β^+ emission to either of the excited states or to the ground state was not considered to be excluded (Pringle *et al.* 1951). Neither γ–γ nor K–γ coincidence experiments were attempted. A half-life of $2{\cdot}0 \times 10^{11}$ yr. was suggested.

---

† Communicated by Professor P. I. Dee, F.R.S.

In a rather insensitive experiment, Pringle *et al.* (1951) assigned an upper limit of 12 counts/min/g La_2O_3 to the number of electrons or positrons emitted with energy > 100 kev. With the aid of a large proportional counter, Mulholland and Kohman (1952) reported β^- emission of maximum energy $(1{\cdot}0 \pm 0{\cdot}2)$ MeV, measured by aluminium absorption methods, and partial half-life of $1{\cdot}2 \times 10^{12}$ yr. In view of the difficulties caused by differing contamination of their absorbers, this result seemed somewhat uncertain.

The aim of the present investigation is to examine the reported β-activity and establish a decay scheme by means of coincidence measurements.

§ 2. EXPERIMENTAL ARRANGEMENTS

To reduce the cosmic ray background, and so increase still further the sensitivity of the apparatus for this and similar investigations, a special laboratory was fitted out about 90 ft. underground in a disused coal-mine beneath this University. Measurements indicated that at this depth the particle component of the cosmic ray flux was reduced by a factor of three. However, lead shielding was still required because of considerable γ-activity due mainly to ^{40}K in the surrounding rocks and brickwork.

The scintillation spectrometer consisted of a 2 in. high × 2 in. diameter NaI crystal mounted on a DuMont 6292 photomultiplier and surrounded on all sides by 8 in. lead. The amplified output pulses were fed into a cable 400 ft. long and analysed at the surface by means of a 100-channel Hutchinson–Scarrott kicksorter. The total background above 70 kev was reduced to 80 counts per minute compared with 250 c.p.m. at ground level.

Coincidence experiments were carried out under the same shielding conditions, the second detector being a NaI crystal of the same size and identically mounted.

For the detection of β-rays the system used was basically that described by Dixon and McNair (1954). The proportional tube spectrometer was surrounded by two rings of Geiger counters and shielded by 4 in. lead and 1 in. iron on all sides. The proportional counter, diameter 14·4 cm, has been modified so that 32·1 cm of its cathode is fully operative, giving an available internal cathode area of 1450 cm^2, an increase of roughly 30%. As previously described, the amplified pulses were displayed oscillographically and filmed. With the counter at a pressure of 4 atm. (argon–methane mixture), the background above 20 kev was 27 c.p.m. as compared with a value of 50 c.p.m. at ground level, and 30 c.p.m. in the basement site used by Dixon and McNair (1954) some 10 ft. below ground level. The reason for the rather disappointing decrease is the increased low energy γ-ray flux, mainly due to ^{40}K, which cannot be completely absorbed by the available shielding.

§ 3. Gamma-Ray Spectrum

The source consisted of 7 g of La_2O_3, distributed uniformly round the crystal, the average source thickness being approximately 70 mg/cm². The activity due to the source was 19 c.p.m. against a background of 49 c.p.m. The spectrum with background subtracted (fig. 1) shows the presence of two γ-rays of energies $(0{\cdot}81 \pm 0{\cdot}01)$ and $(1{\cdot}44 \pm 0{\cdot}02)$ mev. No other γ-ray was observed with energy $< 2{\cdot}5$ mev. In particular, closer investigation failed to reveal either annihilation radiation, which would be expected if β^+-emission occurred, or a γ-ray of energy 0·535 mev. It seems probable that statistical fluctuations caused Pringle *et al.* (1951) to interpret the Compton edge of the 0·81 mev γ-ray as evidence for the existence of a 0·535 mev γ-ray.

Fig. 1

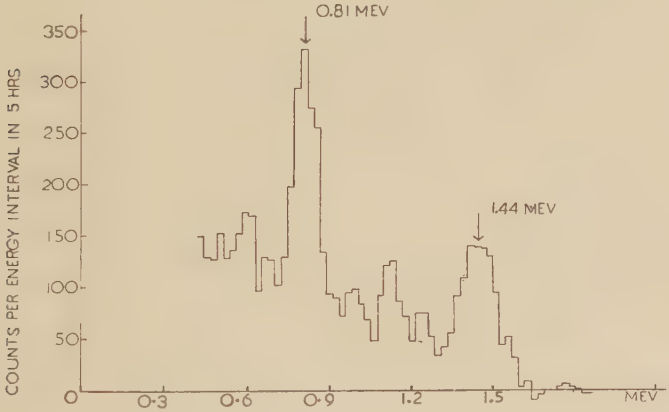

Gamma-ray spectrum of ^{138}La.

The need for sources of very high chemical purity must be emphasised. Spectrographically pure La_2O_3 was found to give a spectrum showing several contamination peaks at energies < 400 kev, their total activity being considerably greater than that of the high energy gamma rays. An extremely pure sample, kindly supplied by Dr. W. Turchinetz of the University of Manitoba, Canada, showed practically no low energy contamination.

§ 4. Beta-Ray Spectrum

0·927 g of the pure finely divided La_2O_3 powder, suspended in amyl acetate containing a drop of Durofix as adhesive agent, was spread over

850 cm^2 of the removable copper lining of the proportional counter, the source being kept well within the effective counting volume. The average source thickness was 1·1 mg/cm^2. The counter was filled to a pressure of 4 atm., and calibrated by means of the 46·7 kev γ-rays of Radium D.

The spectrum obtained (fig. 2) indicated a maximum energy of (205 ± 10) kev for the β-ray. The end point was observed, more clearly (fig. 2 inset), by using a thicker source and lower amplifier gain. There was no indication of a β-ray of maximum energy ~1·0 Mev and partial half-life $1{\cdot}2\times10^{12}$ yr. as reported by Mulholland and Kohman (1952), although such an activity would have been well within the limits of detection of the system used. A thinner source, 0·37 mg/cm^2, was used to examine the spectrum below 50 kev. The shape must be distorted due to the necessary source thickness, but the results suggest that the spectrum exhibits a real rise at low energy. Further investigation with a sufficiently enriched source, as yet not available, is required to confirm that the spectrum shape is indeed similar to that of ^{87}Rb (Curran *et al.* 1952, Lewis 1952).

Fig. 2

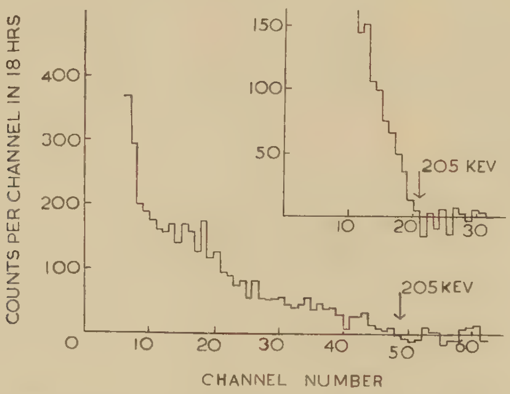

Beta spectrum of ^{138}La. The spectrum in the inset figure was taken over 12 hr. with a thicker source and lower amplifier gain to show the end point more clearly.

§ 5. Coincidence Experiments

The La$_2$O$_3$ source was placed between the two crystals. The output pulses from one photomultiplier, after amplification, were passed through pulse lengthener and brightener circuits and viewed on a cathode ray tube as a spectrum of bright spots in the X-direction. The pulses from the other multiplier were amplified and lengthened, and then applied in the Y-direction, so that a coincidence appeared as a bright spot whose displacement from the X and Y-axes was proportional to the energy spent in each crystal. The resulting pattern was filmed as a series of ten minute exposures and analysed.

For the investigation of possible coincidences between the 0·81 and 1·44 MeV γ-rays, only coincidences in which an energy $>0{\cdot}65$ MeV was spent in both crystals were considered. The total coincidence rates for source + background and background respectively were 106 ± 10 and 96 ± 10 coincidences per 6 hours. From a knowledge of the geometry and the γ-ray counting rates in each crystal, a coincidence rate greater than twice the background rate would have been expected. Hence these two γ-rays cannot be in coincidence. Examination of the energy region 0·35–0·65 MeV gave no evidence of coincidences between annihilation quanta, indicating that β^+-emission, if it occurs, must be of very low intensity, certainly $<1\%$, compared with electron capture.

Fig. 3

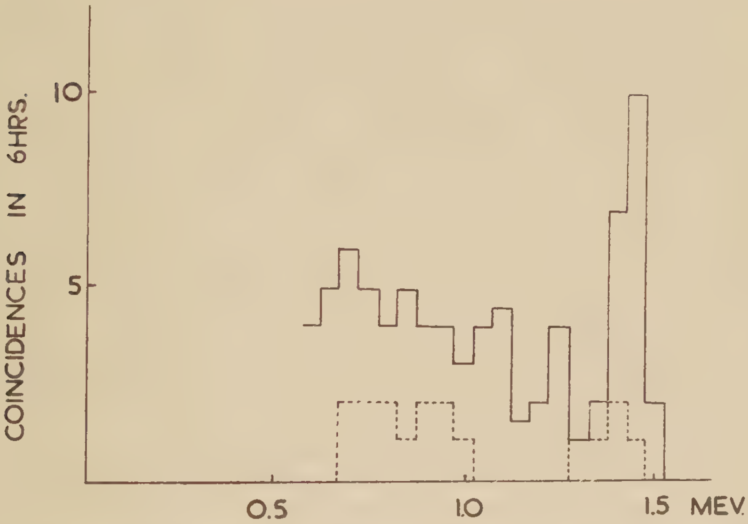

Spectrum of pulses in coincidence with barium K x-rays. The dotted histogram represents the coincidence background.

In the K–γ coincidence experiment a lead absorber, 3 mm thick, was placed between the γ-ray counter and the source to prevent any iodine escape x-rays being observed in the crystal which detected the x-rays since the energy of such x-rays is close to that of barium K x-rays. The spectrum of pulses in coincidence with the barium K x-rays (fig. 3) clearly shows that only the 1·44 MeV γ-ray follows K-capture. The number of coincidences under the 1·44 MeV peak alone is 21 in 6 hr., compared with a background of 4.

To investigate β–γ coincidences, a relatively thin source would be required to permit detection of the β-rays. Because of the very restricted source area available in such an experiment, it was not considered to be feasible.

The decay scheme proposed on the basis of these experiments is shown in fig. 4.

§ 6. Decay Constants

Since the 1·44 MeV γ-ray follows electron capture, the specific activity of this branch can be simply determined by comparison with the ^{40}K 1·46 MeV γ-ray. Using the 2 in. NaI crystal, spectra were taken with sources of La_2O_3 and KCl under identical geometrical conditions. The detection efficiency of the crystal was assumed to be the same for each γ-ray. By measuring the total counts under the ^{138}La 1·44 MeV and ^{40}K peaks, knowing the mass of each source, and using a value of 3·47 gammas/sec/g K for the specific activity of potassium (mean value of the results of Backenstoss and Goebel, 1955, and McNair *et al.* 1956), the specific activity of the electron capture branch was found to be 30·9±1·2 disintegrations/min/g La. Since the abundance of ^{138}La is 0·089% (Inghram *et al.* 1947) the electron capture partial half-life is $(1{\cdot}64\pm0{\cdot}06)\times10^{11}$ yr. This result is in agreement with that of 2×10^{11} yr. determined by Pringle *et al.* (1951), but not with the value of 4×10^{13} yr. estimated by Selig (1954) from the observation of BaK x-rays using a proportional counter.

Fig. 4

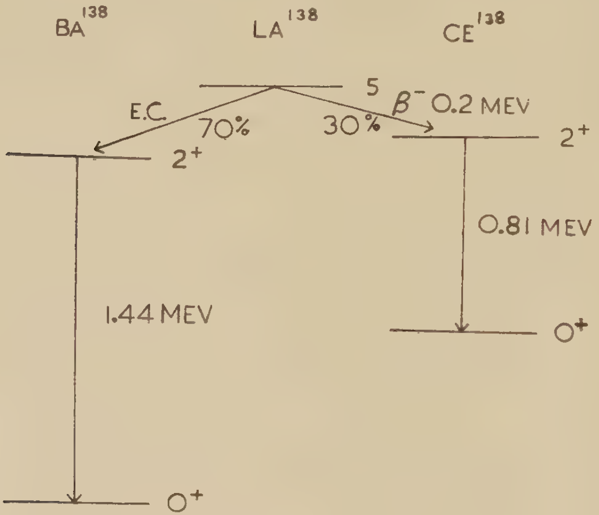

Proposed decay scheme of ^{138}La.

By comparison with the ^{40}K γ-ray spectrum extrapolated to zero energy the counts in the Compton distribution of the ^{138}La 1·44 MeV γ-ray were estimated. Hence, knowing the total counts N_1, N_2 due to the 1·44 and 0·81 MeV γ-rays respectively the partial half-life of the γ branch can be deduced from the formula :

$$t_\beta=\frac{N_1}{N_2}\cdot\frac{1-\exp(-\mu_2 m)}{1-\exp(-\mu_1 m)}t$$

where t_β and t_K are the partial half-lives of the β and K-capture branches and μ_1, μ_2 the total mass absorption coefficients for the 1·44 and 0·81 MeV

γ-rays respectively: m is the average thickness in g/cm^2 of the NaI crystal. The partial half-life thus deduced was $(3{\cdot}5 \pm 0{\cdot}3) \times 10^{11}$ yr., the corresponding specific activity being $(14{\cdot}6 \pm 1{\cdot}2)$ disintegrations/min/g La.

Using the thinner source in the proportional counter, the β-rays with energy >4 kev were counted. By subtracting the BaK x-rays detected following electron capture, extrapolating the β counting rate to zero energy, and correcting for self-absorption and backscattering (45%) (McNair *et al.* 1956), a specific activity of $(12{\cdot}4 \pm 2{\cdot}1)$ betas/min/g La was obtained. The large probable error is mainly due to poor statistics since the observed counting rate from the source was only 2·5 c.p.m. compared with a background of 29·7 c.p.m. The partial half-life is $(4{\cdot}1 \pm 0{\cdot}7) \times 10^{11}$ yr. The specific activity is perhaps slightly lower than that found by the previous method. The suggested spectrum shape would provide a simple explanation, since even the thinner source would absorb an appreciable fraction of those β-rays with very low energy.

From these results, using the mean of the two values for the activity of the β branch, it is concluded that approximately 70% of the disintegrations proceed by electron capture to ^{138}Ba and 30% by β-decay to ^{138}Ce.

§ 7. DISCUSSION

The spin of the ground state of ^{138}La has been reported to be 5 (Sogo and Jeffries 1955). The shell model predicts $(d_{3/2}, g_{7/2})$ configuration and hence even parity. Since the spin of the first excited state of an even–even nucleus is almost invariably 2+ (Scharff-Goldhaber 1953), both the electron capture and β-transitions might be expected to be $\Delta I = 3$, no i.e. unique 2nd forbidden. However, the experimental log ft value for the β-decay is 19·0, corresponding to a 3rd forbidden transition, not 2nd forbidden. Goeppert-Mayer (1955) has pointed out that the odd parity of the ground states of $^{122}_{51}\mathrm{Sb}_{71}$ and $^{124}_{53}\mathrm{I}_{71}$ indicates that the $h_{11/2}$ level can be occupied by an odd number of neutrons in the ground states of odd–odd nuclei. Hence in ^{138}La it is possible that the last odd neutron is in an $h_{11/2}$ level instead of $d_{3/2}$. The parity would then be odd, and a 3rd forbidden $\Delta I = 3$, yes transition would result. Confirmation that the La β-spectrum has the same shape as that of ^{87}Rb would support this suggestion, since ^{87}Rb is the only known $\Delta I = 3$, yes transition.

Since there are several excited states of ^{138}Ba $<$ 2·5 MEV above ground (Thulin 1955), the presence of only the 1·44 MEV β-ray following electron capture indicates that β^+-emission to the first excited state of ^{138}Ba is energetically impossible. Decay to the ground state is obviously highly forbidden because of the large spin change $(\Delta I = 5)$ involved. The inability to detect annihilation quanta experimentally is thus easily understood. Similarly decay to the ground state of ^{138}Ce $(\Delta I = 5)$ with the emission of a 1·0 MEV β-ray is forbidden relative to the excited state. The absence of a 1·0 MEV β-ray (at a conservative estimate its intensity cannot be $>5\%$ of the 0·2 MEV β-ray) is thus not unexpected.

Following the β^--decay of ^{138}Cs, Langer *et al.* (1953) and Thulin (1955) have detected a 1·44 MeV γ-ray, which on the basis of the systematics of Scharff-Goldhaber (1953) was considered to be a transition from the first excited state of ^{138}Ba to the ground state. The present investigation supplies independent confirmation of this view. A 0·80 MeV γ-ray was observed by Handley and Olson (1954) following β^+-decay of ^{138}Pr to ^{138}Ce. Thus the decay scheme proposed is in complete agreement with the most recent experimental data.

ACKNOWLEDGMENTS

We are indebted to Dr. S. C. Curran for suggesting this investigation and to Dr. G. M. Lewis for helpful discussions throughout its prosecution. We would also like to thank Professor P. I. Dee for his interest and encouragement. We are deeply grateful to Dr. W. Turchinetz of the University of Manitoba, Canada, for the loan of the extremely pure sample of lanthanum oxide, without which this investigation could not have been brought to a successful conclusion. One of us (R.N.G.) acknowledges the receipt of a financial grant from the Department of Scientific and Industrial Research ; the other (D.E.W.) of a Strang–Steele Scholarship.

Note added in proof.—Turchinetz and Pringle (August 1956, *Phys. Rev.*, **103,** 1000) have re-examined the γ-ray spectrum of ^{138}La and undertaken coincidence studies. Their results and those of the present investigation are in good agreement.

REFERENCES

BACKENSTOSS, G., and GOEBEL, K., 1955, *Z. Naturforsch.*, **10*a*,** 920.
CURRAN, S. C., DIXON, D., and WILSON, H. W., 1952, *Phil. Mag.*, **43,** 82.
DIXON, D., and MCNAIR, A., 1954, *Phil. Mag.*, **45,** 1099.
GOEPPERT-MAYER, M., 1955, *Classifications of β-transitions* (Siegbahn : β and γ-ray spectroscopy, Chap. 16).
HANDLEY, T. H., and OLSON, E. L., 1954, *Phys. Rev.*, **96,** 1003.
INGHRAM, M. G., HAYDEN, R. J., and HESS, D. C., 1947, *Phys. Rev.*, **72,** 167.
LANGER, L. M., DUFFIELD, R. B., and STANLEY, C. W., 1953, *Phys. Rev.*, **89,** 907.
LEWIS, G. M., 1952, *Phil. Mag.*, **43,** 1070.
MCNAIR, A., GLOVER, R. N., and WILSON, H. W., 1956, *Phil. Mag.*, **1,** 199.
MULHOLLAND, G. I., and KOHMAN, T. P., 1952, *Phys. Rev.*, **87,** 681.
PRINGLE, R. W., STANDIL, S., and ROULSTON, K. I., 1950, *Phys. Rev.*, **78,** 303.
PRINGLE, R. W., STANDIL, S., TAYLOR, H. W., and FRYER, G., 1951, *Phys. Rev.*, **84,** 1066.
SCHARFF-GOLDHABER, G., 1953, *Phys. Rev.*, **90,** 587.
SELIG, H., 1954, *Thesis*, Carnegie Inst. Tech.
SOGO, P. B., and JEFFRIES, C. D., 1955, *Phys. Rev.*, **99,** 613.
THULIN, S., 1955, *Ark. Fys.*, **9,** 183.

Isotopic Spin Selection Rules
IX : The 9·58 Mev State of ^{16}O†

By S. D. Bloom‡, B. J. Toppel§ and D. H. Wilkinson||
Brookhaven National Laboratory, Upton, New York

[Received October 20, 1956]

Abstract

The reaction ^{12}C$(\alpha, \gamma)^{16}$O through the 1 — state of ^{16}O at 9·58 mev is detected and the radiative width measured as 6 mev. This corresponds to $|M|^2=1\times10^{-5}$ in Weisskopf units or to a contamination of the predominantly $T=0$ state with $T=1$ or the ground state with $T=1$ of $\alpha_0{}^2(1)\sim3\times10^{-4}$. Alternatively if the transition is ascribed to a mixing-in by the Coulomb perturbation of the $T=1$ state at 13·09 mev we find $H^{\mathrm{C}}\sim0{\cdot}035$ mev.

§ 1. Introduction

In a recent paper (VII of this series ; Wilkinson 1956 a) a survey was presented of the situation as regards isotopic spin impurity in ^{16}O. It is therefore interesting to investigate any other level of ^{16}O to see how it fits into that general empirical picture, especially if it is a level for which a particular model may make an assignment. This is possible for the broad 1 — $T=0$ state at 9·58 mev (Hill 1953) whose E1 transition to the ground state is forbidden by the isotopic spin selection rule. This state is not included in the recent rather successful account given of certain low-lying odd parity states of ^{16}O by the shell-model (Elliott 1956) in terms of single-particle excitation from the 1p-shell to the mixed 1d–2s shells and so is presumably described as a state of 3-particle excitation. In this case we might expect its combination with the ground state to be rather weaker than one should have anticipated on general grounds or on the grounds of the systematics of VII. This is because the transition must proceed via the mixing into the 3-particle $T=0$ state of some 1-particle $T=1$ state and this is expected to be rather feeble. If on the

---

† Communicated by the Authors. Work performed under the auspices of the U.S. Atomic Energy Commission.

‡ Present address : Cavendish Laboratory, Cambridge, England.

§ Present address : Argonne National Laboratory, Lemont, Illinois, U.S.A.

|| Permanent address : Cavendish Laboratory, Cambridge, England. This work was performed while this author was Visiting Physicist at Brookhaven National Laboratory during the summer of 1956.

other hand the 9·58 MeV state in fact contains a fair proportion of a 1-particle $T=0$ state the isotopic spin mixing will be easier and the E1 transition not so inhibited.

For these reasons the present state is one of particular interest to investigate.

§ 2. EXPERIMENTAL DETAILS AND RESULTS

The only feasible way to detect this transition is by the reaction $^{12}C(\alpha, \gamma)^{16}O$ which should show the broad ($\Gamma_\alpha=860$ keV) resonance observed in the scattering at an alpha-particle energy of 3·24 MeV. Unhappily this investigation is rendered difficult by several sources of background radiation, the most important being the neutrons formed in the reaction $^{13}C(\alpha, n)^{16}O$. The yield of gamma-rays is so small that a simple NaI(Tl) detector is demanded and this is sensitive directly and indirectly to these background neutrons. Because of this the present investigation was carried out using a target of electro-magnetically separated ^{12}C of thickness 450 $\mu g/cm^2$ on a silver backing †. During the course of the experiment natural carbon built up in the usual way on the target until finally it became useless owing to its large neutron yield.

The experimental procedure was to run alternately at alpha-particle energies of 3·00 and 3·45 MeV. Between these energies the greater part of the gamma-ray yield is obtained (the target thickness is also approximately equivalent to this energy range though this is accidental). The pulse height distribution from a 2 in. right cylinder of NaI(Tl) placed close in to the target at 90° to the bombarding alpha-particle beam of about 20 μA from the Brookhaven Research Van de Graaff was recorded on a 20 channel kicksorter. Much of the background present at 3·45 MeV is also present at 3·00 MeV so a subtraction of the two distributions is a first approach to the gamma-ray spectrum. The carbon build-up took place sufficiently slowly and steadily to permit the averaging of a large number of interlaced runs to obtain this subtracted distribution. This subtracted distribution consists of two parts: firstly the desired gamma-ray spectrum, secondly the difference between the background distributions at the two bombarding energies. In fact the raw subtracted distribution shows clearly the high-energy portion of the gamma-ray distribution but to estimate the (small) contribution to it due to this residual difference in backgrounds we made the very reasonable assumption that the *form* of the difference of the backgrounds was the same as that of the background measured at the lower alpha-particle energy. This form was then fitted to the observed difference distribution in the region of small pulse heights and the further subtraction made to reveal the distribution due to the gamma-rays alone. This final distribution is shown in the figure. The standard deviations shown are purely statistical.

We have shown in the dashed line the expected shape and position of the pulse distribution from a gamma-ray of 9·58 MeV. It is seen that there is good agreement in respect of both shape and position between the experimental distribution and that to be expected. It seems then that radiative capture indeed takes place.

---

† Obtained from A.E.R.E., Harwell, England.

Owing to the extremely feeble nature of the capture and the considerable background difficulties it was impossible to investigate in detail the expected $\sin^2\theta$ angular distribution. Runs made at 0° to the alpha-particle beam however also showed the 9·58 MeV radiation in diminished quantity consistent with such an angular distribution and the very bad geometry that had to be employed.

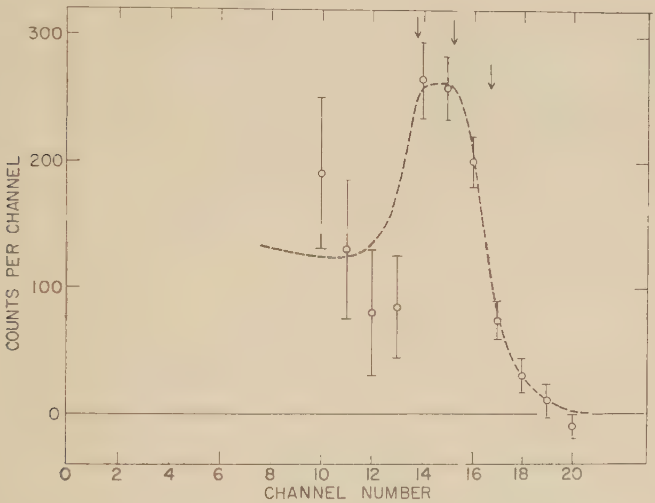

Spectrum, seen in a 2 in. × 2 in. NaI(Tl) crystal of the 9·58 MeV gamma-rays from the reaction $^{12}C(\alpha, \gamma)^{16}O$. The dashed line gives the expected distribution for a gamma-ray of this energy. This spectrum is obtained by a subtraction procedure described in the text. The three arrows show the expected positions of the two, one- and no-annihilation quantum escape peaks.

§ 3. The Radiative Width

From the results displayed in the figure we evaluate a radiative width of 6 MeV for this transition. This figure is probably accurate to a factor of two or better. This width expressed in Weisskopf units for an E1 transition is $|M|^2=1\times10^{-5}$ which may be compared with the most probable value for this quantity for uninhibited E1 transitions in the light elements (Wilkinson 1956 b) of $|M|^2=0{\cdot}032$. If we express our experimental result in the usual way, in terms of the admixture by intensity of $T=1$ state into our predominantly $T=0$ state, and the $T=1$ contamination of the $T=0$ ground state, we should therefore say $\alpha_0^2(1)\sim3\times10^{-4}$. This figure may be compared with the general behaviour in ^{16}O at this region of excitation (Wilkinson 1956 a) from which we should have expected $\alpha^2\sim10^{-3}$ to 10^{-2}. It may therefore seem that this isotopic spin forbidden transition is a little weaker than we might have anticipated *a priori* but certainly not by a big factor.

We may discuss the result in another way. At 13·09 MeV there is a $1-T=1$ state which shows a very strong E1 transition to the ground state of ^{16}O (see Ajzenberg and Lauritsen 1955 for discussion) with $|M|^2=0{\cdot}10$. This is certainly the closest $1-T=1$ state known to our $1-T=0$ state at 9·58 MeV so it is reasonable to suppose that the transition observed in the present work is that from the 13·09 MeV level which takes place by virtue of the mixing of these states by the Coulomb perturbation †. We may now ask for the magnitude of the required matrix element of the Coulomb perturbation between these states. It is $H^C \sim 0{\cdot}035$ MeV. This value is not unusually small and argues, as does the not-particularly-small value of $\alpha_0^2(1)$ obtained by the usual method, that this $1-$ state at 9·58 MeV must contain as a fair proportion (several per cent) of its make-up a description in terms of one-particle excitation from the ground state of ^{16}O. Alternatively, of course, it may be the description of the ground state of ^{16}O as entirely a closed-shell that is defective; an admixture of, say $1p^{-2}$ (2s, 1d)^2 would also enable this transition to take place from a 9·58 MeV state of the predominant description p^{-3} (2s, 1d)^3.

Acknowledgment

We should like to thank Mr. A. G. Rubin who helped with the taking of these measurements.

References

Ajzenberg, F., and Lauritsen, T., 1955, *Rev. Mod. Phys.*, **27,** 77.
Elliott, J. P., 1956 (private communication).
Hill, R. W., 1953, *Phys. Rev.*, **90,** 845.
Wilkinson, D. H., 1956 a, *Phil. Mag.*, **1,** 379; 1956 b, *Phil. Mag.*, **1,** 127.

---

† Note however, that the reciprocal mixing of the 9·58 MeV state $T=0$ into that at 13·09 MeV is not enough to explain the emission of alpha-particles from the latter state because, although the reduced alpha-particle width of the $T=0$ state is roughly a single-particle width the admixture of the $T=1$ into the $T=0$ needed to account for the gamma-ray transition of the latter is only about 1/100% whereas the reduced alpha-particle width of the $T=1$ state is about 5% of the single-particle width.

Isotopic Spin Selection Rules
X : The 7·18 MeV State of ^{20}Ne †

By B. J. Toppel ‡, S. D. Bloom § and D. H. Wilkinson ||
Brookhaven National Laboratory, Upton, New York

[Received October 20, 1956]

Abstract

The possible E1 transition between the 3− state at 7·18 mev and the 2+ state at 1·63 mev in ^{20}Ne is forbidden by the isotopic spin rule. It has been sought using the reaction $^{16}O(\alpha, \gamma)^{20}Ne$ and it has been shown that the radiative width is less than 6 mev. This corresponds to $| M |^2 \leqslant 4{\cdot}3 \times 10^{-5}$ in Weisskopf units or to contaminations $\alpha_0{}^2(1) \leqslant 1{\cdot}3 \times 10^{-3}$ of the 7·18 and 1·63 mev states with $T=1$ states.

§ 1. Introduction

This brief note continues the series of reports in which we study the inhibition imposed on E1 transitions in self-conjugate nuclei when the isotopic spin does not change. By the elastic scattering of alpha-particles in ^{16}O there was established (Cameron 1953) a 3− state in ^{20}Ne at 7·18 mev. Since the (unidentified) first $T=1$ state of ^{20}Ne is expected at about 10·2 mev this 3− state is certainly of $T=0$. Its possible E1 transition to the 2+ state at 1·63 mev is therefore forbidden by the isotopic spin selection rule. The present investigation is a search for this forbidden transition.

§ 2. Experimental Method and Results

The method used in this investigation followed closely that used to detect the reaction $^{12}C(\alpha, \gamma)^{16}O$ and described in the preceding paper of this series (Bloom, Toppel and Wilkinson 1957). In the present reaction the resonance is narrow ($\Gamma_\alpha = 10$ kev) and is found at an alpha-particle energy of 3·05 mev. The bracketing alpha-particle energies were chosen as 3·00 and 3·10 mev and the same subtraction procedure as used in the earlier work was employed to reduce the pulse spectra from the 2 in. × 2 in. NaI(Tl) crystal. The target was of heavily oxidized copper and it was

---

† Communicated by the Authors. Work performed under the auspices of the U.S. Atomic Energy Commission.

‡ Present address : Argonne National Laboratory, Lemont, Illinois, U.S.A.

§ Present address : Cavendish Laboratory, Cambridge, England.

|| Permanent address : Cavendish Laboratory, Cambridge, England. This work was performed while this author was Visiting Physicist at Brookhaven National Laboratory during the summer of 1956.

bombarded with 20 μA beams of alpha-particles from the Brookhaven Research Van de Graaff in a long series of alternating runs at the two energies. The angle of observation was 90° to the alpha-particle beam.

As expected considerable trouble was experienced from the build-up of carbon on the target and the accompanying neutron background from the reaction $^{13}C(\alpha, n)^{16}O$. This trouble was relatively more serious in the present investigation than in the previous one because the energy of the gamma-ray sought is here lower (5·55 MeV as against 9·58 MeV previously) and the pulses from the background radiations increase in abundance rapidly towards lower energies. No 5·55 MeV radiation was detected with certainty and the corresponding limit on the radiative width is 6 MeV.

This figure gives $|M|^2 \leqslant 4{\cdot}3 \times 10^{-5}$ in Weisskopf units. Expressing the contaminations of the 7·18 and 1·63 MeV states through the most probable value for uninhibited transitions namely $|M|^2 = 0{\cdot}032$ (Wilkinson 1956) we find $\alpha^2 \leqslant 1{\cdot}3 \times 10^{-3}$. This is quite a low value but is not startling.

As yet no 3— $T=1$ states are identified in ^{20}Ne. But the density of states of low excitation in ^{20}F is unusually great (see Ajzenberg and Lauritsen 1955). It is then reasonable to suppose that one or more states of 3— will exist within the first 4 MeV of excitation above the first excited state in that nucleus (the ground state is of even parity) since that region contains more than 20 states. This gives us $H^c < 0{\cdot}13–0{\cdot}27$ MeV for contamination of the 7·18 MeV state from the corresponding states in ^{20}Ne.

ACKNOWLEDGMENT

We should like to thank Mr. A. G. Rubin for helping with the taking of the measurements.

REFERENCES

AJZENBERG, F., and T. LAURITSEN, 1955, *Rev. Mod. Phys.*, **27**, 77.
BLOOM, S. D., TOPPEL, B. J., and WILKINSON, D. H., 1957, *Phil. Mag.*, **2**, 57.
CAMERON, J. R., 1953, *Phys. Rev.*, **90**, 839.
WILKINSON, D. H., 1956, *Phil. Mag.*, **1**, 127.

Isotopic Spin Selection Rules
XI : The 8·06 and 6·23 MeV States of ^{14}N †

By D. H. Wilkinson ‡ and S. D. Bloom §
Brookhaven National Laboratory, Upton, New York

[Received October 20, 1956]

Abstract

The decay scheme of the 8·06 Mev $1-T=1$ level of ^{14}N is reinvestigated using the reaction ^{13}C(p, γ)^{14}N at the 550 kev resonance. The relative strength of the isotopic spin forbidden transition to the first excited state is 0·022 corresponding to $\alpha_1{}^2(0)_{8\cdot06}\sim0\cdot061$. Owing to the great strength to it of the transition from the 8·62 Mev 0+ state it seems that the 6·23 Mev $T=0$ state must be 1−. The decay of this state has been determined ; it has been reached by this E1 transition from the 1·16 Mev resonance. The strength of the isotopic spin forbidden transition to the ground relative to the allowed transition to the first excited state is 0·31 corresponding to $\alpha_0{}^2(1)_{6\cdot23}\sim0\cdot078$. The closeness of these two isotopic spin impurities suggests that these two states may be each other's chief contaminators and in this sense the forbidden transitions from the one is the same radiation as the allowed transition from the other and vice versa. If this suggestion is correct $H^C\sim0\cdot45$ Mev which large value suggests some close relationship between the two states. In unravelling the decay schemes subsidiary pieces of information are obtained ; in particular it seems that the 5·69 Mev state is very probably 1+.

§ 1. Introduction

It has been recognized for some time that the 1− state of ^{14}N at 8·06 Mev is chiefly of $T=1$ (see Ajzenberg and Lauritsen 1955 for general references) on account of its width of 10 ev for radiation to the ground state ($|M|^2=0\cdot03$ in Weisskopf units). It was pointed out in an earlier paper of this series (Clegg and Wilkinson 1953) that in this case the possible E1 transition to the 0+ $T=1$ state at 2·31 Mev is forbidden by the isotopic spin selection rule and should be weak. It was shown in that paper that the forbidden transition was indeed much weaker than the ground state transition although the limit there set appears to be somewhat too sharp ;

---

† Communicated by the Authors. Work performed under the auspices of the U.S. Atomic Energy Commission.

‡ Permanent address : Cavendish Laboratory, Cambridge, England. This work was performed while this author was Visiting Physicist at Brookhaven National Laboratory during the summer of 1956.

§ Present address : Cavendish Laboratory, Cambridge, England.

the 8·06 MeV state is in fact quite strongly contaminated with $T=0$. In this paper we make a more detailed examination of these transitions for the reason that we shall now explain.

It has appeared (see Wilkinson and Clegg 1956, Wilkinson 1956 a) that those states such as the 6·89 MeV state of ^{10}B, the 12·95 and 13·05 MeV states of ^{16}O and the presently discussed state of ^{14}N, all of which are states with a very large 2s- or 1d-wave reduced width for a unique parent in the $A-1$ nucleus, are unusually impure from the point of view of isotopic spin. It is then an interesting question where this contamination comes from: does it come from a great number of states of the other isotopic spin, each of which is only lightly contaminated in return by the state in question or does it come from a single state which will therefore be heavily and equally contaminated? In particular may it not be that the state of the other isotopic spin but of the same spin and parity similarly formed by adding a 'loose' 2s- or 1d-nucleon to the same unique $A-1$ parent is the strongly contaminating and contaminated partner? Since these states would be very similar such mixing might be thought to be strong. Within the simple framework of the unique parent and well-defined loose nucleon it seems however that this is not so theoretically (J. P. Elliott and F. C. Barker, private communication). Nevertheless the empirical indication is growing rather strong and the present investigation was carried out because there seemed to be, in ^{14}N, the possibility of identifying such a pair of mutually and strongly contaminating states. Although the work now to be reported does no more than to make this possibility quantitative rather than qualitative and cannot be said to establish the reciprocal relationship, it seems to be suggestive enough to encourage rather strongly further experimental and theoretical investigations.

We seek therefore in ^{14}N another 1− state, chiefly $T=0$, which might be responsible for contaminating the 8·06 MeV state with $T=0$ and which would thereby itself become contaminated with $T=1$. If these two states were indeed each the most important contaminator of the other we would find the amount of $T=1$ introduced into the $T=0$ equal to the amount of $T=0$ introduced into the $T=1$. This would of course be only a minimum requirement for establishing the relationship.

The experimental clue that starts the present work is that the state at 8·62 MeV which seems to be well established as 0+ from ^{13}C(p, p)^{13}C shows a strong radiative transition to the state at 6·23 MeV. If we combine earlier work (Seagrave 1952) on the gamma-ray yield with the decay scheme established here we find that this transition has a radiative width $\Gamma_\gamma - 2·1$ eV which corresponds to a strength $|M|^2=0·24$ in Weisskopf E1 units. So great a strength makes it virtually certain that the transition is indeed E1 (Wilkinson 1956). If the transition were M1 it would have $|M|^2=7·3$, which is much bigger than any known M1 transition and seems most unreasonably large. This then fixes the 6·23 MeV state as 1−. It also is presumably $T=0$ since ^{14}C has no known states between the ground state and the probable 1− state at 6·09 Mev which probably corresponds to the 8·06 Mev state here discussed in ^{14}N. If there were indeed another ^{14}C state between these two we should expect it to be most probably of even parity. The 8·62 Mev state must now be $T=1$ and there seems nothing against this. The present arguments then make the 6·23 Mev state 1− $T=0$ and the question of its radiative decay modes then arises. If it were a well-behaved $T=0$ state it would decay exclusively to the 0+ $T=1$ state at 2·31 Mev and not at all to the 1+ $T=0$ ground state of ^{14}N. In the published literature its behaviour is described as quite otherwise : it reputedly decays only to the ground state. However, at this point we may touch upon an earlier experimental confusion. The expected transitions between the 6·23 and 2·31 Mev states would have an energy of 3·92 Mev which is very close to the energy of the second excited state namely 3·95 Mev. Because of this there has been a tendency to ascribe gamma-rays of about this energy to ground-state transitions from the second excited state. But it is now known (Gove, *et al.* 1956) that this ground-state transition takes place in only about 4% strength and that de-excitation proceeds with 96% probability in the cascade through the first excited state. This requires a re-evaluation of the earlier work and, in the present instance, implies that the expected isotopic spin allowed transition from the 6·23 Mev state may take place, the gamma-ray having been wrongly assigned to the negligibly strong transition to ground from the 3·95 Mev state. Nevertheless, the reported ground-state transition of the 6·23 Mev state is strong and suggests that the contamination of the state with $T=1$ may be considerable and so that this may itself be the contaminating state of that at 8·06 Mev †.

We have therefore carried out an investigation of the decay modes of the 8·06 and 6·23 Mev states in ^{14}N, reaching the former directly through ^{13}C(p, γ)^{14}N at a proton bombarding energy of 550 kev and the latter indirectly by the gamma-ray transition to it from the 8·62 Mev state of ^{14}N, itself formed in the same reaction at a proton bombarding energy of 1·16 Mev. This latter, narrow level sits up on a broad resonance centred on a proton energy of 1·25 Mev which we must therefore also investigate to a certain degree.

§ 2. EXPERIMENTAL METHODS

We have used a target of ^{13}C, 71% enriched, cracked onto gold of thickness 0·004 inches. The thickness of the target was not determined with accuracy but it was about 3 kev for protons of 550 kev and so about 2 kev for protons of 1·16 Mev. The target was soldered onto a water-cooled brass plate and bombarded with proton currents that were generally 5–10 μA and occasionally as high as 20 μA from the Brookhaven Research Van de Graaff.

---

† This suggestion has been made by Dr. A. B. Clegg in a letter to one of us (D.H.W.) following that author's remark that the transition from the 8·62 Mev level appeared to be very probably E1.

The gamma-rays were detected in NaI(Tl) crystals. That used for most of the work as the centre crystal of a three-crystal pair spectrometer and otherwise as the display crystal in the coincidence arrangements was a cylinder of length 5 cm and diameter 4 cm. It had a resolution of 8·8% for the 662 kev gamma-rays following the decay of ^{137}Cs when mounted on a Du Mont 6292 photo-multiplier. The other crystals used in the various types of coincidence arrangement were also cylinders of about $1\frac{1}{2}$ in. dimensions.

§ 3. The 8·06 Mev State of ^{14}N

The resonance at 550 kev proton energy has been observed many times and we will not dwell on our own observations that preceded the investigation of the spectrum except to say that we found nothing different from the constants of the published literature. The width of the resonance as measured with our target of thickness 3 kev was 35 kev as against the 32·5±1 kev of the literature.

Fig. 1

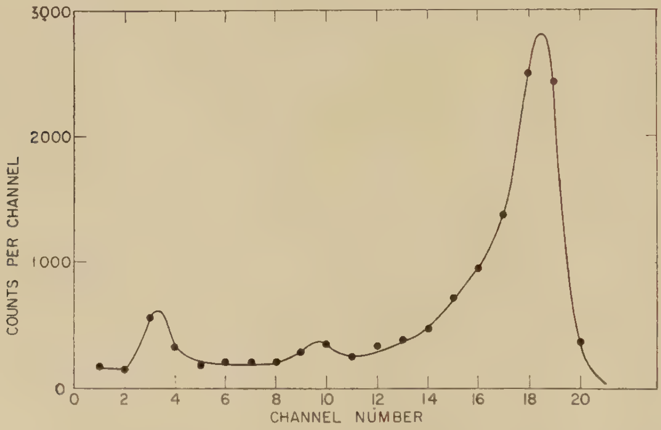

Three-crystal pair spectrum of the gamma-rays from a thin target of ^{13}C bombarded by protons of 550 kev. The peak at channel $18\frac{1}{2}$ is due to the 8·06 Mev ground-state transition. The peak at channel 3 is due to the transition from the 8·06 Mev state to that at 3·95 Mev; its measured energy is 4·14±0·09 Mev. The peak at channel 10 is due to a superposition of the transitions between the 8·06 and 2·31 Mev levels and that to the ground state from the 5·69 Mev level. 6·14 Mev gamma-rays from fluorine impurity would have given a peak at channel 11. The measured energy of the composite peak at channel 10 is 5·77±0·05 Mev. This spectrum was taken with a bias of 9 channels.

To begin with, observations were made at the peak of the resonance. Here the spectrum of gamma-rays was investigated using a three-crystal pair spectrometer. The results of a typical run, of which there were several, are shown in fig. 1. As was to be expected, the strongest gamma-ray is the ground-state transition of energy 8·06 MeV †. This energy was checked roughly using the 4·43 MeV gamma-ray from the first excited state of ^{12}C as a standard. For this purpose a Po–Be source was used. Also clearly seen is the expected gamma-ray from the transition between the 8·06 and 3·95 MeV states. Its energy measured in terms of that of the 8·06 MeV line is 4·14±0·09 MeV. Its intensity relative to that of the ground-state transition we find to be 12%, which agrees with the 12% of the literature. We also see a distinct radiation at an energy which is measured as 5·77±0·05 MeV in terms of the 8·06 and 4·11 MeV lines. This is consistent with the expected 5·75 MeV of the istotopic spin forbidden line. Its abundance relative to the 8·06 MeV radiation we find to be 4·8%.

Whenever radiation of about this energy is sought it is found. It usually comes from the second excited state of ^{16}O formed so prolifically in the reaction ^{19}F(p, α)^{16}O at an energy of 6·14 MeV. The energy measurement is accurate enough to eliminate this possibility here; the ^{16}O gamma-ray would have given a peak a full channel higher. Great care had been taken in preparing the target tube and target chamber for this experiment to eliminate fluorine by making everything from fresh materials. As is well known, however, this precaution fails for at least one important material, namely tantalum, which is always found to have a thin film of fluorine on its surface and from which many regulating slits, defining apertures and so on of the present target assembly were made. All such surfaces were accordingly ground to remove the fluorine and there resulted a very fluorine free arrangement which gave no trouble at this resonance or at the higher one.

This 4·8% of 5·7 MeV radiation cannot be immediately held to be due entirely to the isotopic spin-forbidden transition because there exists a state in ^{14}N at 5·69 MeV which has a known transition to the ground state and so a possible transition from the 8·06 MeV state to this one could lead to radiation of virtually the same energy as the forbidden transition. There is also a state at 5·83 MeV which has a ground-state transition which could be superposed in the present radiation. It is however unlikely that this state is strongly involved because its chief decay mode is by a gamma-ray of 725 kev to the state at 5·10 MeV which then decays predominantly to the ground state. In this event we should see this 5·10 MeV gamma-ray in greater strength than the contribution of the 5·83 MeV line to the radiation near 5·7 MeV. The fact that no such 5·10 MeV line is manifest (see fig. 1) shows that transitions to the 5·83 MeV state are a much weaker contributor to the 5·7 MeV radiation than others, whatever they may be. Also the 725 kev radiation was sought and was certainly not present in any strength corresponding to more than a very small share of the 5·7 Mev radiation. So we must attempt to separate the relative responsibilities of the two possible transitions in giving the 5·7 Mev line.

---

† This line appears unusually broad in this figure because no collimator could be used with the three-crystal spectrometer on account of the feebleness of the source. As a result the resolution suffers owing to loss of bremsstrahlung and other effects.

It is clear that this separation cannot be made by a direct energy measurement using present techniques. It is also clear that to measure the energy of the gamma-ray in coincidence with the 5·7 Mev radiation will not effect a solution either. There does, however, exist one possibility of separating the two possible contributing transitions. This is to take advantage of the fact that the 550 kev resonance is apparently rather well isolated. The next known resonance is that at 1·16 Mev.

Fig. 2

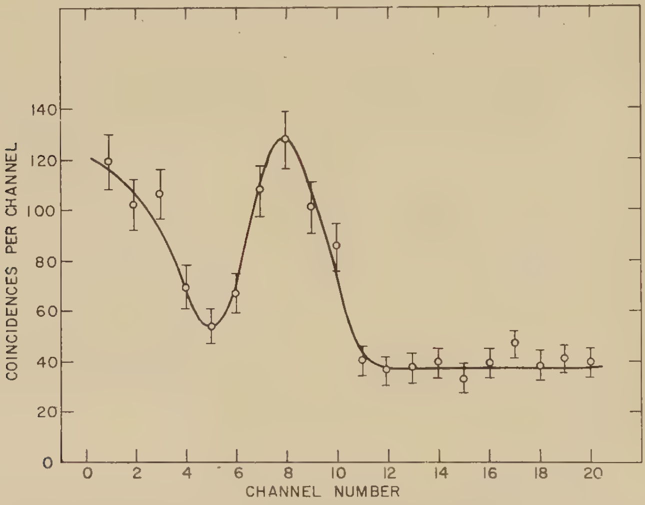

Spectrum of gamma-rays at a proton energy of 550 kev, seen in coincidence with gamma-rays of greater than 4·5 Mev. The peak is due to a superposition of the ground-state transition from the 2·31 Mev level and that between the 8·06 and 5·69 Mev levels. Its measured energy is 2·30 ± 0·05 Mev. This spectrum was taken with a bias of 42 channels.

Initially, at any rate, the yield from proton energies just above the 550 kev resonance is consistent with that to be expected from its own high energy tail. For example, at a proton energy of 700 kev the cross section has fallen to 0·05 of its peak value. The simple dispersion formula with s-wave proton penetrabilities predicts a figure of about 0·08 and so the greater part of the yield may be taken as still due to the 8·06 Mev level. If, then, we investigate the radiations at such a high proton bombarding energy we shall be observing the same state but the two possible components of the 5·7 Mev radiation which were confused on the resonance will now be slightly separated: the isotopic spin-forbidden transition will have an energy increased by about 140 kev while that of the alternative gamma-ray will be unchanged. A more sensitive change is that in the energy of the cascade partner which remains at 2·31 Mev for the forbidden transition but is increased by about 140 kev for the alternative transition. We have used this latter method.

Figure 2 shows the spectrum of gamma-rays in coincidence with all gamma-rays of more than 4·5 Mev when the proton bombardment is carried out at the peak of the resonance. This distribution is as expected for a single gamma-ray or two lines very close in energy. The measured energy of this coincident radiation is 2·30 ± 0·05 Mev. The bias requirement in the other crystal eliminates any contribution to this distribution from the cascade through the second excited state. We may note that this result reinforces the earlier arguments that cascades through the 5·83 Mev state are relatively unimportant because the energy of that cascade partner would be 2·23 Mev. The peak due to this radiation would have fallen almost two channels below that seen in fig. 2, viz. well towards the trough of the distribution and would have caused the summed peaks to be rather ill-defined had it been present in significant amount.

Fig. 3

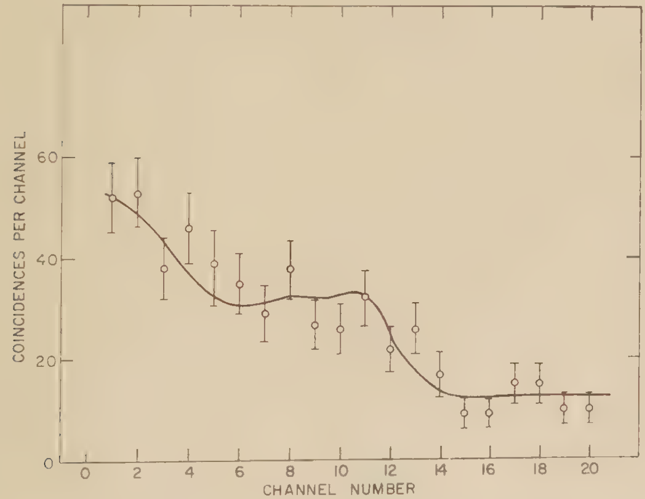

Spectrum of gamma-rays at a proton energy of 700 kev seen in coincidence with gamma-rays of greater than 4·5 Mev. The full line is the distribution calculated for a superposition of 1 part of 2·31 Mev radiation from the first excited state and 1·18 parts of 2·51 Mev radiation from a transition between the compound nucleus state and that at 5·69 Mev. This spectrum was taken with a bias of 42 channels.

When the same measurements are repeated at a proton energy of 700 kev the distribution of fig. 3 is obtained. The well-defined peak of fig. 2 has completely disappeared and is replaced by a quite smeared-out distribution which however cuts off quite sharply as it should if it represents two gamma-rays of about the same energy. From the shape expected from a single gamma-ray, which is close to that of fig. 2, we construct the full line of fig. 3 which shows the theoretical distribution for a mixture of 1 part of radiation of 2·31 Mev to 1·18 parts of radiation of 2·51 Mev.

It therefore appears that the 4·8% of 5·7 Mev radiation observed in fig. 1 is indeed composite, and consists of about 2·2% † due to the forbidden transition between the 8·06 and 2·31 Mev states while the remaining 2·6% comes from the 5·69 Mev state ‡.

We might at this point interpolate a remark about angular distributions and correlations in the present work. At neither of the two resonances here studied need we worry about angular distribution of the individual gamma-rays relative to the proton beam because the 1·16 Mev resonance is of spin zero as is also the broad 1·25 Mev resonance on which it sits, while the 550 kev resonance is formed very largely by s-wave protons as confirmed by the measured isotropy of the strong radiations. The only measurement which could be upset by the existence of a strong angular correlation is that just reported. Here all the spins are known (that of the 5·69 Mev state is evidently 1 as we shall see), so we may compute the angular correlation of our cascade which passes through it. It is $1+0{\cdot}2\cos^2\theta$, so we can neglect its effect because of the poor accuracy of the measurement and because the crystals were large and very close to the target. The competing cascade has of course a rigorously isotropic correlation.

Before leaving this resonance it is profitable to consider the 5·69 Mev state a little more closely because it is of importance also at the 1·16 Mev resonance. According to the review cited, this state cascades through the 2·31 Mev state as well as going directly to ground, the cascade being more probable by a factor of 1·9. According to measurements of gamma-rays following the deuteron bombardment of ^{13}C (Bent *et al.* 1955) this factor is 2·1. According to the present work to be described the factor is 1·4. Although this agreement is not very good it establishes that the intensity of the 2·37 Mev gamma-ray which leads to this state from that at 8·06 Mev is about 2·7 times as great as that of the 5·69 Mev line, viz. about 7% of the ground-state transition from the 8·06 Mev level. Its radiative width is therefore about 0·7 ev with a corresponding strength of $|M|^2=0{\cdot}09$ if the transition is E1 and $|M|^2=2{\cdot}5$ if the transition were

---

† We have not here applied the small (about 12%) correction in the apportioning of the 4·8% due to the differing energies of the competing transitions at proton bombarding energies on and off resonance because this is well covered by the uncertainties of the intensity and intensity-ratio measurements.

‡ Similar conclusions to the present ones concerning the 550 kev resonance have been reached by R. Pick, A. Leveque and P. Lehmann (Report to the 1956 Amsterdam Conference on Nuclear Reactions) who also used the present method for separating the two cascades resulting in 5·7 Mev radiation. These workers used coincidence methods for estimating the absolute intensities whereas we have here chosen to determine the intensities themselves directly and to rely on coincidence methods for estimating relative branching ratios.

M1. These figures make it very probable though not sure that the transition is in fact E1 and so the parity of the state is even. The E1 transition would be allowed by the isotopic spin only because the isotopic spin of the state is presumably zero for the reason discussed earlier in connection with the 6·23 Mev state. The spin must now be $J=0,1,2$, of which $J=1$ is clearly favoured by the decay scheme which also eliminates $J=0$. $J=2$ is eliminated by the strength of the transition to it from the 0+ state at 8·62 Mev as we shall see, so we are left with the assignment $J=1+$. This is supported by the observation (Marion *et al.* 1955) that the reaction ^{13}C(d, n)^{14}N has a very strong slow neutron threshold at a deuteron energy of 0·422 Mev. The slow rise of the yield above the threshold makes these authors suggest that p-wave neutron emission is involved and since the ingoing proton must almost certainly be s-wave at so very low an energy the parity of the state must be even. The fact that it is only this one neutron threshold that shows so very intensely suggests that this state may be a rather simple one and may prepare us for striking radiative properties too.

§ 4. THE 8·62 MEV STATE OF ^{14}N

This state has not been investigated so frequently as the previous one. It is reported as having a width of 6 ±2 kev and so requires rather careful treatment. It is also situated rather close to the maximum of the 1·25 Mev resonance whose width is 500 kev. This state at 8·70 Mev in ^{14}N is 0− and, like that at 8·06 Mev, displays a reduced s-wave width of the order of the single-particle limit. Its large E1 radiative width to the ground state ($\Gamma_\gamma=46$ ev ; $|M|^2=0{\cdot}11$) accords with this description and shows that the state is of $T=1$.

Because all of our work at the 1·16 Mev resonance necessarily included radiation from this underlying 0 − resonance we display in fig. 4 the yield curve across it. This yield curve was measured and all our work at this resonance was carried out using an electrostatic analyser accepting the H_2^+ beam to stabilize and control the proton energy. The units of the abscissa of fig. 4 are those of the potentiometer of the electrostatic analyser ; 5 units correspond to an energy change of 1·33 kev for the proton beam. The yield curve was taken with a low bias setting on the crystal so that all gamma-rays were counted. The curve displayed in the figure was taken at the end of the experiment. That taken at the beginning was a little better, showing a ratio of counts at the peak and 20 kev below the peak of 10·1 to 1. We show the yield curve taken after the experiment to demonstrate that despite the narrowness of the resonance it did not become too badly obscured by carbon deposits in the course of the experimentation.

The narrowness of the resonance is useful in that it enables background effects to be determined accurately. The procedure adopted to eliminate contributions from the 1·25 Mev resonance was to run at the peak of the 1·16 Mev resonance—a potentiometer setting of 4362—then for an equal amount of charge symmetrically either side of it—at potentiometer settings of 4300 and 4430. This is sufficiently far away (17 kev) from the resonance for its own contribution to have become very small, but is a sufficiently small change of energy for that due to the 1·25 Mev resonance to have remained almost constant. The results at the two off-resonance positions were averaged and subtracted from the distribution obtained at the peak of the resonance. This procedure also automatically eliminated any other background such as $^{12}C(p, \gamma)^{13}N$ which had always to be thought of and also $^{19}F(p, \alpha)^{16}O^*$. The latter reaction, although

Fig. 4

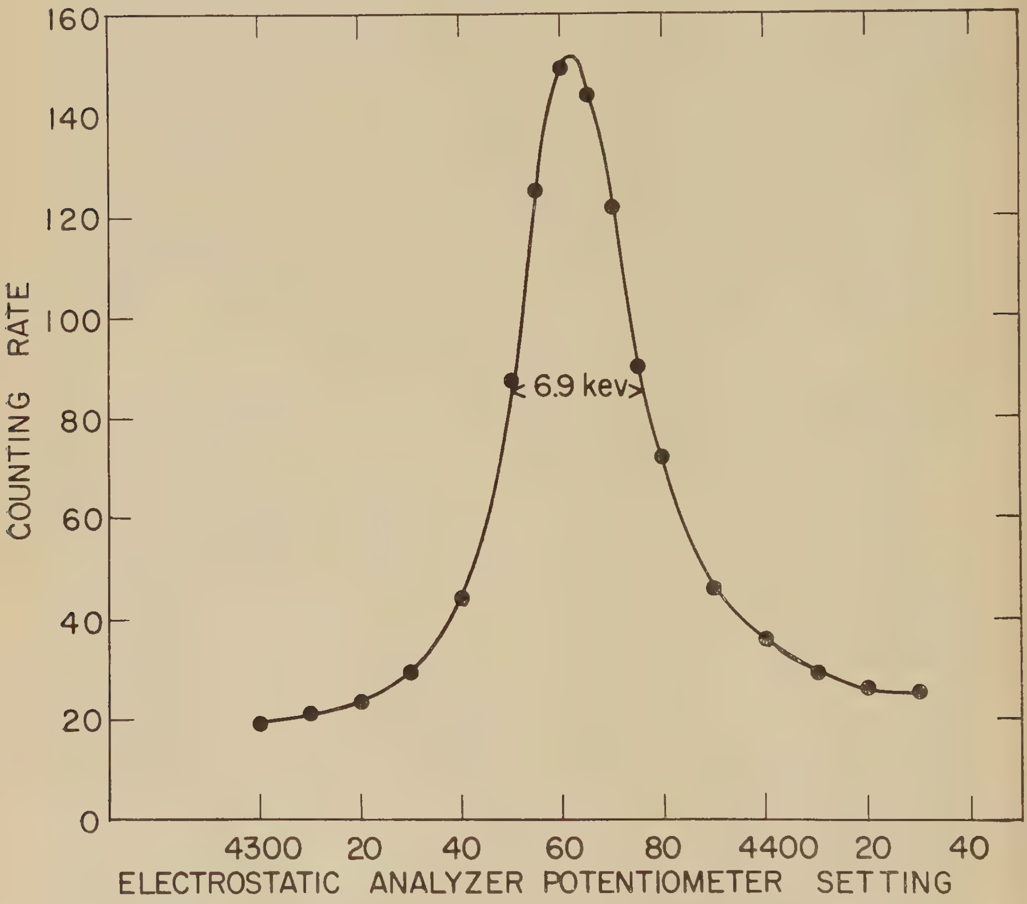

The 8·62 Mev state of ^{14}N seen in $^{13}C(p, \gamma)^{14}N$ at a proton energy of 1·16 Mev. The observed width of 6·9 kev is an upper limit to the true width since the target thickness is not known. The background either side of the peak is due to the broad 8·70 Mev state centred on a proton energy of 1·25 Mev. For purposes of estimating the effect of the 1·16 Mev resonance of this underlying state runs were taken at potentiometer settings of 4300 and 4430, viz. about 17 kev either side of the resonance.

it is resonant, has no sharp resonance in the energy range involved in these energy changes ; it has a broad (130 kev) resonance centred at 1·18 Mev and if this were significant it would also be very well taken care of by the present procedure since the change in proton energy is small, compared with the width of the resonance and, furthermore the (p. α) fluorine resonance almost coincides in energy with our narrow (p, γ) in ^{13}C. This bracketing process was carried out for all our subsequent spectra determinations. Sometimes, however, the subtraction has not actually been made in plotting the figure and this is noted in the figure captions.

The first step was to verify that the 6·23 Mev state does indeed decay to the 2·31 Mev state. This was done by examining the gamma-rays with a three-crystal pair spectrometer with good dispersion. A typical spectrum is shown in fig. 5. The gamma-ray of measured energy (in terms of the 4·43 Mev ^{12}C line) 4·60 ± 0·09 Mev is the expected transition between the 8·62 and 3·95 Mev states. Its intensity has been made the unit in terms of which other intensities from the 1·16 Mev resonance in this work have been measured ; this will be understood in the rest of this report. Because we know that the ground-state transition from the 3·95 Mev level will only give a line of strength 0·04 the other observed

Fig. 5

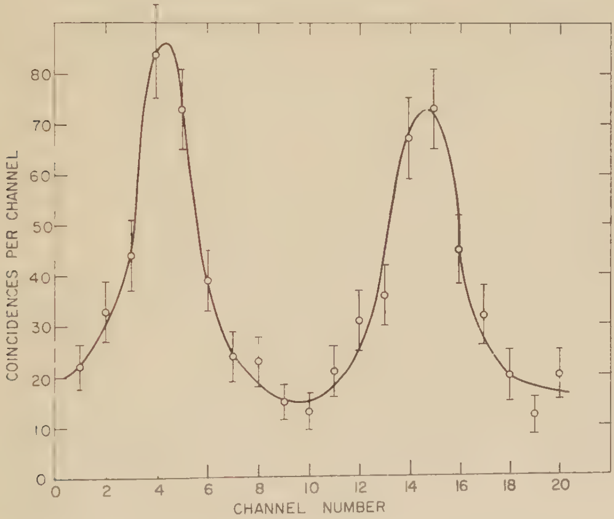

Three-crystal pair spectrum of gamma-rays taken at the 1·16 Mev resonance (potentiometer setting 4362, see fig. 4). The background at settings 4300 and 4430 has not been subtracted ; it amounts to about 5 coincidences per channel in this region. The peak at channel 15 has a measured energy of 4·60 ± 0·09 Mev and is the transition between the 8·62 and 3·95 Mev states. The peak at channel 4 has a measured energy of 3·87 ± 0·07 Mev and is the transition between the 6·23 and 2·31 Mev states. This spectrum was taken with a bias of 33 channels.

gamma-ray of 3·87±0·07 Mev must very largely represent the transition between the 6·23 and 2·31 Mev states. Its intensity is 1·28. The background from the runs in the wings was quite unimportant here. It was generally flattish but showed a very slight tendency to group also at these two energies, probably due to the slight persisting effect of this resonance 17 kev from its peak.

The next problem was to measure the gamma-rays in the region of 6 Mev. A typical spectrum from which this was done is shown in fig. 6. The two lower energy gamma-rays which were measured in fig. 5 are again seen and have measured energies of 3·91±0·09 and 4·61±0·08 Mev. The intensities of the 3·92 Mev line from these results is 1·20 which agrees well with our earlier estimate. The rather flat tail in the higher channels is due to the 8·62 Mev ground-state transition whose peak, measured separately, is not in the present picture. This transition is only of indirect interest to the present investigation in that its strength affects the radiative widths deduced for the other transitions from the 8·62 Mev state. We measured its intensity as 0·95 but this figure is probably quite inaccurate. The presence of radiation of about 6 Mev is very clear. The expected peak positions for the possible ground-state

Fig. 6

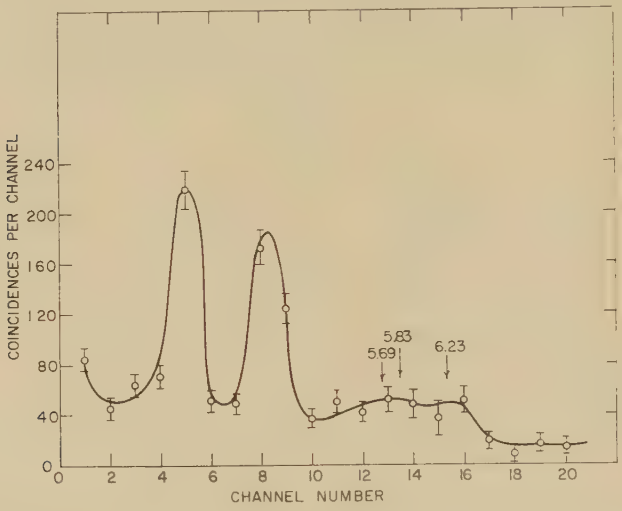

Three-crystal pair spectrum of gamma-rays taken at the 1·16 Mev resonance (potentiometer setting 4362, see fig. 4). The summed distributions taken at settings of 4300 and 4430 and normalized to the same charge have been subtracted. The peaks at channels 5 and 8 have measured energies of 3·91±0·09 Mev and 4·61±0·08 Mev and are the same transitions as are shown in fig. 5. The three arrows show the expected peak positions for gamma-rays of 5·69, 5·83 and 6·23 Mev. The tail in the highest channels is due to the 8·62 Mev ground-state transition. This spectrum was taken with a bias of 8 channels.

transitions from the 5·69, 5·83 and 6·23 MEV levels are shown by the arrows. It is evident that 6·23 MEV radiation is present. But there is not the sharp peak expected for such radiation, rather a sort of step and plateau which extends towards the peak due to the 4·67 MEV line. This then requires the additional presence of some radiation of lower energy. We may construct the expected distribution due to 6·23 MEV gamma-rays with accuracy with the aid of the gamma-rays from fluorine. When this is done the strength of the 6·23 MEV line is found to be 0·39. On subtracting this from the observed distribution the remainder looks quite correct for a gamma-ray of 5·69 MEV and of intensity 0·24. The distribution does not fit nearly so well a line of 5·83 MEV and suggests then that in addition to the cascade from the 8·62 MEV state through that at 6·23 MEV there is another cascade through the 5·69 MEV state.

The distribution of fig. 6 is the subtracted distribution, on peak minus the background distribution taken in the wings. Whereas for fig. 5 the background was very small, and no serious error would have been made in ignoring it, the background for fig. 6 is quite large. In particular the tail from the ground-state transition is important and also there is a substantial amount of background radiation in the region of the 6·2 MEV peak which in the raw distribution taken at the peak of the resonance is much more prominent than in fig. 6. Serious error would have resulted from ignoring the background here ; it is approximately equal to the contribution from the 8·62 MEV level, for the ground-state transition, and the same is true of its importance for the 6·2 MEV radiation.

This suggestion of further complexity in the decay of the 8·62 MEV state must now be pursued to check that we are correct in accepting only a part of the 5·7 to 6·2 MEV radiation as due to the 6·23 MEV ground-state transition. This was done by looking for the lower energy gamma-rays that must be present with the 5·69 MEV line. These are the 2·93 MEV transition between the 8·62 and 5·69 MEV levels and the 3·38 MEV line due to transitions between the 5·69 and 2·31 MEV states which, as we have remarked earlier, is reported to be roughly twice as intense as the ground-state transition from the 5·69 MEV state. Figure 7 displays the spectrum measured in the interesting region. This is the usual subtracted spectrum, peak minus wings. The background here is everywhere unimportant. There is here a special reason for making the background check, namely that $^{12}C(p, \gamma)^{13}N$ at this proton energy would give a gamma-ray of 3·02 MEV which is close to the expected 2·93 MEV. However, the background runs show that this contribution is negligible. Only the lower of the two strong lines of fig. 5 is included in the spectrum of fig. 7 and has a measured energy of 3·85±0·08 MEV. The other strong line has a measured energy of 2·34±0·04 MEV ; it is the superposition of the ground-state transition from the 2·31 MEV state and the 2·39 MEV line due to the transition between the 8·62 and 6·23 MEV states. Its intensity (measured via that of the 3·92 MEV line) is 4·7. In addition to these expected gamma-rays we see a well-defined peak close to the position expected for the gamma-ray of 2·93 Mev which confirms our attribution of the lower energy pulses in the 5·7 to 6·2 Mev range to another cascade via the 5·69 Mev state. The agreement in position is seen to be much better with that expected of a 2·93 Mev line than with that expected for a 2·79 Mev gamma-ray such as would lead to the 5·83 Mev state. The intensity of this 2·93 Mev line is 0·54. We also see the expected line at 3·38 Mev which completes the confirmation of this new cascade. Its intensity is 0·33, which checks quite well, together with the 0·24 measured for the 5·69 Mev line, the 0·54 measured for the intensity of the 2·93 Mev line which precedes these two. However, our branching ratio of 3·38 Mev cascade radiation versus 5·69 Mev ground-state transition is only 1·4 as against the higher figure of about 2 cited earlier in § 3. But our present measurements on this point are not very accurate, as can be judged, and the discrepancy is not worrying. A further check that the 5·83 Mev level is not the one principally involved comes from the absence of the 725 kev radiation from this resonance too ; there is also no suggestion of the 5·10 Mev line (see the argument of § 3 about this level).

Fig. 7

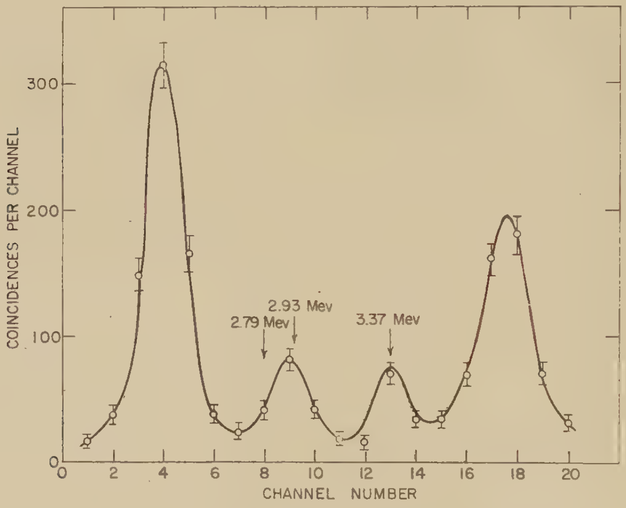

Three-crystal pair of spectrum of gamma-rays taken at the 1·16 Mev resonance (potentiometer setting 4362, see fig. 4) with a subtraction as in fig. 6 for the background measured off-peak. The peak at channel 18 has a measured energy of 3·85±0·08 Mev and is the transition between the 6·23 and 2·31 Mev states. The peak at channel 4 has a measured energy of 2·34±0·04 Mev and is the superposition of the ground-state transition from the 2·31 Mev state and the transition between the 8·62 and 6·23 Mev states. The arrows indicate the expected positions of peaks due to gamma-rays of 2·79, 2·93 and 3·37 Mev. This spectrum was taken with a bias of 8 channels.

From the intensities reported here we can compare the measured and expected strength of the '2·3 MeV' radiation from both sources, viz. the 8·62 MeV to 6·23 MeV state transition and the 2·31 MeV ground-state transition. The transition from the 8·62 MeV state to that at 3·95 MeV, our standard of intensities, contributes 0·96; the cascade through the 5·69 MeV state contributes 0·33 (the intensity of the 3·38 MeV line); the cascade through the 6·23 MeV state contributes 1·24 (the intensity of the transition between the 6·23 MeV and 2·31 MeV states) plus 1·63 (the sum of the intensities of this transition and the direct ground-state transition from the 6·23 MeV state). This makes a total of 4·2 against our measurement of 4·7 which must be regarded as very fair agreement when so many transitions of widely differing energies are involved.

At this point we may regard the decay scheme of the 8·62 MeV state as established but we carried out two further check measurements of a coincidence nature.

The first coincidence measurement was to set up a second NaI(Tl) crystal with a coincidence channel from 2·0 to 2·5 MeV so as to include the full energy peaks of the 2·31 and 2·39 MeV lines and measure the spectrum of gamma-rays in coincidence with this channel. If our decay scheme is correct we should see a line at '2·3 MeV' from the triple cascade through the 6·23 MeV and 2·31 MeV levels, the first or last member falling into the coincidence channel and the last or first member registering in the display crystal. We should also see a 1·64 MeV line from the cascade de-excitation of the 3·95 MeV state. From the intensities we have just presented the relative intensities of the '2·3' and 1·64 MeV lines seen in this coincidence experiment should be 3·1 : 1. There should also of course be many higher energy lines seen in coincidence. It is not satisfactory simply to measure gamma-rays in coincidence with radiation between 2·0 and 2·5 MeV because pulses in this range can be given by higher energy gamma-rays with which the '2·3 MeV' and 1·64 MeV lines are also in coincidence. But such coincidences should not depend critically on where the coincidence channel is set because the singles spectrum of the higher energy lines will be rather flat at 2·5 MeV. On the other hand, if we move the coincidence channel above 2·5 MeV the contribution from the cascades we seek here will vanish completely. We accordingly made several coincidence runs with the coincidence channel set at 2·0 to 2·5 MeV, 2·5 to 3·0 MeV, 2·75 to 3·25 MeV and 3·0 to 3·5 MeV. There was no significant difference between the coincidence spectra obtained with these last three channelling positions, all of which exclude the desired coincidences, so we assumed that this unwanted contribution would be effectively the same on the lowest channel also and so subtracted this suitably normalized contribution derived from the higher channels. The subtraction amounted to about one-half of the total distribution observed with the channel set for 2·0 to 2·5 MeV. This corrected distribution is shown in fig. 8. Chance coincidences were less than 2%. The two expected lines at measured energies of 2·35 ± 0·05 MeV and 1·64 ± 0·05 MeV are well seen. The background on which they sit is due to the higher energy gamma-rays also in coincidence with the ' 2·3 MeV ' line. Because of this background and its unknown behaviour beneath our interesting lines the interpretation of this picture is very inaccurate. Using different treatments of the data our estimates of the ratio of the ' 2·31 MeV ' intensity to that of the 1·64 MeV line ranged from 2·4 to 3·3: 1, which can be taken as agreeing with the expected 3·1.

Fig. 8

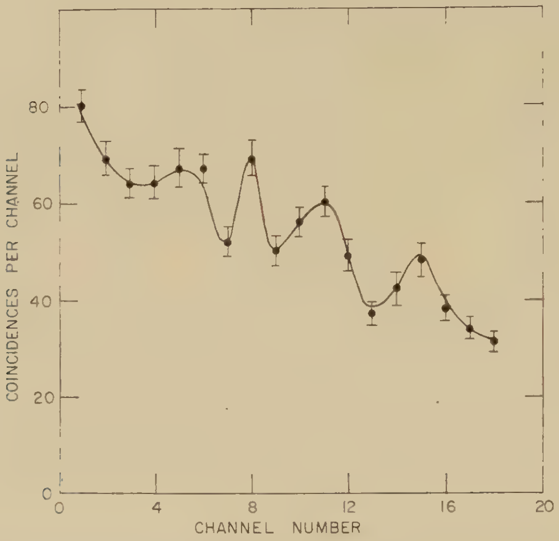

Gamma-rays from the 1·16 MeV resonance seen in coincidences with a channel from 2·0 to 2·5 MeV with a subtraction of spectra obtained by channelling at higher energies (see text). The peak at channel 15 has a measured energy of 2·35 ± 0·05 MeV and is due to a superposition of the gamma-rays of 2·31 and 2·39 MeV observed in fig. 7. The peak at channel 8 has a measured energy of 1·64 ± 0·05 MeV and is the transition between the states at 3·95 and 2·31 MeV. The peak at channel 11 is the Compton edge of the 2·3 MeV radiations. This spectrum was taken with a bias of 8 channels.

The second coincidence measurement was performed to verify the existence of the triple cascade through the 6·23 MeV and 2·31 MeV levels. For this a third NaI(Tl) crystal was placed close to the target. Two of the crystals were set with channels of 2·0 to 2·5 MeV to catch the first and third members of the cascade and the third was displayed in triple coincidence with these. Because of the triple condition we need no longer worry about the effect of higher energy gamma-rays in triggering one of the channelling crystals because this could not be accompained both by the actuation of the other channelling crystal and also the detection in the display of a gamma-ray of energy greater than 3·92 MeV. The resulting coincidence spectrum is shown in fig. 9. While the counting rate is very low and the statistics are very unimpressive it is seen that the distribution is consistent with that expected for a gamma-ray of 3·9 Mev. The important observation is that there are very few counts in the high channels and that the spectrum cuts off rapidly as that of a 3·9 Mev line should. The 4·67 Mev line has been eliminated. For comparison the distribution of single counts obtained by relaxing the triple coincidence condition is almost flat across this picture. The chance coincidence contribution was very small.

Fig. 9

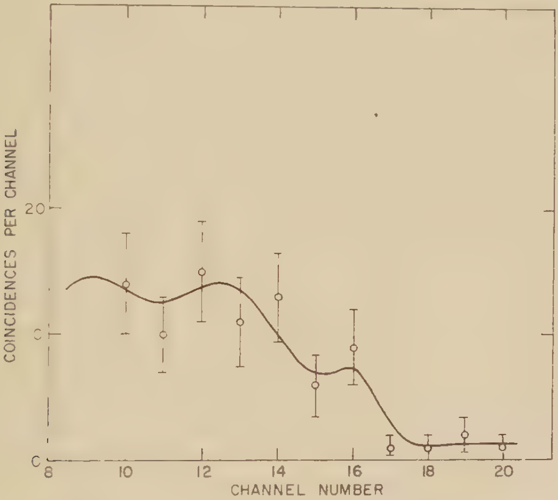

Gamma-rays from the 1·16 Mev resonance seen in triple coincidence with two channels of 2·0 to 2·5 Mev. The full line is the expected pulse distribution for a gamma-ray of 3·9 Mev. This spectrum was taken with a bias of 10 channels.

Before considering the analysis of these results we may examine, as in the decay of the 8·06 Mev state, the transition to the state at 5·69 Mev. In § 3 we concluded that this state was 1+ and also probably a rather simple state because it was so predominantly seen in the neutron threshold experiment. This conclusion is borne out by the decay leading to it from the 8·62 Mev state. If we are correct in the assignments this an M1 transition and its radiative width is 0·7 ev which corresponds to a strength of $|M|^2=1\cdot3$ Weisskopf units. This is a high but quite reasonable figure. Had the state been 2+ the E2 transition would have had $|M|^2=700$, which is impossible, so all evidence points to 1+ for this state.

§ 5. The Decay Schemes

We do not suggest that this work has exhausted the decay schemes of the two states that we have studied, since our primary interest has been the rather specific one described in § 1. We have merely carried the investigation to the point of determining the two branching ratios which bear on the isotopic spin problem. Our results are displayed in fig. 10. The unit of intensity for the 8·06 MeV level radiations is the ground-state transition, while that for the 8·62 MeV level is the first member of the cascade through the second excited state. There is no normalization between the two decay schemes.

Fig. 10

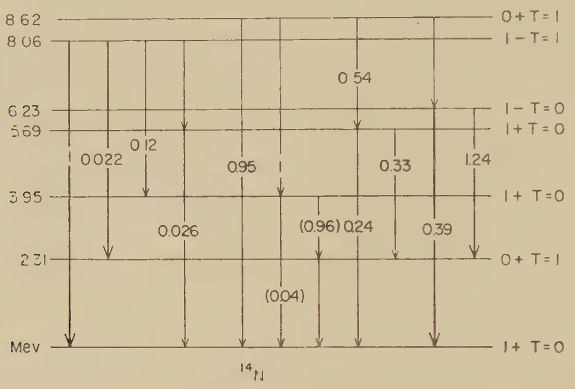

Levels of ^{14}N and the decay scheme of the 8·06 and 8·62 MeV levels as determined in the present work. Only the transitions that were of significance for the present investigation are shown and others not investigated here may well exist. Only the states of ^{14}N of present interest are shown. The four transitions of prime interest for this investigation are shown as heavy arrows. The transitions from the 8·06 MeV have been normalized in strength to the ground-state transition and those from the 8·62 level have been normalized to that between the 8·62 and 3·95 states. The intensities in parentheses are taken from other work. In addition to the intensities shown for the 8·62 MeV state the summed intensities of the ground-state transition from the 2·31 MeV state and that between the 8·62 and 6·23 MeV states was measured as 4·7.

§ 6. Discussion

From the decay schemes of fig. 10 for the two states of interest we see that both E1 transitions forbidden by the isotopic spin selection rule indeed occur. To compare them with the allowed transition from each level we take out the E_γ^3 factor in the transition probability in the usual way. We then find that the strength of the forbidden transition from the 8·06 MeV state is 0·061 of that of the allowed and that the strength of the forbidden transition from the 6·23 MeV level is 0·078 of that of the allowed. With nothing further to guide us the usual procedure would be to say†, for the 8·06 MeV level $\alpha_1^2(0)_{8\cdot06}\sim0\cdot061$, while for the 6·23 MeV level $\alpha_0^2(1)_{6\cdot32}\sim0\cdot078$.

---

† We assume that the ground and first excited states are relatively pure.

If indeed these two levels were each other's chief contaminators we should expect $\alpha_1^2(0)_{8\cdot06}=\alpha_0^2(1)_{6\cdot23}$. In fact the relative strengths of the two forbidden transitions need not be the same of course because the speed of the two allowed transitions may not be the same. There seems no likelihood of measuring this speed for the 6·23 MeV state, although a resonance scattering of the forbidden radiation may eventually be possible. In the meantime the closeness of the two numbers is very suggestive and renders quite plausible the suggestion that we are here seeing the effects of the isotopic spin mixing from both ends. If this is so, then the forbidden transition from the 8·06 MeV level takes place by virtue of the mixing into that state of a fraction $\alpha_1^2(0)_{8\cdot06}$ of the 6·23 MeV state and so in this sense the 5·75 MeV forbidden gamma-ray from the 8·06 MeV state is the same thing as the 3·92 MeV allowed gamma-ray from the 6·23 MeV state ; similarly the 6·23 MeV forbidden line from the 6·23 MeV state is the doppelgänger of the 8·06 MeV allowed transition from the 8·06 MeV state, being present by virtue of the fraction $\alpha_0^2(1)_{6\cdot23}$ of the 8·06 MeV state which has been handed over in return.

The magnitude of H^C, the Coulomb matrix element required to produce this mixing, is about 0·45 MeV. This is quite a large matrix element and tells of a rather close relationship between the $1-T=1$ 8·06 MeV state and the $1-T=0$ 6·23 MeV state. However, as we remarked in § 1, the theoretical indications as to how this relationship can be produced are not clear. It would seem profitable to make a theoretical investigation of isotopic spin mixing between somewhat more complicated states than ^{13}C, 2s, for example to investigate the properties of possible mixed descriptions such as ^{13}C, (2s, 1d). These may then in turn mix via the Coulomb interaction more strongly than states of the simpler type commonly assumed. This in turn suggests that the 8·06 MeV state should be more closely investigated for traces of d-state in its make up for example by careful angular distribution measurements in the high energy wing of the resonance where the relative d-wave penetrability will improve and so show up any admixture of d-state more clearly. A further experimental result that would be most welcome is a confirmation that the 6·23 MeV state is of odd parity. Here use of the ^{13}C(d, n)^{14}N stripping reaction is the obvious approach. It should show an $l=0$ pattern. This should be relatively easy to diagnose even if a full angular distribution is difficult to obtain.

ACKNOWLEDGMENT

We should like to thank Mr. A. G. Rubin who helped with these measurements.

REFERENCES

AJZENBERG, F., and T. LAURITSEN, 1955, *Rev. Mod. Phys.*, **27,** 77.
BENT, R. D., BONNER, T. W., and SIPPEL, R. F., 1955, *Phys. Rev.*, **98,** 1237.
CLEGG, A. B., and WILKINSON, D. H., 1953, *Phil. Mag.*, **44,** 1269.

Gove, H. E., Litherland, A. E., Almquist, E., and Bromley, D. A., 1956, *Phys. Rev.*, **103,** 835.

Marion, J. B., Bonner, T. W., and Cooke, C. F., 1955, *Phys. Rev.*, **100,** 847.

Seagrave, J. D., 1952, *Phys. Rev.*, **85,** 197.

Wilkinson, D. H., 1956 a, *Phil. Mag.*, **1,** 379; 1956 b, *Phil. Mag.*, **1,** 127.

Wilkinson, D. H., and Clegg, A. B., 1956, *Phil. Mag.*, **1,** 291.

Isotopic Spin Selection Rules
XII : The Mirror Reactions ^{6}Li(d, n)^{7}Be and ^{6}Li(d, p)^{7}Li†

By D. H. Wilkinson
Brookhaven National Laboratory, Upton, New York ‡

[Received October 20, 1956]

Abstract

It is remarked that the mirror reactions ^{6}Li(d, n)^{7}Be and ^{6}Li(d, p)^{7}Li leading to the first excited states of the mirror nuclei form an excellent testing place for the prediction following the assumption of charge-independence that such mirror reactions have equal intrinsic probability. This is because the reactions are almost non-resonant which makes for the good operation of the isotopic spin rules and because the protons are emitted well above the Coulomb barrier which makes the interpretation of the experimental neutron to proton branching ratio rather simple. It is also remarked that the experiment may be performed without observing the neutrons and protons by using the gamma rays from the excited states to label the two transitions ; all higher excited states are unstable to heavy particle emission and so do not yield gamma rays. The branching ratio is determined at 31 deuteron energies between 200 kev and 1·8 mev. Over the whole range it agrees to within 15% with that expected from charge independence but there are signs of a resonance like maximum to the ratio at about 450 kev which departure from the isotopic spin rule is in keeping with the behaviour of the ^{6}Li+d total cross sections.

§ 1. Introduction

One of the simplest consequences of the assumption of the charge independence of nuclear forces is that reactions which lead to different members of an isobaric multiplet should have intrinsic rates simply proportional to the squares of the appropriate Clebsch–Gordon coefficients in the isotopic spin. In particular if we form a compond $T_Z=0$ nucleus then the intrinsic probability that it will break up by neutron emission to a given level of the $T_Z=-\frac{1}{2}$ nucleus is equal to the intrinsic probability that it will emit a proton to the mirror level in the $T_Z=+\frac{1}{2}$ nucleus.

---

† Communicated by the Author. Work performed under the auspices of the U.S. Atomic Energy Commission.

‡ Permanent address : Cavendish Laboratory, Cambridge, England. This work was performed while the author was Visiting Physicist at Brookhaven National Laboratory during the summer of 1956.

This rule has never been tested with good accuracy under circumstances where we might reasonably hope that it should be obeyed. As we have discussed earlier (Wilkinson 1956) these circumstances are found either in the low-lying well separated nuclear states which have individually well-defined isotopic spins or in the continuum region of broad overlapping levels where the speed of the reaction defeats the slow mixing of isotopic spins by the Coulomb interaction. Between these regions, where we have resonance structure with close spacing or a continuum but with strong residual effects from the individual levels, we should not expect the rule to work. Indeed in just such a region (at 12·69 MEV in ^{14}N formed by ^{10}B$+\alpha$) we find a level whose reduced width for neutron emission to the ground state of ^{13}N is 5·7 times that for proton emission to the ground state of ^{13}C (Shire and Edge 1955). This very interesting case is one of the clearest examples of the breakdown of charge independence. The reason why such tests are rare is that one must single out the neutron and proton groups leading to the mirror levels ; then the angular distributions of these groups must be measured in order that the total cross sections may be compared because the external effect of the Coulomb field in modifying the angular distribution of the emitted proton must be taken into account if the reaction is not a strictly resonant one and it is not good enough to compare the differential cross sections at a particular angle of emission. This must then be done for every energy of the bombarding particle for which a test is desired. Here again a single bombarding energy is not adequate because of the possibility of a chance result ; the investigation should be carried out with a thin target but over an energy range great compared with the underlying level spacing. Such work involves one in absolute neutron flux measurements and these are very difficult, particularly when they have to be accompanied by resolution of neutron groups. This type of investigation is then extremely difficult and laborious if it is to be carried out with an accuracy of, say, 10% or better at a dozen or more bombarding energies. However, even if this could be done the question of charge independence would remain largely unanswered because this provides only for the equality of the *intrinsic* emission probabilities of neutron and proton viz. the *reduced* widths. In other words the experimental results have to be corrected for the effect on the proton emission of the Coulomb barrier. This is notoriously difficult and uncertain even if the reaction mechanism is known i.e. even if it is known that the proton that is emitted in fact has had to penetrate the barrier. This would be so far for example in a (d, p) reaction that went by compound nucleus formation but not for one that went by a pure stripping reaction. This Coulomb correction is uslly further complicated because we do not know what angular momenta are involved. Accordingly there is no hope of effecting a sharp test of the consequences of charge independence unless the proton emission takes place so far above the Coulomb barrier that the possible correction on that account is small and even then it is highly to be desired that the reaction mechanism should be known so that the small correction may be applied with some confidence. It is for these many reasons that no accurate verification of charge independence has so far been forthcoming from this type of comparison of reduced widths.

Since the charge independence hypothesis does not of itself say anything about the absolute reduced widths but only requires the equality of neutron and proton reduced widths the measurement of absolute yields is not called for. However the only direct way of comparing neutron and proton yields is to measure them both absolutely or perform some measurement equivalent to this which is an unfortunate complication. A method of measuring relative yields of neutrons and protons without making absolute measurements on the particles would be to measure rather the gamma-rays leading from the states to which the particle transitions are made. In this way only relative measurements need be made, gamma-rays acting as a label for the neutron and proton transitions alike. This method however suffers from limitations that generally render it useless. Firstly, the energies of the mirror levels must be sufficiently different to permit easy discrimination between the gamma-rays that label the neutron and proton transitions. Secondly if any gamma-ray branching is possible from the levels to which our particle transitions lead it must be studied too before the answer is obtained because we may not assume that the predictions of charge independence are valid there either. Thirdly the angular distributions of the various gamma-rays must still be measured to get the integrated relative yields because these distributions also will depend on the validity of the charge-independence hypothesis in a trivial and a non-trivial way. The trivial way is that the relative amounts of different spherical harmonics in the outgoing neutron and proton waves will be affected by the Coulomb barrier and so the gamma-ray angular distributions will be affected by Coulomb effects outside the nucleus; the non-trivial way is that the reduced widths for the differing angular momenta will be different if charge independence is being broken by the Coulomb perturbation or for any other reason *inside* the nucleus. Fourthly, and most important, if the state to which the particles lead directly can also be reached by gamma-ray branching from higher states to which other particle groups from the same reaction lead the gamma-ray is no longer just a label for the particle transition that interests us; it is partly a label for other particle transitions. We must therefore study not only it but also all other gamma-rays that could lead to that state. This then becomes very much more complicated and involves relative intensity measurements of gamma-rays of perhaps widely differing energy. The presence of other gamma-rays will also render more difficult the study of the intensity of the gamma-rays of chief interest and so on. For these many reasons and because the study of gamma-ray intensities is usually not very easy in the presence of considerable neutron fluxes this method, although it avoids the necessity for measuring absolute neutron fluxes, is not of very general application.

There is however one pair of mirror reactions where we might hope that the charge independence rules should apply quite well, where the Coulomb barrier has little effect and the mechanism is fairly clear and where the labelling of the transitions by the subsequent gamma-rays is easy and meets none of the difficulties just enumerated. This case is the reactions ^{6}Li(d, n)^{7}Be and ^{6}Li(d, p)^{7}Li leading to the first excited states of the residual mirror nuclei.

When a deuteron is added to ^{6}Li the compound ^{8}Be system has an excitation of 22·3 MeV. The level structure has been fairly well investigated at an excitation of 17–19 MeV where the known level spacing is about 300 400 KeV so the spacing is presumably less than this at the higher excitation. However in the reactions ^{6}Li+d leading to neutron emission (Baggett and Bame 1952, Hirst, Johnstone and Poole 1954) proton emission (Whaling and Bonner 1950 ; Nickell 1954 ; Sawyer and Phillips 1953) or alpha-particle emission (Whaling and Bonner 1950 Sawyer and Phillips 1953, Hirst, Johnstone and Poole 1954) very little sharp resonance structure is found and all the cross sections are smooth. This suggests that we may be in the second region of validity of the isotopic spin rules where the strong overlap of the levels and the speed of the reaction ensure that most of the observed effects are charge-independent ones. Furthermore the cross sections well below a deuteron energy of 1 MeV follow a simple penetrability formula quite well which suggests that compound nucleus formation is the dominant mechanism and so presumably the protons emitted in the (d, p) reaction have come from inside the ^{8}Be compound nucleus. This conclusion is supported by the angular distributions at low energy which are chiefly isotropic although the beginning of a superimposed stripping pattern can be seen at a deuteron energy of about 1 MeV. The Q-value of the (d, p) reaction is 5·02 MeV so the protons leading to the first excited state of ^{7}Li at 477 KeV are emitted well above the Coulomb barrier of about 1·7 MeV. So from the points of view of the reaction and our ability to interpret the relative particle yields the situation seems very favourable to trial of the isotopic spin rules.

From the point of view of the gamma-ray labelling technique we are also very fortunately placed on all four counts listed above. Firstly the first excited states of ^{7}Li and ^{7}Be are at energies of 477 and 430 KeV respectively. Although these energies are not sufficiently far apart to allow a complete separation of the gamma-ray lines the difference in energy is great enough to allow an accurate estimate of relative intensity to be made using a NaI(Tl) crystal. Secondly these are the only gamma-rays that can come from these levels since they are first excited states. Thirdly there is no worry as to angular distributions of the gamma-rays since the states have spin $\frac{1}{2}$. Fourthly the gamma-rays will come virtually entirely from particle transitions directly to the first excited states and only in negligible amount from gamma-cascades from higher states. This is because all higher states are unstable against heavy emission (to ^{4}He+^{3}He or ^{4}He+^{3}H) and this particle break-up will overwhelm any tendency to emit gamma-rays to the lower states. In any case it can be checked that the contribution from such a cascade is negligible by looking for the higher energy gamma-ray which is very different in energy from that from the first excited state (4·22 Mev for ^{7}Be and 4·13 Mev for ^{7}Li).

Because of these favourable indications that the experiment would be clean in interpretation as well as in execution we have measured the yield of low energy gamma-rays from the bombardment of ^{6}Li with deuterons over the energy range above 200 Kev. It was originally hoped to carry the observations to deuteron energies of several Mev but for reasons that will be explained the present measurements have an upper limit at a deuteron energy of 1·8 Mev.

§ 2. EXPERIMENTAL DETAILS AND RESULTS

The target used was of ^{6}Li$_2$O with a thickness of 40 μg/cm^2 deposited on platinum of thickness 0·005 in. The stopping power was therefore about 60 Kev for deuterons of 200 Kev and 20 Kev for deuterons of 1 Mev. The target was bombarded with very tiny beams of deuterons from the Brookhaven Research Van de Graaff. The radiations were examined with a NaI(Tl) crystal, a cylinder of length 5 cm and diameter 4 cm, placed close to the target in the 'end-on' position at 0° to the deuteron beam. Between the ^{6}Li$_2$O target and the crystal the gamma-rays traversed 1 mm of brass.

A typical spectrum is shown in fig. 1. This was taken at a low deuteron energy where the background corrections are small. Corrections have been made for the background in the crystal immediately after the deuteron beam is interrupted and for the flattish spectrum observed at slightly higher energies due to gamma-rays of higher energy from the target, from elsewhere in the machine and from neutrons. The first correction amounts to 3% of the spectrum shown while the second correction is of 10%.

To analyse such spectra the response of the crystal to several gamma-rays was determined. These were the 411 Kev line from the decay of ^{198}Au, the same 477 Kev line as follows proton emission to ^{7}Li (obtained from the decay of ^{7}Be), and annihilation radiation. From these lines the response of the crystal to the 430 Kev line of ^{7}Be following neutron emission could be accurately determined. Spectra corresponding to pure 430 Kev and pure 477 Kev radiation were then mixed together to give the best fit to the experimental spectrum of the mixed radiations. This fitting is shown on the figure where it is seen to be quite good. The fitting is quite sensitive to changes in the proportions and it is felt that it is good to ±4% in the peak heights. This does not mean that this accuracy also obtains for the determination of the relative intensities because several corrections must now be applied of which the most important (apart from the differing widths of the two peaks which is accurately known) are the different sensitivity of the crystal for the two radiations and the different fraction of all the gamma-rays detected by the crystal that give pulses in the peaks of the distributions for the two radiations. These two corrections are in the same sense, the higher energy gamma-ray being less efficiently detected and also giving a smaller fraction of pulses in the peak, and amount together to a correction factor of 1·19. While this type of correction has

Fig. 1

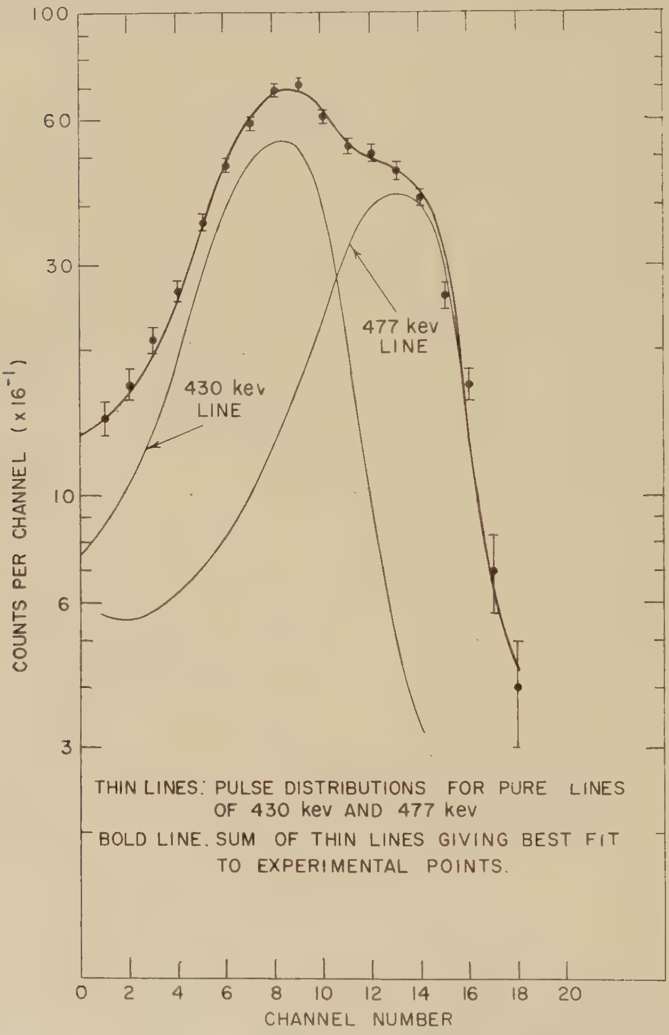

Spectrum seen in NaI (Tl) crystal of the mixed radiations of 430 kev from the first excited state of ^{7}Be formed in the reaction ^{6}Li(d, n)^{7}Be and of 477 kev from the first excited state of ^{7}Li formed in the reaction ^{6}Li(d, p)^{7}Li. The deuteron energy was 200 kev. The thin lines show the shapes of the distributions for pure 430 kev and pure 477 kev radiation with intensities adjusted so that the sum of these pure distributions, shown by the bold line, gives the best fit to the experimental points. This spectrum was taken with a bias of 35 channels ; it has been corrected as described in the text for the background observed when the deuteron beam is interrupted and for the effects of higher energy gamma-rays.

been quite well studied for the crystal used we feel that because of this and other uncertainties in the fitting we should not claim better than 10% systematic accuracy in the determination of the relative gamma-ray intensities.

At the lower deuteron energies the corrections were small and interpretation of the composite spectrum was easy. However as the deuteron energy was raised two difficulties of similar origin arose. Both were due to the production in the bombardment of positron active bodies. The first to show up was ^{13}N of half-life 10 min made by $^{12}C(d, n)^{13}N$ from stray carbon. At the low energies the annihilation line observed with the deuteron beam interrupted was almost negligible and, in equilibrium had a peak height of only about 3% of that of the interesting lines. By the time a deuteron energy of 750 kev had been reached however, it had increased to the point where it was about 15% in relative peak height. Above this energy the proportion was almost constant. Accurate corrections could still be made because the runs with deuterons were only 1 minute long and each was followed immediately by the background run for 1 minute with the beam interrupted and then immediately by the next deuteron irradiation. The ^{13}N increased slowly from run to run and, because the cycle was considerably shorter than the half-life of the ^{13}N the subtraction could be made with confidence. By the time the deuteron energy had increased to 2·0 Mev the new positron background, namely the 66 second activity of ^{17}F made by $^{16}O(d, n)^{17}F$ with a threshold at 1·84 Mev from the oxygen of the Li_2O was evident. This had too short a half-life to be accurately taken care of by the present technique and caused the abandoning of work at higher energies. Even before the ^{17}F activity set in there were some indications of a possible short-lived positron activity. This could possibly be 150 of half-life 2 min made by $^{14}N(d, n)^{15}O$ from nitrogen present as nitride in the target. The target had been prepared by oxidation in air of electromagnetically-deposited lithium metal. Under these conditions nitriding should be very slight. The activity if present was very small compared with that of ^{13}N but it would not be well allowed for by our subtraction procedure. For this reason the results above a deuteron energy of about 1·2 Mev are less reliable than the rest. The second background discussed above namely the counts in the channels above the peaks of the low energy gamma-rays increased steadily. It increased from 10% at the lowest energies to 30% at a deuteron energy of 1 Mev and at 2 Mev it was 50%. This is a big correction and obviously the necessary assumption that this background is flat underneath the interesting peaks is doubtful. Because of these two increasing backgrounds accuracy in estimating the intensity ratios decreases considerably at the higher deuteron energies.

As a check on the origin of these low energy gamma-rays a search was made for the gamma-rays of 4·13 Mev from ^{7}Li and 4·22 Mev from ^{7}Be that could give rise to them by cascade deexcitation from the second excited states of the two nuclei in the unlikely event that gamma-ray emission competed significantly with heavy-particle decay of these states. The search was made at a deuteron energy of 1·8 MeV and no trace of the high energy lines was found. Their intensity was certainly less than 10% of that of the low energy lines and so their importance in leading to the first excited states is negligible. The 3·09 MeV line from the first excited state of ^{13}C formed by $^{12}C(d, p)^{13}C$ showed up very well in keeping with the production of ^{13}N in the mirror reaction.

Fig. 2

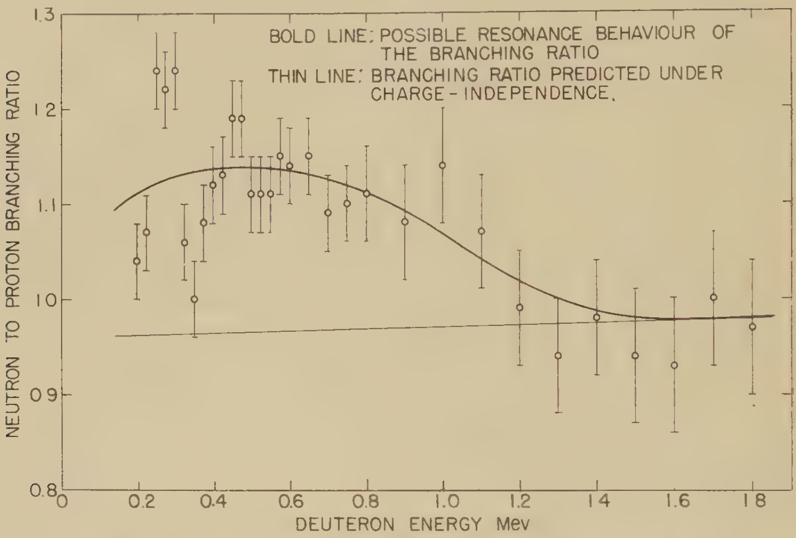

The experimentally determined neutron to proton branching ratio for transitions to the first excited states of ^{7}Be and ^{7}Li as a function of bombarding deuteron energy. The bold line shows the possible resonance behaviour indicated by the experimental results. The thin line shows the prediction of the branching ratio under charge independence corrected for the influence of the Coulomb barrier on the proton emission.

Other possible sources of the 477 KeV gamma-rays are the decay of the ^{7}Be formed in the (d, n) reaction and inelastic deuteron scattering into the first excited states of residual ^{7}Li in the ^{6}Li target. The first origin need not concern us because it was negligible on account of the 53 day half-life and in any case would have been accurately taken care of by our background procedure. The second origin has an energetic threshold at 614 KeV. but an effective threshold at a considerably higher energy an account of the Coulomb barrier. The fact that emission of high energy neutrons and protons will always give larger cross sections than the emission of low energy deuterons and the stated purity of greater than 99% of the electromagnetically separated ^{6}Li combine to make this source of trouble negligible also.

The results of these investigations corrected for the two backgrounds in the manner described and for the crystal factors discussed above are displayed in fig. 2. The errors there shown indicate the uncertainties in the ratios of peak heights and do not include the possible 10% systematic error mentioned earlier. It is felt that this error if it exists is in the sense that the neutron to proton branching ratio as indicated in fig. 2 is too big.

§ 3. Discussion

We must now compare the experimental results displayed in fig. 2 with what is expected on the basis of charge independence. That principle requires that the neutron and proton reduced widths be the same. To translate this into a neutron to proton branching ratio we must correct for the differing momenta of the two particles which is done exactly and then for the differing penetrabilities. This latter correction cannot be made exactly because we do not know what angular momenta are involved in the outgoing particle waves. Nor are we sure of the relative importance of stripping and compound nucleus formation. As we remarked earlier there are some indications that at low bombarding energies at least compound nucleus formation is the more important mechanism and we have made this assumption over the whole range of interest here. Since to a very rough approximation the total effect of the potential barrier on the outgoing particles is the sum of the effects of the centrifugal barrier, common to both neutrons and protons, and the Coulomb barrier felt only by the protons we have applied as correction factor simply the s-wave Coulomb barrier penetrability. This was computed with a radius constant of $1{\cdot}35 \times 10^{-13}$ cm resulting in penetrabilities ranging from 0·85 for the protons produced by deuterons of 0·2 Mev to 0·88 for the protons made at 1·8 Mev bombarding energy. It is because these factors are quite close to unity and presumably cannot be greatly in error that the present comparison of neutron and proton yields is significant. When these phase-space and barrier factors are inserted the theoretical neutron to proton-branching ratio is as shown by the thin line of fig. 2. The branching ratio has only a slight dependence on the deuteron energy because the phase space factor favours the neutrons relative to the protons as the deuteron energy rises but the change in the barrier factor simultaneously favours the protons.

It is seen from fig. 2 that the experimental and theoretical branching ratios are very closely the same. Since the measurements extend over a range of excitation that probably covers a dozen levels of the compound nucleus this good behaviour is unlikely to be the result of an accident and argues for the validity of charge independence (or, more properly, for charge symmetry since we are involved with $T_Z = \pm\frac{1}{2}$ mirror systems as the residual nuclei). But it seems probable that the figure also shows some deviations from the theoretical expectation though this is not sure. Our possible systematic error of 10% would, as already noted, most likely lower the experimental ratio and so give better accord with theory. Again the correction for the Coulomb barrier was about 15% and so the theoretical line also carries some uncertainty. The most significant observation would be a marked variation of the experimental ratio with deuteron energy. This we appear to see, the ratio declining at the higher energies. But this is the sense to be expected if there were indeed some short-lived positron contamination of importance there. However the lowered ratio remains more-or-less constant over a 600 Kev increase in deuteron energy in a region where we should expect the $^{14}N(d, n)^{15}O$ reaction to become more important and this argues that the results are probably reliable. The sharp change in ratio at a deuteron energy of 250–300 Kev appears to be significant but we cannot be sure of it. So although we cannot maintain for certain that all our experimental ratio measurements are not consistent with the values of, say, 1·1 and although we cannot argue in view of the various corrections and uncertainties that this is inconsistent with complete charge independence, there is some slight indication of a general 'resonance-like' change in the ratio as indicated by the bold line of fig. 2, reaching a maximum around a deuteron energy of about 450 Kev. As we remarked earlier in § 1 if reactions such as the present one show in their total cross section traces of resonance structure in the region of generally overlapping and broad levels then we might anticipate that the Coulomb perturbation may break down the isotopic spin rules despite the speed of the reaction. We could then expect in such a region to find isotopic spin forbidden processes taking place and also departures from other consequences of charge-independence such as that studied here. If our branching ratio indeed shows a resonance around a deuteron energy of 450 Kev then we may expect a resonance also to show in the conventional sense of a maximum in the cross section. However, whereas the effect as we detect it in this investigation, in a partial relaxation of the isotopic spin rule, will be strongest at the true resonance position of the compound nucleus, the resonance in the cross section will be shifted in energy because of the superimposed effect of the Coulomb barrier. In fact the $^{6}Li(d, p)^{7}Li$ reaction (Whaling and Bonner 1950) is weakly resonant at a deuteron energy of about 1 Mev ; when the Coulomb barrier is removed the true resonance position of the compound nucleus is found as about 400 Kev, rather close to our own possible ' resonance '. The $^{7}Li(d, \alpha)^{4}He$ reaction investigated by the same authors has a maximum cross section at about 600 Kev deuteron energy which corrects similarly to a true energy of 347 Kev. The $^{6}Li(d, n)^{7}Be$ reaction (Baggett and Bame 1952) shows no resonance to the total cross section itself but when the Coulomb barrier is removed a resonance appears at a deuteron energy of about 450 Kev. All these reactions then indicate that a resonance is formed at a true position corresponding to just about the deuteron energy at which our results may indicate an anomaly in the branching ratio and this is just what we should expect. All the observed resonances are broad, of the same order as our own.

We may conclude then that the predictions of charge independence are borne out with an accuracy of better than 15% and that the possible anomaly that we observe is in accord with what might be expected from the behaviour of the total cross sections in this region.

Another possible interpretation of the change in branching ratio at the higher energies may be touched upon and that has to do with the mechanism of the reaction. If the reaction goes chiefly by compound nucleus formation then the proton yield is diminished because the proton has difficulty in getting out of the nucleus. On the other hand if the chief mechanism is stripping the neutron yield is now diminished because the proton has difficulty in getting into the nucleus. So if we change over from compound nucleus formation to stripping we might expect an accompanying diminution in the neutron to proton branching ratio such as we observe. As we have remarked earlier in § 1 stripping seems to become important in the present reactions at about 1 MEV which is where our branching ratio falls off. If in addition the structure of the nucleus departed from the provisions of charge independence in the sense that neutrons were denser at the surface than protons this change of ratio accompanying the change of mechanism would be accentuated because a larger neutron than proton reduced width means that neutrons escape more easily from a compound nucleus reaction but are accepted more easily in a stripping reaction.

ACKNOWLEDGMENT

I should like to thank Mr. A. G. Rubin for his help in making these measurements.

REFERENCES

BAGGETT, L. M., and BAME, S. J., 1952, *Phys. Rev.*, **85**, 434.
HIRST, F., JOHNSTONE, I., and POOLE, M. J., 1954, *Phil. Mag.*, **45**, 762.
NICKELL, W. E., 1954, *Phys. Rev.*, **95**, 426.
SAWYER, G. A., and PHILLIPS, J. A., 1953, Los Alamos report LA 1578.
SHIRE, E. S., and EDGE, R. D., 1955, *Phil. Mag.*, **46**, 640.
WHALING, W., and BONNER, T. W., 1950, *Phys. Rev.*, **79**, 258.
WILKINSON, D. H., 1956, *Phil. Mag.*, **1**, 379.

Observation of Helicoidal Dislocation Lines in Fluorite Crystals†

By W. Bontinck and S. Amelinckx
Laboratorium voor Kristalkunde, Rozier, 6, Gent, Belgium

[Received June 22, 1956]

Dislocations, irregular dislocation networks and related features have been observed in natural (Bontinck and Dekeyser 1956) and in synthetic fluorite crystals (Bontinck, unpublished results).

After a thermal treatment of synthetic fluorite crystals at very high temperature (1100°c), in a reducing atmosphere with an excess silver, decorated helix shaped lines were observed (photo. 1, Plate). They were identified as helicoidal dislocations. It is the object of this note to interpret their formation.

The theory of dislocations predicts a number of mechanisms of conservative and non-conservative motion of dislocations, which lead to the formation of either plane or conical spirals (or concentric loops) (Seitz 1952, Cottrell and Bilby 1951, Bardeen and Herring 1952, Bilby 1954, Suzuki 1954, Frank and Read 1950, Read 1953).

In every case the resulting shape of the dislocation line is either a plane spiral or a helix of which the step is equal in magnitude to the Burgers vector of some screw dislocation. The step of the observed helices is far too large to allow an explanation on this basis. Moreover the characteristic configuration of dislocation lines which should be present e.g. in the case of mechanical twinning, according to the pole mechanism is not observed. Even allowing for some climbing after mechanical twinning would not account for the observed configuration of lines.

So far, discussions of the mechanism of climb have been restricted to the case of pure edge dislocations (Bardeen and Herring 1952, Barnes 1954, Read 1953). Dislocations of mixed character however are also capable of climbing. We suggest that this can lead to the formation of a helix with an arbitrary step. Let us consider e.g. the dislocation line AB, fig. 1(*a*) which is pinned at both ends e.g. at nodes of the dislocation network. One can imagine that this dislocation line is a zig-zag line (lying in the plane determined by the line and the Burgers vector) of a number of small sections which are alternatively pure edge and pure screw, fig. 1(*a*). The edge components jog from one lattice plane (climb plane) to the next. When two edge sections climb they will eventually bend somewhat and pull the screw part, which is in between, with them. In this manner the dislocation line will be able to climb as a whole, the easier the less it has screw character.

As the endpoints are fixed the dislocation will wind up in a similar way as in the Bardeen–Herring case (or spiral prismatic case) (Seitz 1952);

---

† Communicated by the Authors.

there is however an essential difference, for in general no closed loops can be formed because no two arms of the spirals will meet in the same climb plane during winding up. The result will be a helix with an arbitrary step, connecting the two endpoints, fig. 1(*c*).

Fig. 1

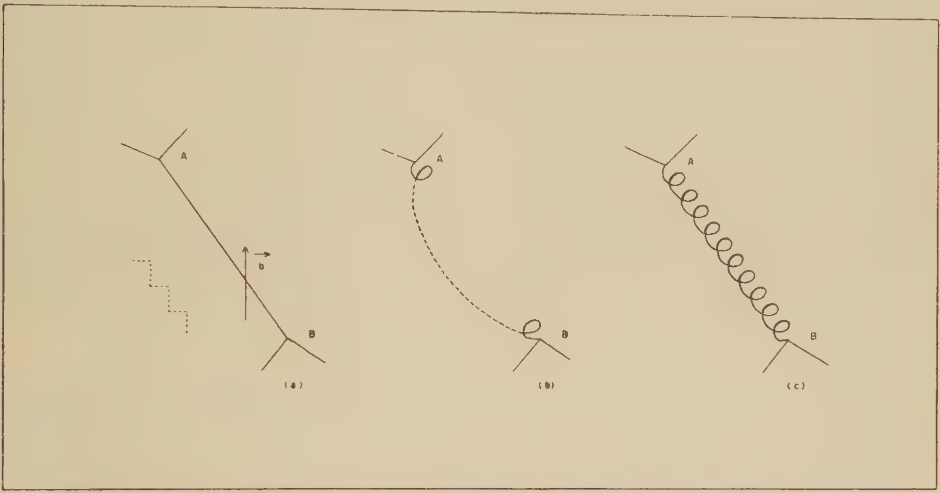

The winding up into a helix of a climbing dislocation of mixed character.

There will be a minimum radius of curvature for the dislocation line for a given concentration of vacancies ; this is one of the factors determining the shape of the helix. During winding up the dislocation line lengthens, i.e. its line energy increases ; there will as a consequence be a limit at this process when no longer energy is gained by the loss of vacancies at the dislocation line.

The intersection of windings of the helix with other dislocation lines of a suitable Burgers vector may occasionally result in the formation of closed loops (photo. 2, Plate).

Fig. 2

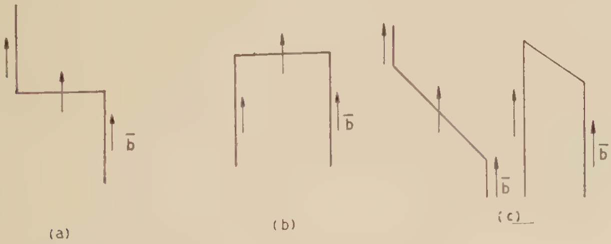

Configuration of dislocation lines responsible for :
(*a*) Spiral Prismatic Dislocation (Seitz 1952)
(*b*) Bardeen–Herring mechanism (1952)
(*c*) the here discussed phenomenon.

Seitz pointed out that there is a relation between the described mechanism and the spiral prismatic dislocation (Seitz 1952) on one hand, and the Bardeen–Herring mechanism (1952) on the other hand. The configuration of dislocation lines responsible for the three mechanisms are shown for comparison on fig. 2. It is now evident that our mechanism (*c*) is intermediate between (*a*) and (*b*).

As the fluorite crystals which contain the described helicoidal dislocation lines have been in temperature conditions where climb is important it is reasonable to consider the phenomenon just described as responsible for their formation.

Acknowledgments

The authors are grateful to Prof. Dr. W. Dekeyser for the stimulating interest taken in this work which is part of a research programme (C.E.S.) supported by I.R.S.I.A. We are also very much indebted to Prof. F. Seitz for interesting discussions.

References

Bardeen, J. and Herring, C., 1952, *Imperfections in Nearly Perfect Crystals* (New York : John Wiley & Sons Inc.), p. 277.
Barnes, R. S., 1954, *Acta Metallurgica*, **2,** 380.
Bilby, B. A., 1954, *Report of the Bristol Conference on Defects in Crystalline Solids* (London : Physical Society), p. 132.
Bontinck, W., 1956 (to be published).
Bontinck, W., and Dekeyser, W., 1956, *Physica* (in the press).
Cottrell, A. H., and Bilby, B. A., 1951, *Phil. Mag.*, **42,** 573.
Frank, F. C., and Read, W. T., 1950, *Phys. Rev.*, **79,** 722.
Read, W. T., 1953, *Dislocations in Crystals* (McGraw-Hill), p. 79.
Seitz, F., 1952, *Advances in Physics*, **1,** 43.
Suzuki, T., 1954, *Sci. Rep. Res., Tohoku University*, **A6,** 309.

Magneto-Resistance in Metals †

By D. K. C. MacDonald
Division of Pure Physics, National Research Council, Ottawa, Canada

[Received June 12, 1956]

Abstract

Experiments are reported in which novel results are found on the magneto-resistance of sodium and rubidium. Measurements have been made both on plate-like specimens which show very strong anisotropy in the magnetic field, and on a cylinder of diameter large compared with the mean free path, l, of the electrons. The anomalous behaviour appears certainly to depend on the attainment of large values of the ratio l/r, where r is the orbital radius of a free electron in the magnetic field.

As the theory stands today, magneto-resistance in metals is ascribed essentially to anisotropic features of the electron velocity and/or relaxation time. The detailed theory, as developed by Bethe (1931), Peierls (1931), Wilson (1953), and others, leads one to expect in a given metal that the magnitude of the resistive increase $\{(R_{\mathrm{H}} - R_{\mathrm{H}=0})/R_{\mathrm{H}=0}\} \equiv \{\Delta R_{\mathrm{H}}/R_{\mathrm{H}=0}\}$ will depend closely on the ratio l/r, where l is the electron mean free path and r the radius of an electron orbit in the applied magnetic field. This is found to be in generally good agreement with the experimental facts, and it is also broadly true that the metals usually considered to be nearly 'ideal' (in particular sodium, and to a lesser degree the group I metals as a whole) show a lower order of magneto-resistance for a given value of l/r than polyvalent metals such as antimony or gallium (cf. e.g. the reviews by MacDonald and Sarginson 1952, or MacDonald 1956). It is also a general prediction that in bulk metal (i.e. where all dimensions are much larger than the mean free path) a magnetic field will only cause an *increase* in resistance ; it has also been found experimentally that the magnitude of magneto-resistance does not vary greatly with the relative orientation of magnetic field and specimen current except in single crystals of some metals.

However much still remains unexplained in magneto-resistance in metals, such as the remarkably linear increase of resistance with magnetic field observed in certain metals where the theory would predict either a saturation law or a simple quadratic increase of resistance with magnetic field.

In connection with an investigation of the Hall effect in the alkali metals a series of measurements has been made on the resistance of thin plates of pure sodium and rubidium in magnetic fields at low temperatures :

---

† Communicated by the Author.

these in turn have led to some experiments on the apparent resistance of a 'thick' cylinder of sodium, and the results appear sufficiently remarkable to call for some publication at this time. We are as yet unable to make any very significant theoretical suggestions to explain these results, although it is clear that their occurrence depends on the fact that by experiments on extremely pure sodium† at liquid helium temperatures and in relatively high magnetic fields (up to ~25–30 kgauss) we have been able to achieve very high values of the ratio l/r (up to at least 50). The theory of magneto-resistive effects based on the Boltzmann equation is in fact only valid for $l/r \ll 1$, although it has often been assumed that the theoretical predictions would not be seriously affected when $l/r \gtrsim 1$. It is of course possible that some relatively trivial cause can be found to account for the observations, or for part of them, but quite numerous experiments have shown a very satisfactory degree of reproducibility and no obvious explanation has yet been found.

In fig. 1 are shown measurements in liquid helium ($T \approx 4{\cdot}2^\circ$K) on a 'plate' of very pure sodium. The sodium was cast under high vacuum into a suitable soft glass mould (see inset sketch). This makes it difficult to assess dimensions at all exactly. After the experiments the specimen was broken to attempt to measure the internal dimensions optically with some precision, but unfortunately the mould disintegrated rather completely; rough estimates (using resistivity and Hall data) are given on the sketch. The resistance was measured using the current and potential leads (of platinum) sealed into the relatively large end-bulbs on the specimen. The Hall voltage was measured using the three central leads; these however were entirely disconnected at the specimen during the resistance measurements to ensure that they could not contribute somehow to a false reading. In a second specimen (see fig. 2) no leads at all were inserted on the plate section.

It will be seen that with the plane of the specimen parallel to the magnetic field‡ (curves B) the resistance rises linearly (and rather precisely so) to a value about twice that observed in zero magnetic field. This magnitude and rate of increase agrees with that observed in the past (cf. e.g. MacDonald, loc. cit.) on cylindrical specimens and generally accepted as 'bulk' behaviour §. However when the specimens are turned through 90° about their axis, so that the plane of the specimens is now perpendicular to the magnetic field, the resistance then rises rapidly with increasing field (the rate being somewhat less than quadratic—curves A); with $H \approx 25$ kgauss the resistance in specimen No. 1 was more than 20 times that in zero field, and in specimen No. 2 the ratio approaches 10. In this same position the Hall voltage was measured in specimen No. 1 (curve C) and its behaviour appears quite normal. In fig. 3 is shown the detailed variation of resistance with rotation of the specimen about its axis perpendicular to the magnetic field. Deducing l from the conductivity formula $\sigma = Ne^2l/mv$ for measurements in zero magnetic field, and r from the expression mvc/eH, we find that $l/r \approx 1$ for $H \approx 500$ gauss; consequently $l/r \gg 1$ obtains in figs. 1 and 2. Further experiments which have been made to explore the behaviour of sodium specimens of this kind in more detail in the region $l/r \approx 1$ will be reported later.

---

† For which I am indebted to Messrs. Philips of Eindhoven, Netherlands and Mitcham, Surrey.

‡ Throughout all these experiments the magnetic field remains perpendicular to the nominal axis of current flow.

§ We note however that the work of White and Woods (1956) has also drawn attention to some doubt about what should be accepted specifically as the bulk behaviour.

Fig. 1

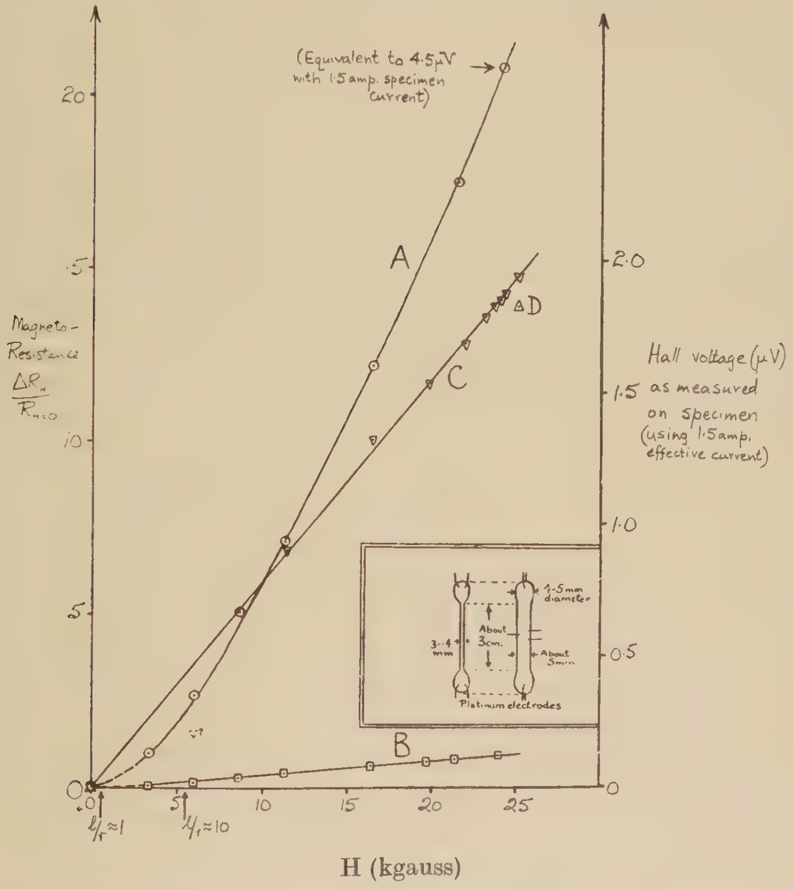

Magneto-resistance and Hall voltage of Sodium No. 1 plate specimen ($R_{4\cdot2°\mathrm{K}}/R_{294°\mathrm{K}} \approx 2\cdot8_5 \times 10^{-4}$).

A : Resistance as measured with plane of specimen perpendicular to H.
B : Resistance as measured with plane of specimen parallel to H.
C : Hall voltage.
D : Hall voltage as measured at room temperature.

A rubidium 'plate' specimen was next measured whose mean free path was such that $l/r \approx 1$ should occur at about $H \approx 6\cdot5$ kgauss. The results in fig. 4 confirm rather strikingly how the anomalous behaviour depends vitally on the onset of $l/r \gtrsim 1$. The rotational pattern is similar to that for the sodium specimen in fig. 3.

Following these experiments on plates, we were led to examine the behaviour of cylinders of sodium whose diameter was very large compared with the mean free path. Figures 5 and 6 show the results obtained in liquid helium on a specimen of pure sodium cast in a glass mould about 5 mm in diameter (see inset sketch). In a specimen of this size the resistance at 4°K is naturally very low (about 2×10^{-8} ohm), so that even with a measuring current of 5 amperes considerable sensitivity was required from the galvanometer amplifier used for the work. The results are sufficiently surprising to require careful checking for spurious effects†; we are reasonably confident that no 'trivial' artefact is responsible and the reproducibility is rather satisfactory. In fig. 5 is shown the variation of apparent resistance (i.e. the potential difference

Fig. 2

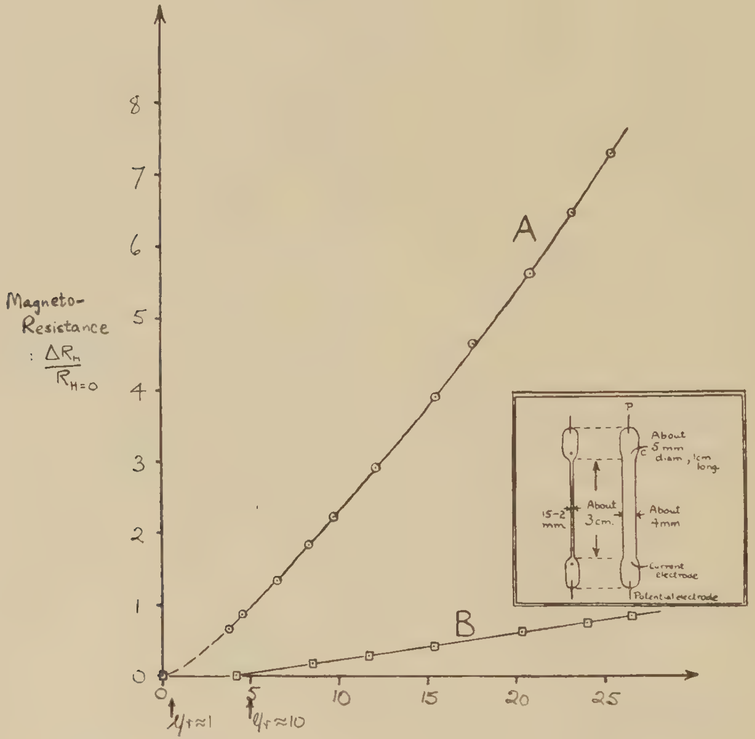

Magneto-resistance of Sodium No. 2 plate specimen ($R_{4\cdot2°K}/R_{294°K}\approx2\cdot2\times10^{-4}$).

A : Resistance as measured with plane of specimen perpendicular to *H*.

B : Resistance as measured with plane of specimen parallel to *H*.

---

† I am grateful to Dr. R. G. Chambers for his comments and suggestions.

observed at the terminals 1 when current is passed through the terminals 2) when the specimen was placed with its axis perpendicular to the magnetic field†. The surprising feature, when one recalls that the diameter of the specimen is at least 25 times the electron mean free path, is that the apparent resistance at the higher fields falls far below that in zero field.

Fig. 3

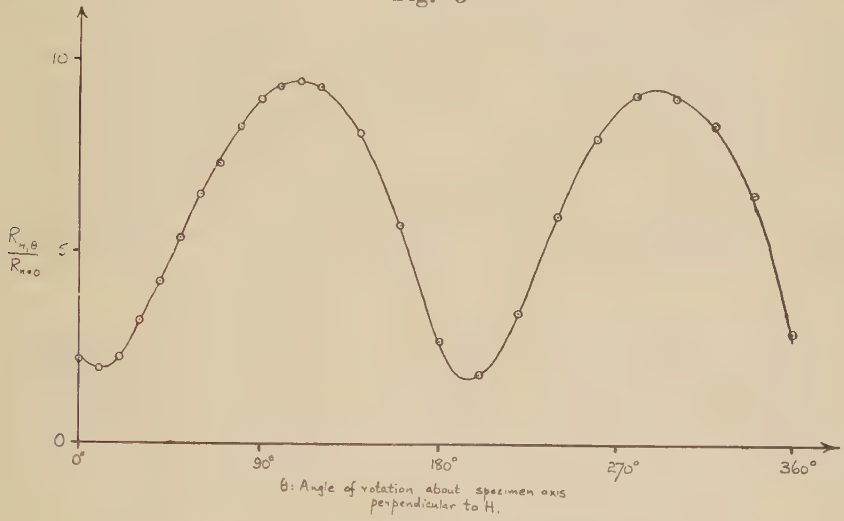

Variation of resistance of Sodium No. 2 plate specimen with rotation ($H \approx 24{\cdot}5$ kg ; $\theta=0°$ corresponds approximately to curve B in fig. 2 ; $\theta=90°$ corresponds approximately to curve A in fig. 2).

Figure 6 shows the variation of apparent resistance with rotation of the specimen about its axis perpendicular to the magnetic field. The apparent resistance now actually becomes *negative* at certain angular settings (that is to say, the potential difference measured *reverses* in sign compared with that measured in zero magnetic field). One could suggest that this must mean that a relatively strong electric field of opposite sign to that in the main body of the specimen is generated at the ends of the cylinder. Evidently further experiments are needed to explore the potential distribution‡.

The rotational pattern of fig. 6 shows also that the potential measured is *not* symmetrical with reversal of H (in contrast to the plate results—

---

† The apparent resistance varies with rotation about the axis (fig. 6) and fig. 5 corresponds to one particular setting.

‡ In the *plate* specimens the current density in the ' bulbs ', which have a relatively large volume, must be very small compared with that in the plate section, and any electric fields generated in the bulbs should therefore be small. This was confirmed by interchanging current and potential leads in the experiments on the plate specimens, which had little effect on the results. On the other hand, interchange of the leads in the case of this cylindrical specimen markedly altered the rotational pattern, and suggested an effect similar to an angular displacement of the specimen.

see fig. 3). This suggested that the magnitude of the potential might also be found to depend on the direction of current in the specimen. The data in figs. 5 and 6 would not show this directly, since they were taken with complete reversal of specimen-current to double the sensitivity of measurement, instead of simply switching the current on and off.

Fig. 4

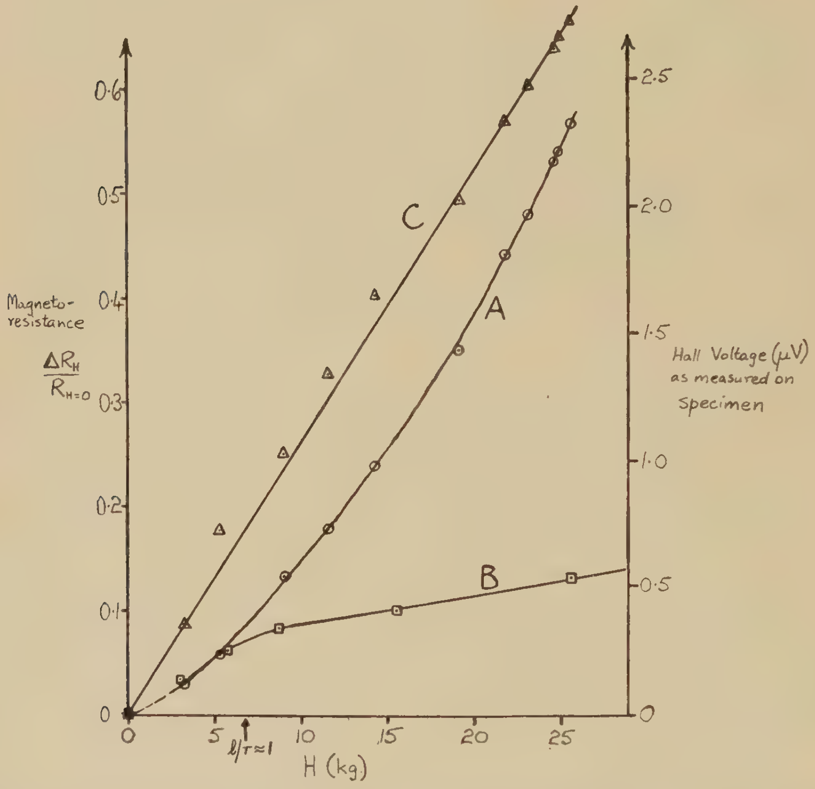

Magneto-resistance and Hall voltage of Rubidium plate specimen (plate length : 4·2 cm ; plate breadth : about 7 mm., plate thickness : 0·5–0·6 mm ; end bulbs (spherical) : about 6 mm diameter ; $R_{4\cdot2^\circ\mathrm{K}}/R_{294^\circ\mathrm{K}} \approx 3\times10^{-3}$.
A : Resistance as measured with plane of specimen perpendicular to *H*.
B : Resistance as measured with plan of specimen parallel to *H*.
C : Hall voltage.

It was indeed found that while in *zero* magnetic field the potential was essentially symmetric in the current, marked asymmetry occurred under the magnetic field (see table). This again suggests further experiments to explore symmetry relations between current and magnetic field.

It is possible that the glass moulds themselves cause some physical strain on the metal (this always presents itself as somewhat of a problem with work on the alkali metals) which may play *some* rôle in these experiments ; the rather low residual resistance ($R_{4\cdot2^\circ\mathrm{K}}/R_{294^\circ\mathrm{K}} \approx 2\text{–}4\times10^{-4}$)

suggests however that it cannot be very important and I do not think this can be a dominant factor.

Fig. 5

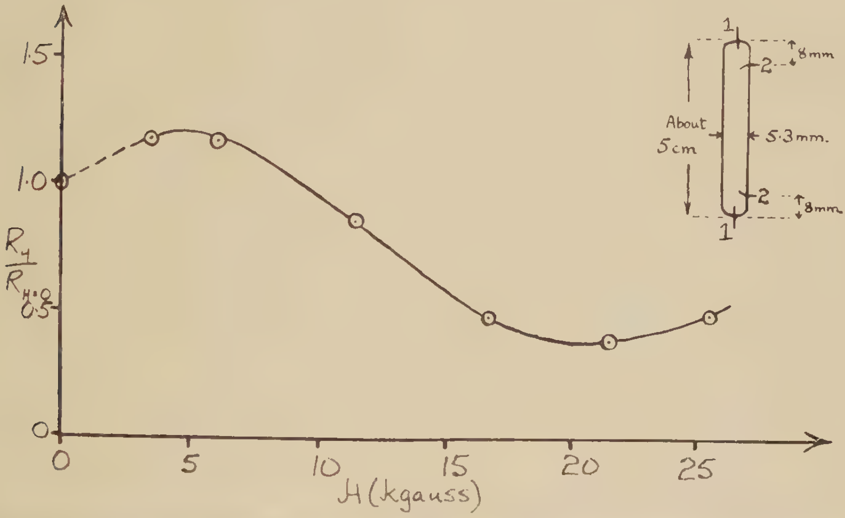

Variation of apparent resistance of sodium cylindrical specimen with intensity of magnetic field at a particular angular setting $(R_{4\cdot 2^\circ\mathrm{K}}.\ R_{294^\circ\mathrm{K}} \approx 4\cdot 2 \times 10^{-4})$.

Fig. 6

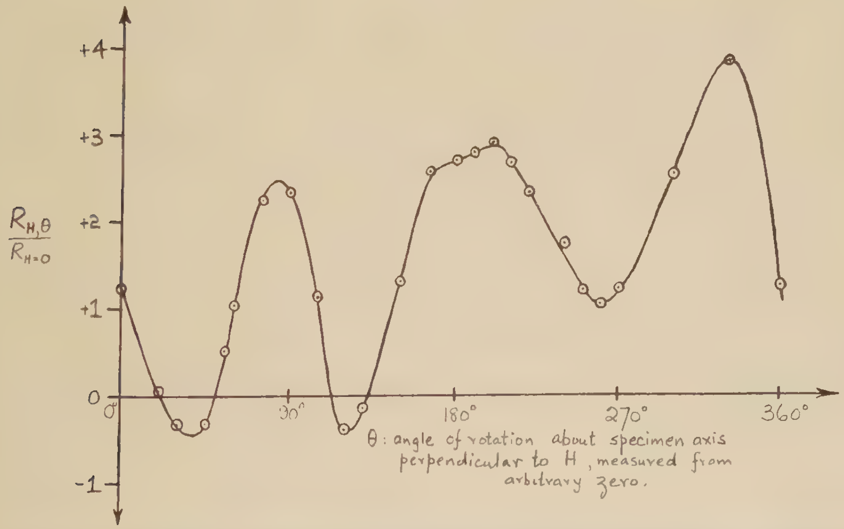

Variation of apparent resistance of sodium cylindrical specimen with rotation about axis perpendicular to magnetic field $(H \approx 24\cdot 5\ \mathrm{kg})$.

As far as I know, the only magneto-resistive work at all similar to the present results is that of Olsen and Rinderer (1954) on wires of copper where, using very high pulsed magnetic fields (up to ~150 kgauss) a value of $l/r \approx 8$ was achieved. Their results show that above $l/r \approx 2$

H (kgauss)	θ	I (amps)	Potential deflection on galvanometer (cm)
0	—	+5 −5	+1·12 −1·20
24·5	30°	+5 −5	0 ; +0·05 +0·8
24·5	330°	+5 −5	+3·55 −5·70

the increasing longitudinal magneto-resistance (magnetic field parallel to specimen current) appears rather abruptly to become *linear* with magnetic field, while the transverse magneto-resistance continues to rise approximately quadratically.

Note added in proof (*November* 1956)

In later experiments on Corbino disks it has been found that this type of apparent asymmetry with direction of measuring current can occur in zero magnetic field if the measuring current is sufficiently great. Current-reversal, however (used otherwise generally in this work), eliminates the effect from the reading. Presumably then in the sodium cylinder the asymmetry observed when the magnetic field is applied must be ascribed to a magneto-thermoelectric effect arising from high current density near the electrodes. Dr. Chambers, in correspondence, found the asymmetry with measuring current very hard to accept as an intrinsic effect.

Further measurements on sodium cylinders of similar size (but of different electrode structure) to that shown in fig. 5 showed no appreciable asymmetry with measuring current, but still displayed rather bizarre patterns of resistance variation with angular rotation when $l/r \gg 1$.

ACKNOWLEDGMENTS

I am grateful to Mr. A. A. M. Croxon for his able technical assistance with these experiments, to Mr. B. Evans for his patience and skill in making the soft glass moulds, and to my colleagues for their interest in the results and for discussions ; Dr. T. H. K. Barron's comments on this note were particularly helpful. I should also like to thank Dr. R. G. Chambers for correspondence.

REFERENCES

BETHE, H. A., 1931, *Nature, Lond.*, **127,** 336.
MACDONALD, D. K. C., 1956, *Handb. d. Phys.*, Vol. 14, pp. 137–197.
MACDONALD, D. K. C., and SARGINSON, K., 1952, *Rep. Prog. Phys.* (London : Physical Society), **15,** 249.
OLSEN, J. L., and RINDERER, L., 1954, *Nature, Lond.*, **173,** 682.
PEIERLS, R. E., 1931, *Ann. Phys., Lpz.*, **10,** 97.
WHITE, G. K., and WOODS, S. B., 1956, *Phil. Mag.*, **1,** 846.
WILSON, A. H., 1953, *The Theory of Metals* (Cambridge : University Press), 2nd edition.

On the Mechanism of Work Hardening in Face-Centred Cubic Metals, with Special Reference to Polycrystalline Copper†

By P. FELTHAM and J. D. MEAKIN
The University, Leeds

[Received February 17, 1956; and in revised form July 10, 1956]

ABSTRACT

Tensile specimens of oxygen-free polycrystalline copper (99·991%) were annealed for various periods *in vacuo*, in the range 500–700°C so as to obtain variations in the grain sizes and yield points. The initial rate of work hardening of all specimens was linear up to strains of about 1·5%, and independent of the magnitude of the yield stress. This hardening appeared to be of the type responsible for the linear hardening which follows easy-glide in single crystals, the theory of which has recently been developed by Friedel. At higher strains parabolic hardening occurred. In this stage the coefficient of work hardening, χ_p, defined as the ratio $d\sigma^2/d\epsilon$, where σ and ϵ are the tensile stress and strain respectively, was found to obey the relation $\chi_p \simeq G\sigma_Y \pi$, i.e. it was proportional to the product of the shear modulus G, and the tensile yield stress σ_Y. This equation is derivable from Mott's theory, in which parabolic hardening is regarded as resulting from the action of the long range stress fields of piled up dislocation arrays on Frank–Read sources in the grains.

§ 1. INTRODUCTION

IN a recent paper Friedel (1955) developed the theory of the linear hardening which is observed after the cessation of easy-glide in face-centred cubic single crystals at sufficiently low temperatures. He assumes that all the Frank–Read sources of the operative slip system in the crystal are in action after the termination of easy-glide, and form small active slip planes bounded on all four sides by Cottrell barriers. The linear stage should then be characterized by short slip bands, measuring about 10^{-3} cm, distributed at random throughout the crystal. The lengths and number of the bands should remain essentially constant during this stage of hardening. Experimental evidence supporting these conclusions has been obtained by Blewitt and co-workers (1954) in the case of copper single crystals deformed in the range 4–300°K, and by Lozinskii (1954), who studied slip in the thermally etched surface grains (by hot-stage microscopy) in pure face-centred cobalt at 713°K.

Friedel's theory does not preclude the possibility of observing this type of linear hardening also in well annealed polycrystalline metals of face-centred cubic symmetry. In fact Lozinskii's work and the observations

---

† Communicated by the Authors.

(Crussard 1948) that the stress–strain curves of a number of pure polycrystalline metals cannot, in general, be represented adequately by parabolae over the entire plastic range suggest that under suitable experimental conditions linear hardening should also be observable in face-centred cubic polycrystals.

The principal object of the present work was therefore to make a careful study of the initial stages of work hardening in well annealed pure polycrystalline copper and, if possible, to interpret the results theoretically.

§ 2. Materials and Method

Wires of 2 mm diameter were drawn by means of steel dies from 3 mm thick strips of oxygen-free high-conductivity copper which had been received in the ‘ as rolled ’ condition. An analysis of the metal gave the following results (in parts per million) : Cu 99.991 ; Fe 40 ; Ni 5 ; Pb 4 ; As 0 ; Ag 6 ; Sn 0 ; S 8, and Bi 0. The wire was then cut into equal lengths measuring about 10 cm, and these were annealed *in vacuo* in batches of 3 before being subject to tensile tests in a motor-driven Hounsfield Tensometer. Self-centring long solder grips were used to hold the wires. Careful examination showed that no slipping whatsoever occurred in the grips. The annealing times and temperatures, as well as the true spatial mean grain diameters D, are given in table 1. The grain sizes were determined by the line-intercept method, using a Vickers projection microscope. D was taken to be 1·5 times the mean line-intercept (Spektor 1955). Each tabulated value represents the mean of ten

Table 1

(1)	(2)	(3)	(4)	(5)	(6)	(7)	(8)
1	297	540	75 min at 700°c	1·81	1·92	30·3	24
1a	310	548	75 min at 700°c	1·76	2·25	29·0	32
2	340	619	75 min at 600°c	1·83	2·03	33·2	5·0
2a	349	554	75 min at 600°c	1·58	2·25	33·0	5·0
3	323	568	105 min at 600°c	1·72	2·39	32·8	5·7
4†	329	625	Slow cool from 550°c	1·70	2·91	33·4	3·9
5	386	645	120 min at 550°c	1·67	2·53	37·2	4·6
6†	517	860	105 min at 500°c	1·67	1·94	34·5	2·6
7	386	710	220 min at 550°c	1·84	2·18	36·1	3·0
7a	384	674	220 min at 550°c	1·76	2·15	37·8	3·2
8	390	730	510 min at 500°c	1·87	2·62	38·6	3·3
8a	414	770	510 min at 500°c	1·84	2·17	39·4	3·2

(1) Specimen ; (2) σ_Y kg/cm^2 ; (3) σ_C kg/cm^2 ; (4) annealing ; (5) σ_C/σ_Y ; (6) $\chi_l \times 10^{-4}$ kg/cm^2 ; (7) $\chi_p \times 10^{-6}$ (kg/cm^2)^2 ; (8) $D \times 10^3$ cm.

† Incompletely annealed.

determinations, each obtained with a different line†. The wires were extended at room temperature (18°c) at a constant strain rate of approximately 10^{-3} per second.

§ 3. Experimental Results

The true stress–strain curves of all the specimens were of a similar character, typified by that of specimen 7a (viz. table 1) shown in fig. 1. The points represent measured values. A linear part can be seen to extend over the range of strains from 0·2 to about 1·7%. This is then followed by a parabolic portion. As the initial yielding was not sharp the yield point was in each case taken to be the intersection of the extrapolated straight lines representing the elastic and linear hardening ranges respectively. Experimentally determined conjugate values of σ and ϵ were substituted into the equation

Fig. 1

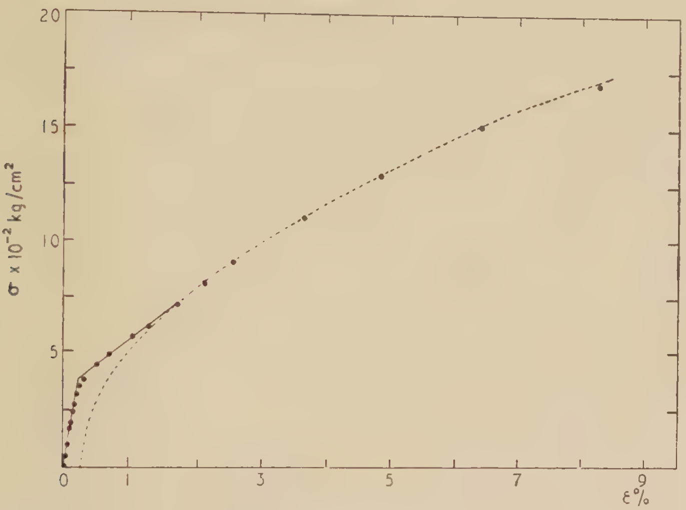

Stress–strain curve of specimen 7a. The equation of the parabola is given by eqn. (2).

$$(\sigma-\sigma_0)^2=\chi_p(\epsilon-\epsilon_0) \qquad (1)$$

in order to determine the origin (σ_0, ϵ_0) of the parabola, and the coefficient of work hardening χ_p. After about half the curves had been analysed in this manner it became apparent that within experimental error σ_0 was equal to zero and ϵ_0 to about $\frac{1}{2}\%$ in all cases. Thus, for example, the equation of the parabola drawn through the non-linear part of the work hardening curve shown in fig. 1 is given by

$$\sigma^2=3{\cdot}8\times10^7(\epsilon-0{\cdot}003)\ (\text{kg/cm}^2)^2. \qquad (2)$$

---

† Larger grain-sizes than those given in table 1 were not used as the ratio (specimen diameter)/(planar grain size) should not be appreciably less than 10 if the specimen is to be regarded as truly polycrystalline.

As $\sigma_0=0$, eqn. (1) yields

$$d\sigma^2/d\epsilon=\chi_p, \qquad (3)$$

and this relation was utilized to obtain the tabulated values of χ_p, i.e. χ_p was found from the slopes of the straight parts of the curves relating σ^2 and ϵ, as is shown in fig. 2 for specimen 7a. The results for all specimens are given in table 1, together with the coefficients of linear work hardening $\chi_l(=d\sigma/d\epsilon)$ obtained from the actual stress–strain curves (e.g. fig. 1). The values of σ_Y, σ_C and of σ_Y/σ_C are also tabulated, σ_C denoting the tensile stress at which the transition from linear to parabolic hardening takes place.

Fig. 2

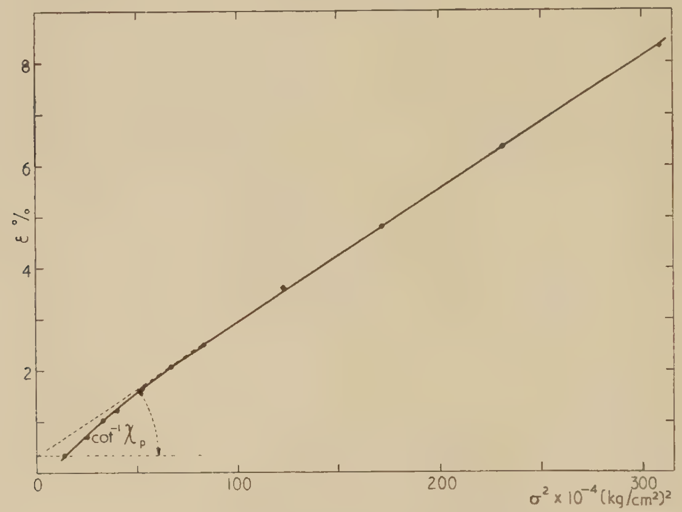

Determination of the coefficient of work hardening χ by means of the σ^2/ϵ -plot. Measured points from specimen 7a.

The linearity of the first part of the work hardening curve is particularly evident from log–log plots of $\sigma-\sigma_Y$ against $\epsilon-\epsilon_Y$. Such a representation of the stress-strain curves of the specimens 7 (full circles) and 7a (empty circles) is shown in fig. 3, where the slope of the line extrapolated to the right has been drawn to be unity, i.e. its slope is

$$d\log(\sigma-\sigma_0)/d\log(\epsilon-\epsilon_0)=1,$$

while, similarly, the slope of the line extrapolated to the left is equal to $\frac{1}{2}$, corresponding to a parabolic law of hardening.

§ 4. THEORY

4.1. *Linear Hardening*

Friedel estimates the coefficient of work hardening of single crystals in the linear stage to be of order $10^{-2}G$, where G is the shear modulus. Actual values of the slopes of the shear stress versus shear strain curves of copper single crystals of various orientations with respect to the tensile axis, deformed between 4 and 300°K (Blewitt *et al.* 1954), lie in the range $1{\cdot}6\times10^4$ to $2{\cdot}4\times10^4$ kg/cm². The mean value of the coefficient of work hardening (in tension) obtained in the present experiments (not including the values of the incompletely annealed specimens No. 4 and No. 6) is $\chi_l = 2{\cdot}25\times10^4$ kg/cm² ($\simeq 5\times10^{-2}G$), which is in very satisfactory agreement with the single crystal values.

Fig. 3

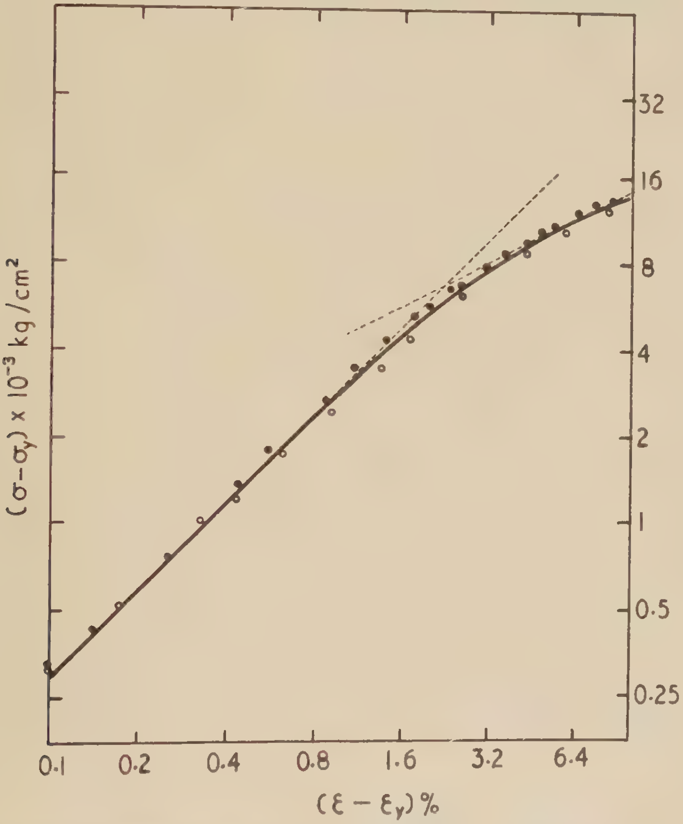

The stress–strain curves of specimen 7a on log–log coordinates, with the yield point taken as origin. The straight lines extrapolated to the right and left respectively represent linear and parabolic work hardening laws.

There appeared to be no relation between χ_l and D, as is evident from table 1. This is to be expected, as Friedel's mechanism should lead to intragranular hardening in which the grain boundaries should play, at best, only a secondary role. Further, the mean value of σ_C (column 3 in table 1) is 638 kg/cm², which is also in good agreement with the value for copper crystals quoted by Friedel, namely $\sigma_C \simeq 600$ kg/cm². (Friedel actually gives the corresponding shear stress τ_C, which we take to be approximately equal to $\frac{1}{2}\sigma_C$.) Thus except for the shorter linear hardening range in polycrystalline copper, due to the higher yield point, the process of linear hardening at any given temperature takes place by the same mechanism in single crystals and polycrystals ; in particular the values of χ_l and σ_C are common to both.

This can also be seen from the temperature-dependence of σ_C shown in table 2. The first four entries are those given by Friedel for single crystals ; the last four were obtained by the authors with polycrystalline specimens in a continuation of the present work. The specimens were annealed at 650°C for $\frac{1}{2}$ hour prior to testing. According to theory the product $\sigma_C{}^2T$ should be constant, as is indeed the case.

Table 2

σ kg/cm^2	°C	$\sigma_C{}^2T \times 10^{-7}$ (kg/cm^2)°K
>4000	−267	> 6·8
1300	−195	13·2
800	− 73	12·8
600	27	10·8
600	20	10·6
430	450	13·4
390	500	11·7
350	550	10·2

Friedel estimates that in single crystals of copper deformed at room temperature about 2500 dislocations are on the average piled up against the Cottrell barriers surrounding a source by the time the yield stress of the crystal has risen from σ_Y to σ_C. As this number of dislocations is proportional to the plastic strain up to the point at which the stress is σ_C, and since at room temperature that range is smaller in polycrystals than in single crystals by a factor of about 2, the corresponding number of dislocations in the grains of polycrystalline copper should be of the order of 1000.

4.2. *Parabolic Hardening*

Jacquet (1954) obtained electron-micrographs of grains of polycrystalline alpha-brass deformed a few percent at room temperature after careful prior annealing. These showed dislocation arrays piled up at the grain boundaries. The uniformity of the spacing between adjacent pile-ups suggests that the mode of hardening of the metal was of the interaction type, which leads to a parabolic work hardening law (Mott 1952). In view of the similarity between the materials and the amount of strain as used by Jacquet and in this research, it seemed appropriate to investigate the applicability of some relations derived from the interaction theory to the present results.

If, to conform with the method of extending the wire, the applied shear stress is replaced by $\frac{1}{2}\sigma$, and the tensile strain is equated to the shear strain†, Mott's theory gives

$$\chi_p \simeq G^2bn/\pi^2L, \quad . \quad . \quad . \quad . \quad . \quad . \quad . \quad . \quad (4)$$

where L is the slip distance which, according to Jacquet's micrographs, should be equal to about $\frac{1}{2}D$. G, as before, is the shear modulus, b the

Fig. 4

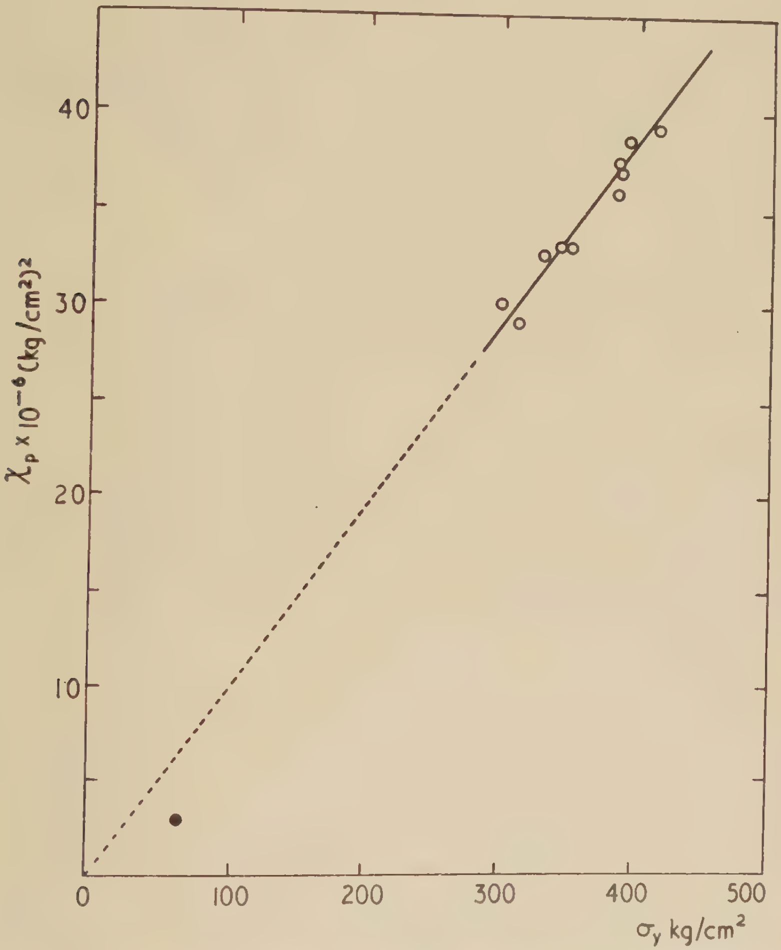

The relation between the coefficient of work hardening in the parabolic stage and the initial yield stress (eqn. (6)). Points for the incompletely annealed specimens No. 4 and No. 6 are not shown. The full circle relates to a single crystal of copper having a cube face approximately perpendicular to the tensile axis (curve 305a, 300°K, Blewitt *et al.* 1954).

---

† Mott uses the engineering shear strain, which is twice the corresponding deviatoric shear strain.

interatomic spacing in the slip direction, and n the number of dislocations per pile-up, given by

$$n \simeq (\pi L/Gb)\sigma_Y, \qquad (5)$$

where $\tau_Y \equiv \frac{1}{2}\sigma_Y$ is the yield stress in shear of the undeformed metal. Substitution from eqn. (5) into eqn. (4) yields

$$\chi_p \simeq G\sigma_Y/\pi, \qquad (6)$$

which is independent of L and n. Thus the relation between χ_p and σ_Y should be linear; the line should pass through the origin, and its slope should be about G/π, i.e. $1{\cdot}4 \times 10^5$ kg/cm² in the case of copper, taking G to be $4{\cdot}5 \times 10^5$ kg/cm². This value is in reasonable agreement with the slope of the line through the experimentally determined points (fig. 4), namely $1{\cdot}0 \times 10^5$ kg/cm². Points for the incompletely annealed specimens are not shown. The full circle has been obtained from the parabolic stress–strain curve of a copper single crystal, having a cube face almost perpendicular to the tensile axis, deformed at 300°K (curve 305a, Blewitt *et al.* 1954).

On substituting into the right-hand side of eqn. (5) the appropriate values of the parameters for the specimen 7a, n is found to be about 120. This is of the same order of magnitude as the number of dislocations per pile-up observed by Jacquet, i.e. about ten times less than the number of dislocations estimated by Friedel to be piled up at Cottrell barriers at the stress σ_C. However, a more detailed analysis (Stroh 1956) shows Friedel's estimate to be too high, the more likely range of values in copper at room temperature being 150–500. This is of the same order as n obtained from eqn. (5). It appears therefore as if the dislocations in a pile-up at a grain boundary are those suddenly released by the breakdown of one of the sides of a rectangular enclosure of Cottrell barriers of the type postulated by Friedel.

REFERENCES

BLEWITT, T. H., COLTMAN, R. R., and REDMAN, J. K., 1954, *Report of the Bristol Conference on Defects in Crystalline Solids* (London : The Physical Society).
CRUSSARD, C., 1948, *Recent Developments in Rheology* (London : Nelson).
FRIEDEL, J., 1955, *Phil. Mag.*, **46,** 1169.
JACQUET, P. A., 1954, *Acta Met.*, **2,** 752, 770.
LOZINSKII, M. G., 1954, *Izv. Akad. Nauk S.S.S.R.* (O.T.N.), No. 10, 3.
MOTT, N. F., 1952, *Phil. Mag.*, **43,** 1115 ; 1953, *Ibid.*, **44,** 742.
SPEKTOR, A. G., 1955, *Zavod. Lab.*, **21,** 193.
STROH, A. N., 1956, *Phil. Mag.*, **1,** 489.

Electronic Subtraction of Background with a Hutchinson-Scarrott Kicksorter †

By C. W. McCutchen
Cavendish Laboratory, Cambridge

[Received May 16, 1956]

Abstract

A semi-automatic background subtracting system has been developed for the Hutchinson–Scarrott kicksorter. It provides for direct measurement of 'live time', i.e. total counting time minus dead time. The statistical implications of background subtraction are discussed.

§ 1. Introduction

The subtraction and live time measuring systems were grafted on to one of our existing kicksorters so the circuits all refer to Hutchinson–Scarrott kicksorters as now operated in the Cavendish Laboratory. For a general description of the instrument the reader is referred to the original article by Hutchinson and Scarrott (*Phil. Mag.*, **42**, 792, 1951). The present machines differ from the original in detail but not in logic so no difficulty should be experienced in relating the modifications to the machine as a whole.

While the paper relates specifically to the Hutchinson–Scarrott machine it is believed that the remarks on live time measurement and on the statistics of background subtraction are of more general interest.

§ 2. Subtraction

Much effort in the recording of pulse-height spectra can be saved if the kicksorter rather than the experimenter performs the subtraction of background. It was found that a Hutchinson–Scarrott kicksorter can easily be modified to subtract. The procedure, based on the idea of complement addition, is as follows. The experimental spectrum, i.e. the spectrum wanted plus that of the background, is recorded in the normal way. In the Hutchinson–Scarrott machine it is stored in binary notation in the 'memory', an acoustic delay line. This signal is then 'reversed', each *nought* being converted into a *one* and vice versa. This replaces the number in each channel by its complement with respect to 2^n-1 where n is the number of digits per channel. Then the background run is recorded: the background spectrum is added to the complement of the experimental spectrum. Finally the memory is again reversed: that gives us the experimental spectrum minus the background spectrum as required.

---

† Communicated by Professor O. R. Frisch, F.R.S.

Statistical fluctuations will, in general, cause negative counts to appear in some channels. A negative number $-N$ is represented as 2^n-N where n is the number of digits per channel. A channel with a small negative count will contain nothing but *ones* except for a few *noughts* near the bottom. The pattern of *noughts*, interpreted as if they were *ones* gives us $N-1$, a count of -1 being represented by a channel containing

Fig. 1

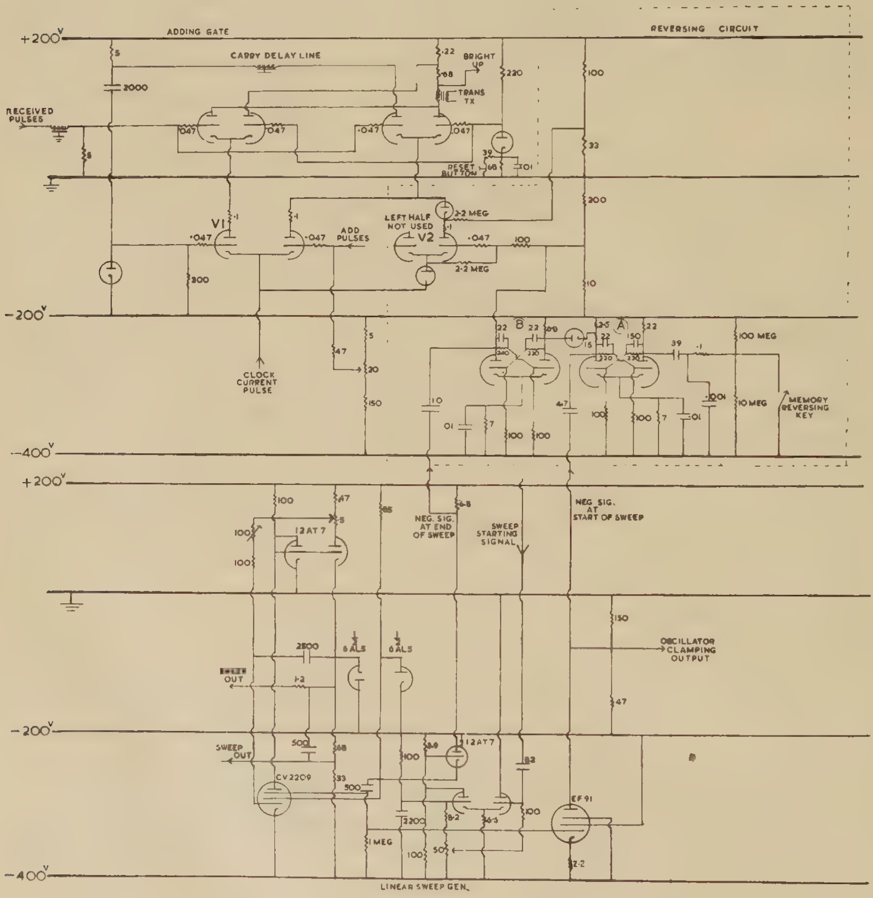

Notes on Figures

Resistance values are in *k* ohms except where otherwise stated.

Capacity values >1 are in pf.

Capacity values <1 are in μf.

All triodes are 6J6's except where noted.

All diodes are CV448 crystal diodes except where noted.

entirely *ones*. A negative count of less than 2^n-1 in channel k causes 1 to be subtracted from channel $k+1$. Decoding of negative numbers is easier if the memory is reversed again, converting the pattern of *noughts* into a pattern of *ones* with which we are more familiar.

The memory reversal is preformed by one extra valve in the adding gate ; this valve is controlled by a timing circuit comprising two bistable pairs. In fig. 1 the modified adding gate, the timing circuit and the kicksorter sweep circuit are shown, with all the additions to the original Hutchinson–Scarrott circuit being within the dotted outline. The sequence of events in memory reversal is started by closing the memory reversal key. This produces a pulse which flips pair A which remains flipped until reset by a pulse produced by the kicksorter sweep circuit at the beginning of the sweep. By this means, closing of the key—which is necessarily random in time—initiates a process which is synchronized with the sweep. The resetting of pair A flips pair B which remains flipped, producing the memory reversing signal, until reset by a pulse produced by the kicksorter sweep circuit at the end of the sweep. In the resting state the left hand half of pair B is conducting, holding V2 cut off and isolated from the adding gate by the two diodes. During one cycle of the memory the left half of pair B is cut off holding V2 conducting which diverts the clock pulses from V1 through which they would otherwise pass. If a *nought* is received the clock current pulse passes through the transmitter transformer and a *one* is transmitted. If a *one* is received the clock pulse does not go through the transmitter transformer so nothing (a *nought*) is transmitted. A negative pulse does go down the carry delay line but as V1 is already cut off, it produces no further effect. The only subtlety is that the leading edge of the memory reversing signal is slowed by the 100 k resistor so that V2 starts conducting after the synchronizing pulses have been transmitted, otherwise they are eliminated and the memory cycle is destroyed.

The complement addition method of subtraction has one advantage over direct subtraction by an adding and subtracting gate in that it allows us to leave the simple reliable adding gate virtually undisturbed except during the reversal process which is itself very straightforward. There is further the advantage of being able to reverse the picture when decoding negative counts.

§ 3. LIVE TIME MEASUREMENT

A meaningful background run, whatever the method of subtraction, requires that the kicksorter be ' live ', i.e. ready to receive a pulse, for the same total time as in the experimental run. The dead time of the Hutchinson–Scarrott kicksorter is long enough for the machine to be dead for an appreciable fraction of the total time even with apparently moderate counting rates. The average dead time per count is not constant but depends on the counting rate and on the spectral shape. This rules out the possibility of calculating the live time by determining the total dead time from the total number of counts and the average dead time and subtracting it from the total time. Live time must therefore be measured directly. Experimental and background runs are then taken for equal live times and a great simplification of procedure and saving of labour results.

Our method of live time measurement is to switch a standard current to a current integrator during the live time. The current is thus switched on at the end of one sorting operation and switched off at the arrival of the next pulse. The total charge recorded by the integrator is proportional to live time. The integrator and standard current are calibrated together when the kicksorter is receiving no pulses, so that all the time is live time. It is unnecessary to know the exact value of the standard current or the exact calibration of the integrator: all that is required is the time per integrator cycle. We used a beam current integrator because we had one, but there is no reason why an integrating motor or velodyne should not be used. They would avoid the problems inherent in the rapid switching of small currents.

Fig. 2

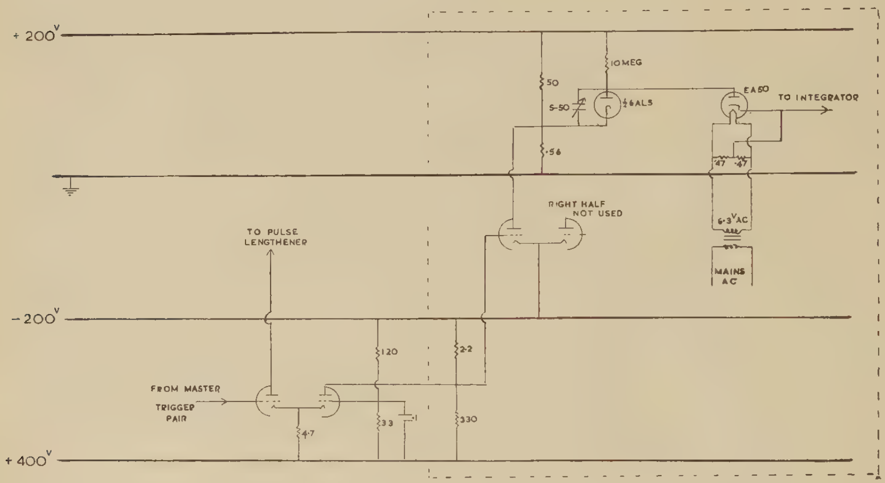

The switching circuit is shown in fig. 2 with the addition to the original kicksorter circuit within the dotted outline. During live time the current flowing through the 10 meg resistor is carried to the integrator by the EA 50 while during dead time it is diverted by the ½ 6AL5. The isolated heater supply for the EA 50 avoids any trouble which might be caused by heater cathode leakage. The trimmer condenser compensates for the capacity of the circuit comprising the anodes of the two diodes, the bottom of the 10 meg resistor, and the connecting wiring (which should be kept short). The live-time waveform applied to the grid of V1 is obtained from the free anode of the dual triode which controls the discharge of the pulse lengthener.

The live time integrator has been tested with random pulses at average repetition rates up to 1000 c.p.s. The number of pulses recorded by the kicksorter has been proportional to the input rate to well within 1%, as it should be if the integrator really is measuring live time. At this input rate it takes about two minutes to add up one minute of live time so the error made by counting for a given total time rather than a given live time is enormous. 1000 c.p.s. is about as high a count rate as is profitable with the Hutchinson–Scarrott kicksorter as further increase produces a rapidly diminishing increase in recorded count rate.

One accessory which we have found useful is the ‘ dead meter ’ which instantaneously measures the fraction of the time during which the machine is dead to incoming pulses. In our machine it is simply an anode current meter in one anode of the dual triode which controls the gate.

It should be pointed out in passing that though the live time measuring technique was developed specifically for the background subtracting problem it is valuable whenever the absolute value of the kicksorter spectrum is required instead of merely the shape.

§4. Statistical Implications

With a spectrum from which background has been subtracted there is no relation between the number of counts in each channel and the standard deviation to be expected. Accordingly it is wise for the experimenter to have some idea of the experimental spectrum before he subtracts the background so that he knows what sort of statistics to expect. If the kicksorter channel width is much narrower than the resolution of the instrument whose output is being analysed bad statistics will betray itself by producing wiggles which the instrument cannot.

Background subtraction inevitably hurts statistics, although even in the worst case, that of a minute wanted spectrum and a huge background, the standard deviation is only increased by $\sqrt{2}$ if the background is counted for an *additional* time equal to that allowed for the experimental spectrum.

The best use of a given total counting time requires that it should be divided between experiment and background runs as the square root of the recorded (not input) count rates. Unequal counting times require that the results of the background run be multiplied by the ratio of counting times before performing subtraction. With automatic subtraction, the obvious method is to multiply the background run as it is being recorded by a suitable power of 2 by making the machine add into the first or higher digit position instead of the zeroth. Counting time ratios of 2, 4, 8, etc. are thus allowed. This can be done, as I verified, by the simple expedient of delaying the add pulse with 2500 ohm delay cable (Rocke International H H 2500).

As the count rate ratio will seldom be an even power of 2, i.e. 2^{2k}, this method will not in general produce optimum statistics. It can be shown that, for any available set of multiplying factors, the worst cases occur when the count rate ratio is such that the ideal counting time ratio is the geometric mean of the nearest available factors. With powers of two available, the supreme worst case is a count rate ratio of 2, demanding a counting time ratio of $\sqrt{2}$. Even in this case the relative standard deviation obtained with a counting time ratio of either 1 or 2 is only 1·015 times that which results from the ideal ratio of $\sqrt{2}$. Thus, provided that one remembers to use the counting time ratio geometrically closest to the ideal, the kicksorter will provide nearly optimum statistics. In fact, a kicksorter which can only multiply by 8 (and, of course, 1) will handle any count rate ratio from 1 to infinity with a relative standard deviation in the worst case (count rate ratio of 8) only 1·06 times the ideal.

While a counting time ratio determined, as described above, by the ratio of the total count rates gives the best statistics for the spectrum as a whole it will not, in general, be optimum for a particular channel. This is especially sinister when one uses a large counting time ratio and then looks at a part of the spectrum which is nearly all background. No doubt it will often pay to suit the counting time ratio to the most interesting part of the spectrum at the expense of statistical damage to the remainder. The magnitude of the damage is given by

$$\frac{\text{Standard Deviation (counting time ratio} = X)}{\text{Standard Deviation (counting time ratio} = \sqrt{N})} = \sqrt{\left(\frac{1+X}{X} \cdot \frac{N+X}{(1+\sqrt{N})^2}\right)}$$

where N is the count rate ratio.

ACKNOWLEDGMENTS

The writer wishes to thank Professor O. R. Frisch and Dr. G. A. Jones for helpful suggestions and discussion.

The Effects of Incomplete Resolution on Surface Distributions Derived from Strip-Scanning Observations, with Particular Reference to an Application in Radio Astronomy †

By S. F. Smerd and J. P. Wild
Division of Radiophysics, C.S.I.R.O., Sydney, Australia

[Received July 31, 1956]

Abstract

A surface distribution can be measured by scanning in a number of directions with an observing instrument that has high resolution in only one direction. O'Brien has described a method which can be extended to reconstitute a two-dimensional distribution from a number of such 'strip scans'. Because of the finite width of the strip and the associated lack of resolution, the 'derived' distribution differs, in general, from the 'true' distribution. But, because this method of measuring a two-dimensional distribution is indirect and complex, the exact form such deviations may take is not apparent.

It is shown that the derived distribution is identical with that which would be recorded directly by two-dimensional scanning with a particular 'spot'-instrument; the power response of this equivalent 'spot' has radial symmetry and is such that a line scan of it along any diameter is the same as the power response of the 'strip' in the direction of high resolution.

An application of this to the determination of two-dimensional distributions of radio brightness over the sun's disc is discussed.

§ 1. Introduction

A surface distribution can be measured by two-dimensional scanning with a 'spot'-instrument, and the limitations associated with the finite size of the spot are known. The spot must be small compared with the distribution or, in other words, the observing instrument must have good resolution in all directions. Such resolution is not always attainable because of instrumental limitations. Examples of this occur in measurements of the radio-brightness distribution of celestial objects. At the relatively long radio wavelengths (some 10^4 to 10^7 times the optical wavelengths) good resolution requires very large, perhaps even impracticable, radio telescopes. For instance, it has not yet been possible to produce a radio 'spot' small enough to resolve detail on the sun. Nevertheless surface distributions of radio brightness over the sun's disc have recently been published by O'Brien (1953), O'Brien and Tandberg-Hanssen (1955), and by Christiansen and Warburton (1955). They were, each, derived from a number of one-dimensional scans of the sun with ' strip '-instruments ; that is, with radio telescopes which are very large, and thus have high resolution, in only one direction. From a number of such ' strip scans ' taken over a wide range of directions a two-dimensional distribution can be reconstituted. In the derivation a theorem on two-dimensional Fourier transforms has been used in a manner described by O'Brien (1953). However the limitations in this derived distribution due to the finite width of the strip are not obvious. It can be surmized that, the wider the strip, the less detail of the true distribution will be reproduced in the derived distribution. But the interpretation of such derived distributions demands more precise knowledge and it is the purpose of this note to show, quantitatively, how any lack of resolution in the ' strip '-instrument reflects in the derived distribution.

---

† Communicated by E. G. Bowen.

Sections 2 to 4 give a formal presentation of strip-scanning observations and their reduction to a derived distribution ; this includes a proof of the theorem on Fourier transforms used in the analysis. In § 5 the meaning of the derived distribution is established in terms of a hypothetical instrument which would give the derived distribution directly by 'spot-scanning ' the true distribution. The characteristics of this ' equivalent ' instrument are related to those of the observing instrument. Section 6 illustrates the relation between equivalent and observing instruments for the two kinds of radio telescopes used in the above mentioned radio surveys of the sun. The results are discussed in § 7.

§ 2. STRIP-SCANNING A TRUE DISTRIBUTION

A two-dimensional distribution, $f(x', y')$ say,† is to be measured ; it will be referred to as the ' true ' distribution. The observing instrument has high resolution in one direction and practically none at right angles to it. The two-dimensional power response of such an instrument (which, in the radio-astronomy application, looks characteristically like that of fig. 2 (a)) will be referred to as a ' strip '. One observation consists in scanning the true distribution with the strip instrument in the direction of high resolution. This process will be referred to as ' strip-scanning '. A number of such strip scans are carried out for a wide range of directions.

Now, let the x'-axis (arbitrarily chosen in the first place) be a scanning direction. Then, with the instrument directed at the point x along the scanning direction, the corresponding value, $f_S(x)$, in the recorded strip scan is given by

$$f_S(x)=\iint a(x'-x)\, f(x', y')dx'\, dy',$$

where $a(X)$, which determines the observing instrument, is the profile of the strip and the integrals here, and subsequently, extend over the whole distribution. Integration at right angles to the scanning direction is not affected by the strip profile and may be carried out independently. This is done here by introducing the one-dimensional distribution $f_L(x')$ say, each point of which is a line integral of the true distribution along y'; i.e.

---

† In radio measurements of the brightness distribution over the sun's disc, the angular size of the source is sufficiently small for rectangular co-ordinates (x', y') to be used in specifying position on the disc of the sun.

$$f_L(x')=\int f(x',y')\,dy'.$$

The operation represented by taking the line integral $f_L(x')$ for all values of x' will be referred to as 'line-scanning' the true distribution along x'; it is the limiting case of 'strip-scanning' with the strips infinitely thin.

The strip-scanning process may be thought of as consisting of two successive steps, namely: line scanning the true distribution and smoothing the line scans by the strip profile. This then reduces the expression for a point in the strip scan to the type of expression given by Bracewell and Roberts (1954) who considered aerial smoothing of one-dimensional brightness distributions; i.e.

$$\begin{aligned} f_S(x)&=\int a(x'-x)\,f_L(x')\,dx' \\ &=\int a[-(x-x')]\,f_L(x')\,dx'. \qquad \ldots\ldots \quad (1)\end{aligned}$$

The former expression is known as the unnormalized cross-correlation function of $a(x)$ and $f_L(x)$, the latter as the 'convolution' or 'Faltung' of $a(-x)$ and $f_L(x)$. The convolution may be written as

$$f_S(x)=a(-x')*f_L(x').$$

The observations may be said to result in strip scans which are, each, the convolution of the reversed † strip-profile and of a line scan of the true distribution.

§3. THE FOURIER TRANSFORM OF STRIP SCANS

O'Brien (1953) described a method of deriving a two-dimensional distribution from the Fourier transform of a number of variously orientated strip scans. To use this method here it is necessary first to find an expression for the Fourier transform of a strip scan.

The convolution theorem (cf. Sneddon 1951, pp. 23–24) states that

$$p(x)*q(x)=\int_{-\infty}^{\infty}\bar{p}(\xi)\,\bar{q}(\xi)\exp(-ix\xi)\,d\xi,$$

where $\bar{f}(\xi)$ denotes the Fourier transform of $f(x)$. Applying the theorem to eqn. (1) for the strip scan and inverting the transformation gives

$$\bar{f}_S(\xi)=\bar{a}(-\xi)\,\bar{f}_L(\xi). \qquad \ldots\ldots\ldots \quad (2)$$

In words, the Fourier transform of a strip scan is the product of the Fourier transforms of the reversed strip profile and of a line scan.

---

† There is no need to reverse the profile in the case of symmetrical instruments, such as those normally used in radio astronomy, since there $a(-X)=a(X)$.

Two kinds of aerial systems have been used in the solar applications; one, the variable spacing two-element interferometer used on 60 cm (O'Brien and Tandberg-Hanssen) and 1·4 m (O'Brien) observations of the sun, the other, the multiple element, or 'grating'-type, interferometer used in 21 cm (Christiansen and Warburton) observations of the sun. In the case of the two-element interferometer each observation results in a record from which the modulus and the phase of the Fourier component, corresponding to the spacing of the elements, can be obtained. In practice the phase has not always been measured. A number of observations at different spacings have to be taken in each scanning direction to give a set of Fourier components for one strip scan. The Fourier transform of each strip scan is then taken to be given by a smooth line through the set of points. A strip scan, if required, can be obtained by inverse transformation of this. In the case of the multiple element interferometer each strip scan is recorded directly in one observation. The Fourier transforms of the strip scans have been obtained by numerical transformation.

In both cases the Fourier transforms of variously orientated strip scans form the basis for the derivation of a two-dimensional distribution from the observations.

§ 4. The Derivation of a Distribution from Strip Scans

The following theorem in the theory of two-dimensional Fourier transforms has been used to derive a two-dimensional distribution, $g(x, y)$ say, from the strip-scanning observations.

Theorem A: A two-dimensional function is obtained from its two-dimensional Fourier transform by *two-dimensional* inverse transformation. However, the values of the function along any line through the origin may also be obtained by taking the *one-dimensional* inverse Fourier transform of the line scan (in this direction) of the two-dimensional Fourier transform.

Thus, if $p(x, y)$ is the function, then

$$p(x, 0)=\frac{1}{2\pi}\int_{-\infty}^{\infty}\left[\int_{-\infty}^{\infty}\bar{p}(\xi, \eta)\, d\eta\right]\exp(-ix\xi)d\xi, \quad . \quad . \quad \text{(A)}$$

where, without loss of generality, the line through the origin along which the function is evaluated is taken as the x-axis.

(*Inverse*) *Theorem B*: The values of the *two-dimensional* Fourier transform along any line through the origin may also be obtained by taking the *one-dimensional* Fourier transform of a line scan (in this direction) of the two-dimensional function.

Thus

$$\bar{p}(\xi, 0)=\frac{1}{2\pi}\int_{-\infty}^{\infty}\left[\int_{-\infty}^{\infty}p(x, y)dy\right]\exp(i\xi x)dx. \quad . \quad . \quad . \quad \text{(B)}$$

Proof: The relations between a two-dimensional function $p(x, y)$ and its two-dimensional Fourier transform $\bar{p}(\xi, \eta)$ may be written

$$\bar{p}(\xi, \eta)=\frac{1}{2\pi}\int_{-\infty}^{\infty}\int_{-\infty}^{\infty} p(x, y)\exp\left[i(\xi x+\eta y)\right]dx\,dy,$$

or

$$p(x, y)=\frac{1}{2\pi}\int_{-\infty}^{\infty}\int_{-\infty}^{\infty} \bar{p}(\xi, \eta)\exp\left[-i(x\xi+y\eta)\right]d\xi\,d\eta.$$

Introduce the co-ordinate system (x', y') rotated through an angle θ with respect to (x, y). The two are related by

$$x=x'\cos\theta-y'\sin\theta, \quad y=x'\sin\theta+y'\cos\theta, \quad \text{and} \quad dx\,dy=dx'\,dy';$$

similar relations hold for the spatial 'frequencies' (ξ, η) and (ξ', η') Values of the two-dimensional function along the x'-axis (that is, along a line through the origin of the (x, y) co-ordinates making an angle θ with the x-axis) and in the (x', y') co-ordinates are then

$$\begin{aligned} p(x', 0) &= \frac{1}{2\pi}\int_{-\infty}^{\infty}\int_{-\infty}^{\infty} \bar{p}'(\xi', \eta')\exp\{-i[x'\cos\theta(\xi'\cos\theta-\eta'\sin\theta) \\ &\qquad +x'\sin\theta(\xi'\sin\theta+\eta'\cos\theta)]\}d\xi'\,d\eta' \\ &=\frac{1}{2\pi}\int_{-\infty}^{\infty}\int_{-\infty}^{\infty} \bar{p}'(\xi', \eta')\exp(-ix'\xi')d\xi'\,d\eta' \end{aligned}$$

where

$$\bar{p}'(\xi', \eta')\equiv\bar{p}(\xi, \eta);$$

this may be written

$$p(x', 0) = \frac{1}{2\pi}\int_{-\infty}^{\infty}\left[\int_{-\infty}^{\infty} \bar{p}'(\xi', \eta')\,d\eta'\right]\exp(-ix'\xi')\,d\xi'; \quad . \quad \text{(A}'\text{)}$$

similarly

$$\bar{p}(\xi', 0) = \frac{1}{2\pi}\int_{-\infty}^{\infty}\left[\int_{-\infty}^{\infty} p'(x', y')\,dy'\right]\exp(i\xi' x')\,dx'. \quad . \quad \text{(B}'\text{)}$$

The last two expressions are symbolic forms of the theorems.

We may now enumerate the steps that have been taken in the derivation of a two-dimensional distribution from strip-scanning observations:

(*a*) Fourier transform each strip scan.
(*b*) Plot (*a*) in polar co-ordinates.
(*c*) Interpolate between the scanning directions to obtain a transform contour map.
(*d*) Line scan (*c*) in a number of directions.
(*e*) Inversely Fourier transform each line scan.
(*f*) Plot (*e*) in polar co-ordinates and form a contour map of a two-dimensional function.

The two-dimensional function in (*f*) is the 'derived distribution' $g(x, y)$.

The steps (*d*) to (*f*) are an application of the above theorem (A). This means that the contour map of Fourier transformed strip scans in (*c*) is also a graphic representation of the two-dimensional Fourier transform of the derived distribution. Symbolically this may be written

$$\bar{f}_S(\xi)=\bar{g}(\xi, 0). \quad . \quad . \quad . \quad . \quad . \quad . \quad . \quad . \quad . \quad . \quad (3)$$

It is this identification of the transformed strip scans with values of the Fourier transform of the derived distribution which defines the latter.

In practice the strip scans of radio brightness over the sun's disc were found to be symmetric about the centre of the disc (i.e. $f_S(x)$ was an even function). In the case of an even function the Fourier transform reduces to the cosine-transform. If a function is anti-symmetric (i.e. an odd function) the Fourier transform reduces to the sine-transform. In the general case, that of an asymmetric function, the Fourier transform is complex. So, for instance, the Fourier transform of an asymmetric strip scan may be written

$$\bar{f}_S(\xi)=\mathrm{Re}\{\bar{f}_S(\xi)\}+i\,\mathrm{Im}\{\bar{f}_S(\xi)\}.$$

Generally writing the two-dimensional Fourier transform of a two-dimensional, real function, $p(x, y)$ say, as

$$\bar{p}(\xi,\eta)=\mathrm{Re}\{\bar{p}(\xi,\eta)\}+i\,\mathrm{Im}\{\bar{p}(\xi,\eta)\}$$

the above theorem (A) may be stated in the form

$$\begin{aligned} p(x', 0)= & \frac{1}{2\pi}\int_{-\infty}^{\infty}\left[\int_{-\infty}^{\infty}\mathrm{Re}\{\bar{p}'(\xi',\eta')\}\,d\eta'\right]\cos(x'\xi')\,d\xi' \\ & +\frac{i}{2\pi}\int_{-\infty}^{\infty}\left[\int_{-\infty}^{\infty}\mathrm{Im}\{\bar{p}'(\xi',\eta')\}\,d\eta'\right]\sin(x'\xi')\,d\xi'. \end{aligned}$$

From this it is apparent that the steps in the derivation of a two-dimensional distribution from asymmetric strip scans will be :

(*a*) Fourier transform each strip scan.

(*b*) Plot the real and imaginary parts of (*a*) separately in polar co-ordinates.

(*c*) Interpolate between the scanning directions in both plots to obtain contour maps of the real and imaginary parts of the Fourier transforms of strip scans.

(*d*) Line scan both contour maps in a number of directions.

(*e*) Inversely cosine-transform the line-scanned real parts, inversely sine-transform the line-scanned imaginary parts and add the results of the two inverse transformations.

(*f*) Plot (*e*) in polar co-ordinates and form a contour map of a two-dimensional function.

The function in (*f*) is again the derived distribution $g(x, y)$.

From the definitive step in the derivation, as expressed in eqn. (3), and theorem (A) it follows that

$$\bar{f}_S(\xi)=\bar{g}_L(\xi). \quad . \quad . \quad . \quad . \quad . \quad . \quad . \quad . \quad . \quad (3')$$

The Fourier transform of a strip scan of the true distribution is also the Fourier transform of a line scan of the derived distribution.

This and eqn. (2) give

$$\bar{g}_L(\xi)=\bar{a}(-\xi)\,\bar{f}_L(\xi). \quad . \quad . \quad . \quad . \quad . \quad . \quad . \quad . \quad (4)$$

This means that, apart from a constant multiplier, the Fourier-transformed line scans of true and derived distributions are equal only if the

Fourier transform of the reversed strip-profile is constant over the whole range of the Fourier transform of any line scan of the true distribution. Clearly, the same condition applies to identity between true and derived distributions.

The identity condition may be described as requiring 'complete resolution' (range of Fourier transform) and 'equal weights of all Fourier components' (constant Fourier transform) from the observing strip instrument.

Of the two requirements that of 'complete resolution' is the more stringent.

'Unequal weights' of the Fourier components in any strip scan can, in principle, be restored to equality from a knowledge of the Fourier transform of the strip profile (cf. Bracewell and Roberts 1954).

In the case of 'incomplete resolution' the higher Fourier components in line scans of the true distribution are not 'seen', and therefore not recorded, by the strip instrument. The missing information cannot be restored unambiguously in the reduction of the observations.

The consequences of incomplete resolution are here explicit as far as the difference between transformed line-scans of true and derived distributions (cf. eqn. (4)). How this instrumental limitation reflects in the derived distribution itself, after the remaining steps in the derivation, will be discussed later.

§ 5. THE MEANING OF THE DERIVED DISTRIBUTION

It remains to determine the meaning of the derived distribution when the latter is not the true distribution.

For this we invoke a hypothetical instrument of two-dimensional power response $A(X, Y)$, say. The hypothetical instrument is defined to be that instrument which would record directly any point in the derived distribution if it were pointed at the corresponding position in the true distribution.

Then a point in the derived distribution may be represented by

$$g(x, y)=\int\int A(x'-x, y'-y)\, f(x', y')\, dx'\, dy'. \quad . \quad . \quad . \quad . \quad (5)$$

We now make use of eqn. (4) which relates the Fourier transforms of line scans of true and derived distributions and of the strip profile. Inverse transformation leads to

$$g_L(x)=\int a(x'-x)\, f_L(x')\, dx'. \quad . \quad . \quad . \quad . \quad . \quad . \quad . \quad (6)$$

In words, line scanning the derived distribution is equivalent to strip scanning the true distribution along the same scanning direction.

This may also be written as

$$\int g(x, y)\, dy=\int\int a(x'-x)\, f(x', y')\, dx'\, dy'. \quad . \quad . \quad . \quad . \quad . \quad (6')$$

Substituting from (5) in (6′) gives

$$\int\int\int A(x'-x, y'-y) f(x', y')\, dx' dy' dy=\int\int a(x'-x)\, f(x', y')\, dx' dy'. \quad (7)$$

This is satisfied if

$$\int A(x'-x, y'-y)\,dy = a(x'-x)$$

or, in terms of the instrument co-ordinates, if

$$a(X) = \int A(X, Y)\,dY. \quad . \quad . \quad . \quad . \quad . \quad . \quad . \quad . \quad (8)$$

The hypothetical, 'equivalent' instrument has a circular beam; its two-dimensional power response $A(X, Y)$, is such that a line scan of this along any diameter is the same as the one-dimensional strip-profile $a(X)$, of the observing instrument.

Equation (8) may be re-written

$$a(X) = 2\int_X^\infty \frac{A(R)R\,dR}{\sqrt{(R^2-X^2)}}, \quad . \quad . \quad . \quad . \quad . \quad . \quad . \quad (8')$$

where $A(R)$ is the radial power response of the equivalent instrument and the radius R, is measured from the centre of the beam. This can be transposed into a form of Abel's integral equation. The solution of the integral equation (cf. Bôcher 1926, pp. 8–9) is

$$A(R) = -\frac{1}{\pi}\int_R^\infty \frac{a'(X)\,dX}{\sqrt{(X^2-R^2)}}.$$

Alternatively, the integral eqn. (8′) may be solved for $A(R)$ by an application of the above theorems on Fourier transforms. By theorem (B) (in the direction function to transform) and eqns. (8) or (8′) the values of the two-dimensional Fourier transform of the circular beam along any diameter are those of the Fourier transform $\bar{a}(\xi)$, of the strip profile. The two-dimensional Fourier transform of the circular beam is thus a radially symmetrical form $\bar{a}(\rho)$ say, of $\bar{a}(\xi)$. Again by theorem (A) (in the direction from transform to function) the values of the radial power response $A(R)$ along any diameter are obtained by inverse transformation of a line scan (along any diameter) of the circular transform $\bar{a}(\rho)$.

A point in the derived distribution may then be said to be the response of a circular-beam, 'equivalent' instrument centred on the corresponding point of the true distribution. The equivalent and the observing instruments are related in such a way that a line scan of the circular power response of the equivalent instrument along any diameter results in the one dimensional strip-profile of the observing instrument.

§ 6. EXAMPLES OF EQUIVALENT INSTRUMENTS

Two examples may serve as illustration: they are the observing instruments and their equivalents used in the radio studies of the sun described above.

Let us consider first the variable-spacing two-element interferometer of maximum spacing l and used for observations at a wavelength λ.

The strip profile, normalized so that $\int_{-\infty}^{\infty} A(\theta)\, d\theta = 1$, where θ is the angular displacement, may be written

$$a(X) = \frac{2l}{\lambda} \frac{\sin X}{X},$$

where $X = (l/\lambda) 2\pi\theta$. The Fourier transform of the strip profile

$$\begin{aligned} \bar{a}(\xi) &= \frac{2\pi l}{\lambda} && \text{for } \xi < 1 \\ &= 0 && \text{for } \xi > 1. \end{aligned}$$

Fig. 1

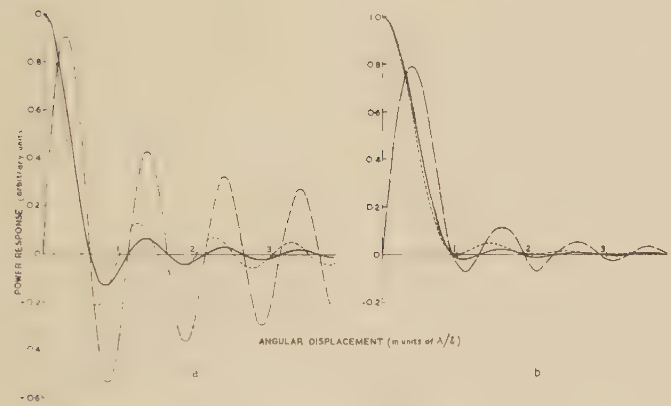

The power response of strip instruments and their circular equivalents.

‐ ‐ ‐ ‐ ‐ ‐ ‐ ‐ ‐ ‐ ‐ ‐ strip profile, $a(X)$, of observing instrument,

———————— radial power response, $A(R)$ ⎫ of equivalent

—— —— —— circular power response. $R\,A(R)$ ⎭ instrument.

(*a*) The variable-spacing two-element interferometer of maximum spacing l used at a wavelength λ.

(*b*) The multiple-element interferometer of overall length l used at a wavelength λ.

The cut-off at $\xi = 1$ in the ξ–'spectrum' corresponds to a cut-off 'frequency' of l/λ in the angular 'spectrum' of the instrument. Line scanning a radially symmetrical form $\bar{a}(\rho)$, of the above transform gives the Fourier transform $\bar{A}(\rho)$, of the radial power response of the equivalent instrument. Thus

$$\bar{A}(\rho) = \frac{4\pi l}{\lambda} \sqrt{(1-\rho^2)}.$$

Inverse transformation leads to the radial power response of the equivalent instrument

$$A(R) = \frac{\pi l}{\lambda} \frac{J_1(R)}{R}.$$

It should be noted that the response of a circular beam, whose radial power response is given by $A(R)$, to a true distribution $f(R, \Phi)$ say, in polar co-ordinates around the point on which the beam is centred is given by

$$\int R\,A(R)\left[\int_0^{2\pi} f(R,\Phi)\,d\Phi\right]dR.$$

The term $R\,A(R)$ will be referred to as the circular power response. In the case of an extended distribution this term will result in increasingly enhanced side-lobe effects with increasing distance from the beam's centre. This is illustrated in fig. 1, part (*a*) of which shows the strip profile $a(X)$, the 'equivalent' radial power response $A(R)$, and the 'equivalent' circular power response $R\,A(R)$, for the instrument discussed above.

Fig. 2

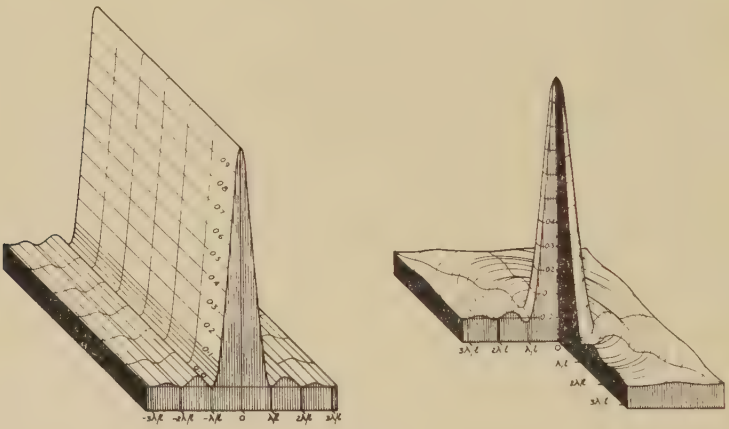

(*a*) (*b*)

An isometric projection of the power response of the multiple-element interferometer (*a*) and its circular equivalent (*b*).

We consider secondly the multiple-element interferometer of overall length l used at a wavelength λ. The strip profile, normalized and in the previous notation, may be written

$$a(X)=\frac{l}{\lambda}\frac{\sin^2(X/2)}{(X/2)^2}\;.$$

The Fourier transform of the strip profile

$$\begin{aligned}\bar{a}(\xi)&=\frac{2\pi l}{\lambda}(1-\xi) &&\text{for } \xi<1\\ &=0 &&\text{for } \xi>1.\end{aligned}$$

The cut-off at $\xi=1$ and the corresponding cut-off 'frequency' l/λ are the same as in the first example. A line scan of a radially symmetrical form of the above transform again leads to the transform of the 'equivalent' radial power response. In the present case

$$\bar{A}(\rho)=\frac{2\pi l}{\lambda}\{\sqrt{(1-\rho^2)}-\rho^2\cosh^{-1}(1/\rho)\}.$$

The inverse transformation yielding the radial power response, $A(R)$, of the equivalent instrument was done numerically. The result, together with the circular power response $R\,A(R)$, and the strip profile of the observing instrument, is illustrated in fig. 1 (*b*) and more graphically in fig. 2.

As may be seen from fig. 1 the main lobes of the strip profile and of the 'equivalent' radial power response are similar; the greater difference between the main lobes in the case of the two-element interferometer is due to the more pronounced side-lobe structure of this observing instrument. The side lobes of the equivalent instrument, alternately positive and negative in both cases, are smaller than those of the observing instruments.

This then means that the present method of observing leads to a derived distribution which could also be obtained directly by a circular-beam, 'equivalent' instrument whose resolution tends to be lower, and whose response to distant parts of the true distribution tends to be greater, than that of the observing instrument.

§7. Conclusion

The most direct way of measuring a surface distribution is by two-dimensional scanning with a 'spot' instrument. Practical considerations seem to make it necessary at times to carry out such measurements by the more indirect method of one-dimensional scanning with a 'strip' instrument and subsequently deriving a two-dimensional distribution from a number of such strip scans taken over a wide range of directions. If, in such cases, the 'true' and 'derived' distributions are to be identical the strip instrument must be capable of 'complete resolution' and 'equal weights' must be attached to all observed Fourier components.

In the idealized case of infinite resolution both requirements are fulfilled, whatever the true distribution. It should be noted, however, that in any particular case a finite resolution can also be complete, that is, it too can give an exact answer. This occurs when there are no Fourier components in any line scan of the true distribution which are higher than the highest that can be 'seen' by the observing instrument. Unfortunately the absence of such 'invisibly high' Fourier components cannot be inferred with any certainty from the observations. Similarly, if there are invisibly high Fourier components in the true distribution, they are filtered out in the observations and cannot be restored in the subsequent analysis. On the other hand, unequal weights attached to observed Fourier components can, in principle, be restored to equality in the reduction of the observation (cf. Bracewell and Roberts 1954). It is clear therefore that if resolution is complete the derived distribution can be identical with the true distribution, subject only to experimental errors and their possible enhancement in a weight-restoring process.

In the case of incomplete resolution the derived distribution is a smoothed and distorted version of the true distribution. This is partly due to sheer lack of resolution associated with the finite width of the main beam but also to considerable side-lobe effects when the observations are carried out with such 'multiple-strip' observing instruments as, for instance, the interferometers used in 21 cm, 60 cm and 1·4 m radio surveys of the sun (see figs. 1 and 2(*a*)). Unlike the case of an incompletely resolving spot, the limitations in the derived distribution due to incomplete resolution of the strip are not apparent. At the same time it is necessary that these limitations should be known so that valid inferences may be drawn from derived distributions.

It is shown here that the derived distribution could also be obtained directly by two-dimensional scanning of the true distribution with a hypothetical spot instrument. The circular beam of this 'equivalent' instrument is found to be such that a line scan of its power response along any diameter is the same as the strip profile of the observing instrument. Examples of observing and equivalent instruments are illustrated in figs. 1 and 2 for the two interferometers used in radio studies of the sun. It should be noted that the side-lobe structure of the equivalent to the variable-spacing two-element interferometer (which attaches equal weights to all observed Fourier components) is much more pronounced than that of the equivalent to the multiple-element, or 'grating'-type, interferometer (where the weights of Fourier components decrease gradually towards the high frequency cut-off). This means that when resolution is incomplete—that is, probably in all radioastronomy applications so far—a gradual decrease in the weights of observable Fourier components will tend to result in less distortion than would constant weights up to the same cut-off.

Generally, if resolution is incomplete, the derived distribution is not the true distribution. If resolution is complete, but the instrument does not *per se* attach equal weights to different Fourier components, these weights could be restored to constancy in the reduction of the observations. If resolution is incomplete, but the instrument attaches equal weights to all Fourier components, these weights could, with advantage, be gradually reduced towards the cut-off in the Fourier spectrum of the observing instrument's power response.

ACKNOWLEDGMENTS

The authors are indebted to Drs. J. L. Pawsey and J. A. Roberts of the Radiophysics Laboratory for many stimulating discussions.

REFERENCES

Bôcher, M., 1926, *An Introduction to the Study of Integral Equations* (Cambridge: University Press).

Bracewell, R. N., and Roberts, J. A., 1954, *Aust. J. Phys.*, **7**, 615.

Christiansen, W. N., and Warburton, J. A., 1955, *Observatory*, **75**, 9.

O'Brien, P. A., 1953, *M.N. Roy. Astr. Soc.*, **113**, 597.

O'Brien, P. A., and Tandberg-Hanssen, E., 1955, *Observatory*, **75**, 11.

Sneddon, I. N., 1951, *Fourier Transforms* (New York: McGraw-Hill Book Company).

The Nature of Persistent Slip Bands in Fatigued Copper†

By D. S. Kemsley
Department of Supply, Aeronautical Research Laboratories, Melbourne

[Received May 22, 1956]

Wadsworth and Thompson (1954), and Thompson *et al.* (1956) have reported the presence of 'persistent slip bands' in annealed polycrystalline and single crystal specimens of high-conductivity copper tested at constant cyclic stress in push-pull. These bands were observed when a test was interrupted before failure, and the specimen electrolytically polished. Most of the slip bands produced by the cyclic stress were removed, but some persisted, and even appeared to be made more prominent by polishing. These persistent markings were approximately one grain diameter deep, i.e. confined to the surface layer of crystals. As the test was continued to failure, with intermediate polishes, the same persistent slip bands remained, some new ones appeared, and unmistakable fatigue cracks resulted when certain persistent bands spread into neighbouring crystals. The conclusion from this work was that the persistent bands were incipient cracks, and were characteristic of fatigue deformation in copper.

Some evidence of the nature of persistent slip bands has recently been obtained during metallographic work on rotating cantilever fatigue specimens of annealed high conductivity copper. These specimens were fractured at several stress levels (from ±10 000 p.s.i. to ±25 000 p.s.i.) and two frequencies (21 c.p.m. and 6000 c.p.m.), giving specimen lives ranging from $3{\cdot}6\times10^4$ to $3{\cdot}1\times10^7$ cycles. The low-stress conditions used by Thompson *et al.* resulted in fatigue lives near the top of this range.

Following Thompson, these fractured specimens were electrolytically polished in orthophosphoric acid solution to remove slip bands produced by the cyclic stress, but in no case did any slip bands persist, although the depth of polish was only approximately 4% of the grain diameter. This result, anomalous in the light of Thompson's findings, was considered as possibly arising from differences in testing technique. Such differences were (i) type of stress used (rotating cantilever against push-pull); (ii) frequency of testing (21 c.p.m. and 6000 c.p.m. against 60 000 c.p.m.); and (iii) the stage at which electrolytic polishing was carried out (at failure against half the life or less). A check was initially made on the last point, in that a specimen was tested at ±10 000 p.s.i. and 6000 c.p.m. for approximately 10% of the life at this stress, i.e. for $3{\cdot}7\times10$ cycles, and then electrolytically polished. Persistent slip bands were clearly visible. Thus we have the situation that persistent slip bands were observed, after electrolytic polishing in a specimen cycled to 10% of its life, but were absent in a specimen cycled direct to fracture. Furthermore the type of stress and the testing frequency appear to be unimportant in this connection.

---

† Communicated by the Author.

The specimen in which persistent slip bands had been observed was next etched in dilute acid ferric chloride solution, which had been shown (Kemsley 1956) to reveal fatigue deformation markings (striations) both on the surface and in the interior of copper specimens cycled at low stresses (in the region of ±12 000 p.s.i.). It was found that the persistent slip bands were clearly associated with certain of the striations (see fig. 1, Plate). However, a similar specimen when cycled to fracture under the same conditions but without intermediate electrolytic polishing showed no persistent slip bands, although the striations were much more numerous (see fig. 2, Plate).

Another specimen was tested at ±25 000 p.s.i. and 6000 c.p.m.. and was electrolytically polished and then etched at 10% of its life (i.e. at $3{\cdot}6\times10^3$ cycles) and also at fracture. Neither persistent slip bands nor striations were observed at either stage.

Thus, persistent slip bands were only found when a low-stress long-life specimen was electrolytically polished at a relatively early stage of the test. They were not visible in a similar low-stress specimen run direct to failure, nor in a high-stress specimen either at 10% of the life or after complete fracture. They therefore do not seem to be truly characteristic of fatigue. These results suggest that ‘ persistent bands ’ are produced by the rapid attack, during electrolytic polishing, of certain striations formed early in the fatigue life, resulting in the production of a groove. The reason why some striations behave in this manner soon after their formation but not at fracture, is unknown. Fatigue cracks have been observed to lie along certain striations in fractured low-stress specimens (Kemsley 1956), but whether the striations involved would have produced a persistent slip band early in the fatigue life is not certain. Crack formation from persistent slip bands as observed by Thompson *et al.* (1956) may only be due to the stress concentrating action of the grooves.

A more detailed account of the nature of striations, and the variation in microstructure of fractured specimens with stress and frequency, will be published shortly.

ACKNOWLEDGMENTS

Thanks are due to Dr. A. K. Head for helpful discussions, and to the Chief Scientist, Department of Supply, for permission to publish this note.

REFERENCES

KEMSLEY, D. S., 1956, *Nature*, **178,** 653.
THOMPSON, N., WADSWORTH, N. J., and LOUAT, N., 1956, *Phil. Mag.*, **1,** 113.
WADSWORTH, N. J., and THOMPSON N., 1954, *Phil. Mag.*, **45,** 223.

Angle Distribution by Pair Production in Photographic Emulsions†

By J. P. Roalsvig
Fysisk Institutt, University of Oslo, Norway ‡

[Received June 20, 1956 ; and in revised form August 21, 1956]

Ilford G-5 nuclear photographic plates were exposed at the 30 Mev betatron at the Norwegian Radium Hospital in Oslo. The plates were scanned for electron-pairs, and the energy of each pair was calculated by the multiple scattering method. The energy spectrum for the gamma-rays thus found is given in a previous paper by Hisdal and Roalsvig (1955). At the same time some angles in the pair production were measured, their frequency distributions are given in this letter.

In fig. 1 is shown the measured distribution for the angle $\phi_{\rm p}$ between the photon direction and the direction of any one of the two pair-electrons.

Fig. 1

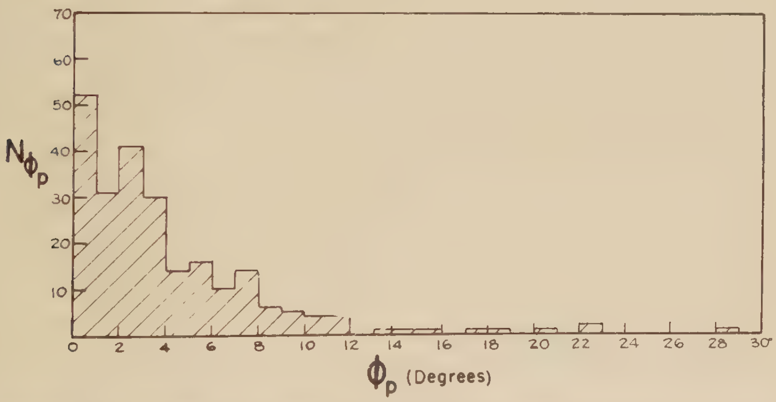

The number of angles $N_{\phi_{\rm p}}$ versus $\phi_{\rm p}$. $\phi_{\rm p}$ is the angle between photons and electrons.

A theoretical distribution for $\phi_{\rm p}$ for mono-energetic photons is given by Bethe (1934). This has a maximum at $\phi_{\rm p}$ (radians) $= \dfrac{1}{\sqrt{3}}\dfrac{m_0c^2}{\bar{E}}$ where $\bar{E}$ is the mean energy of the electrons. With $\bar{E} \simeq 6$ Mev (see Hisdal and Roalsvig 1955), this maximum should occur at $\phi_{\rm p} \approx 3°$. No absolute maximum at this value was found when using the whole gamma-spectrum from the betatron.

---

† Communicated by the Author.
‡ Now at the University of Saskatchewan, Saskatoon, Canada.

In fig. 2 is shown the determined variations of ϕ_p with the energy of the electron $\bar{E}$. The stripped line is given by ϕ_p (degrees)$=20{\cdot}5\,\dfrac{1}{\bar{E}(\text{MeV})}$ or $\bar{\phi}_p$ (radians)$=\dfrac{1}{\sqrt{2}}\,\dfrac{m_0c^2}{E}$. This shows that $\bar{\phi}_p$ is of the order given by Bethe (1934).

Fig. 2

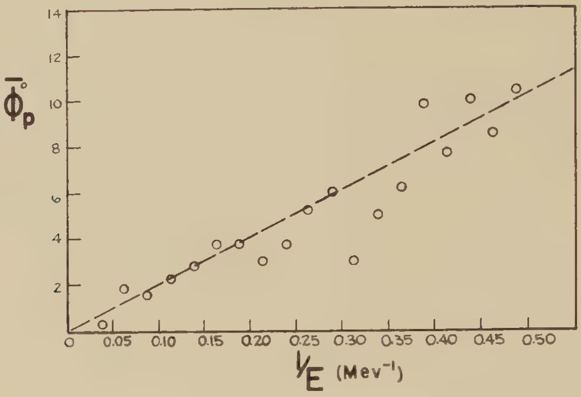

The average angle $\bar{\phi}_p$ pr. $1/E$ interval of 0·025 (MeV)$^{-1}$.

The experimentally determined distribution for the angle ψ_p, between the two pair-electrons is shown in fig. 3. This follows the form predicted by Groshev (1940), but is in contradiction to the experimental results of Voyvodick and Pickup (1952) and King (1950).

Fig. 3

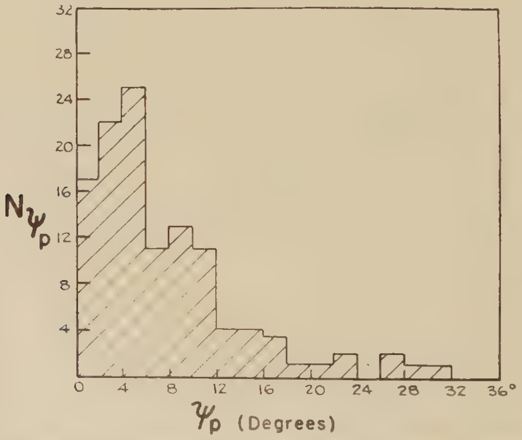

The number of angles N_{ψ_p} versus ψ_p . ψ_p is the angle between the two pair electrons.

In fig. 4 is given $\bar{\psi}_p$ as a function of the pair-energy, in intervals of 5 MeV (circles). On the same figure is also shown the values found by McDiarmid (1953) (crosses). The agreement is fairly good for medium energies.

A theory involving the angle ψ_p is proposed by Borsellino (1953). He derives a theoretical distribution for the value $Q = h\nu)^2 - P_p^2|^{1/2}$, where $h\nu$ is the energy of the photon and P_p is the momentum given to the nucleus, expressed in energy units (equal to the real momentum multiplied by the velocity of light). The value Q thus represents the total pair-energy in the centre of mass system for the two electrons. Borsellino derives the probability function for Q:

$$\Phi(Q)dQ = 4\overline{\Phi}\frac{F}{Q^3}dQ \qquad \text{. . . . . . (1)}$$

where $\overline{\Phi} = \frac{z^2}{137}\cdot\frac{e^4}{m_0^2c^4}$, and F is a function of $h\nu$ and Q, the expression for F is given in the above paper. The Q-distribution that will correspond to our energy-spectrum is given in fig. 5 in arbitrary units as the drawn line.

Fig. 4

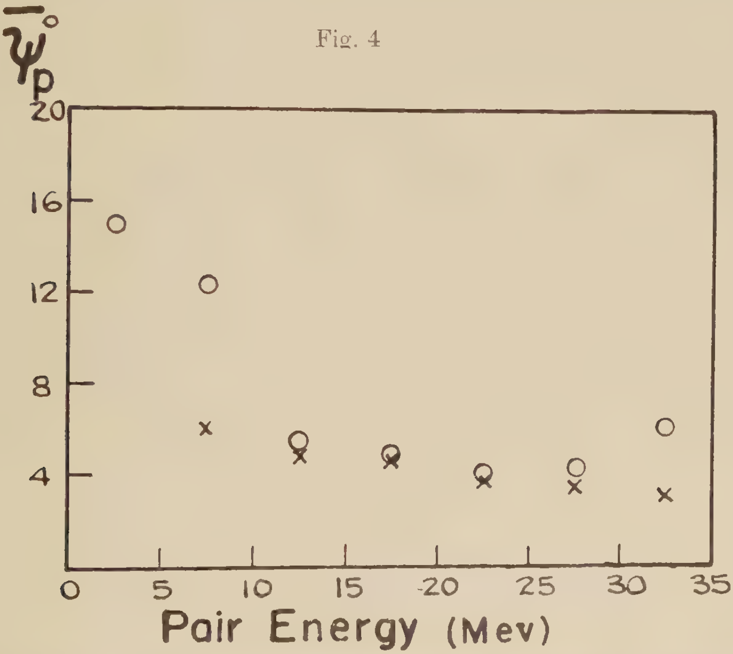

The average angle ψ_p pr. pair-energy interval of 5 Mev (circles). Former values found by McDiarmid (crosses).

Now for high energies with E_+ and $E_- \gg m_0c^2$, E_+ and E_- is the total energy of the positron and negatron respectively, one has:

$$\begin{aligned} Q^2 &= (h\nu)^2 - P_p^2 = (E_+ + E_-)^2 - (P_+ + P_-)^2 \\ &\cong 2m_0^2c^4 + m_0^2c^4\left(\frac{E_+}{E_-} + \frac{E_-}{E_+}\right)\cos\psi_p + 2E_+E_-(1 - \cos\psi_p) \qquad (2) \\ &\cong \frac{m_0^2c^4(h\nu)^2}{E_+E_-} + E_+E_-\psi_p^2. \end{aligned}$$

The Q values were calculated from eqn. (2) for all the electron pairs, and this experimentally determined Q distribution is also shown on fig. 5 (histogram). The two distributions are normalized for $Q/2m_0c^2 \leqslant 3$. We see that the conformity of experiment with theory is tolerably good, the experimental distribution having somewhat too many small Q values. A similar result is also obtained by Baroni *et al.* (1953) and by Hinterman (1954 a, b).

Fig. 5

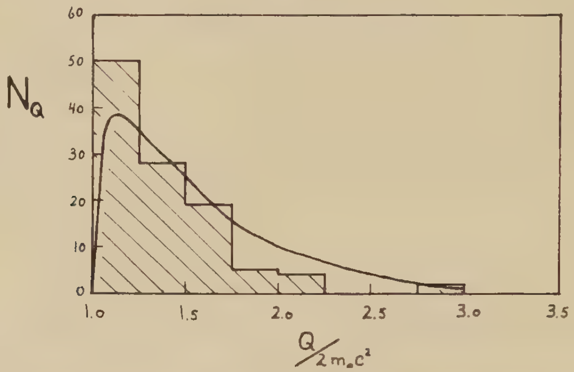

Theoretical and experimental distribution for Q, normalized for $Q/2m_0c^2 \leqslant 3$.

Fig. 6

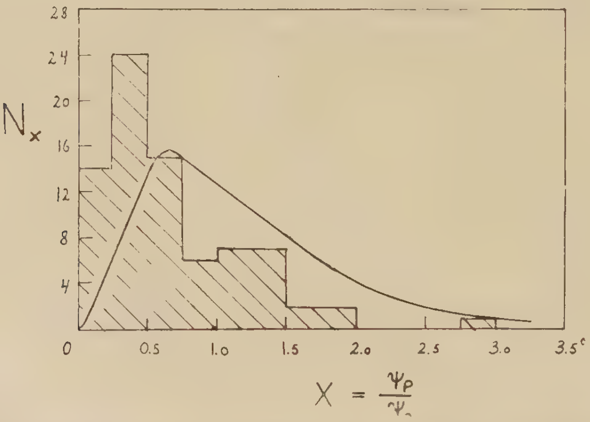

Theoretical and experimental distribution for $x=\psi_{\rm p}/\psi_0$, normalized for $x \leqslant 3$.

Another application of Borsellino's Q-distribution may be obtained as follows. If we put :

$$\psi_0=\frac{h\nu m_0c^2}{E_+E_-},\quad a=\frac{E_+}{h\nu},\quad x=\frac{\psi_{\rm p}}{\psi_0}, \quad \ldots \ldots \quad (3)$$

eqn. (2) can be written :

$$Q^2 \simeq E_+E_-(\psi_0{}^2+\psi_{\rm p}{}^2)=(4a(1-a))^{-1}\left(1+\frac{\psi_{\rm p}{}^2}{\psi_0{}^2}\right)$$
$$=(4a(1-a))^{-1}(1+x^2).$$

By substituting (3) into (1) we get :

$$\frac{\Phi(x)}{\overline{\Phi}}\,dx = 16a(1-a)\,F\,x\,dx/(1+x^2)^2. \qquad (4)$$

In the special case with $a=0{\cdot}5$, equipartition, $Q^2 \simeq 1+x^2$, and

$$\frac{\Phi(x)}{\overline{\Phi}}\,dx = 4F\,\frac{x}{(1+x^2)^2}\,dx. \qquad (5)$$

This distribution for x is drawn on fig. 6 in arbitrary units.

To find the corresponding experimental distribution, one should take into account only the pairs where $a=0{\cdot}5$. In practice no such pairs are found. However, for $0{\cdot}25 \leqslant a \leqslant 0{\cdot}75$ the probability function for x will not vary appreciably, as shown by Borsellino, and all electron-pairs with a-values within this range were used. This experimental distribution for x is also shown on fig. 6 (histogram). The experimental and theoretical distributions are normalized for $x \leqslant 3$. We see that experimentally there are too many small x-values. Baroni *et al.* (1953) have also arrived at a similar result.

References

Baroni, G., Borsellino, A., Scarsi, L., and Vanderhaeghe, G, 1953, *Nuovo Cimento*, **10,** 1653.

Bethe, H. A., 1934, *Proc. Camb. Phil. Soc.*, **30,** 524.

Borsellino, A., 1953, *Phys. Rev.*, **89,** 1023.

Groshev, L. V., 1940, *C. R. U.S.S.R.*, **26,** 424.

Hintermann, K., 1954 a, *Helv. Phys. Acta*, **27,** 125 ; 1954 b, *Phys. Rev.*, **93, 898.**

Hisdal, E., and Roalsvig, J. P., 1955, *Arch. Math. & Naturv.* B, **53,** No. 4.

King, D. T., 1950, *Nature, Lond.*, **165,** 526.

McDiarmid, I. B., 1953, *Canad. J. Phys.*, **31,** 337.

Voyvodick, L., and Pickup, E., 1952, *Phys. Rev.*, **85,** 91.

CORRESPONDENCE

An Investigation of Neutron Groups from the Reaction $^{10}B(d, n)^{11}C$ at 7·0 MeV Deuteron Energy †

By A. GRAUE and B. TRUMPY
Department of Physics, University of Bergen, Norway

[Received June 11, 1956]

SYNOPSIS

Energy spectra and angular distributions of the neutrons from the reaction $^{10}B(d, n)^{11}C$ have been measured at 7·00 7 ± 0·01 MeV bombarding energy using the photographic plate technique. Levels in ^{11}C were found at 8·5, 9·0, 10·0, 10·5 and 10·85 MeV excitation energy.

§ 1. INTRODUCTION

IN previous measurements made in this laboratory the reaction $^{10}B(d, n)^{11}C$ has been investigated at 1·0 MeV deuteron energy (Graue 1955, 1956) and angular distributions were obtained for the ground state neutrons and the three first neutron groups. No angular distribution measurements have yet been made at higher deuteron energy. At 3·64 MeV deuteron energy Johnson (1952) has measured the energy spectra of the neutrons at 0° and 80°, finding a number of neutron groups corresponding to excited states in ^{11}C up to 9 MeV.

§ 2. EXPERIMENTAL PROCEDURE

The deuterons were accelerated in the 8 MeV Van de Graaff generator at M.I.T., Mass., U.S.A. A ^{10}B target on tantalum backing was used. The target thickness was 200 $\mu g/cm^2$. The neutrons were detected in 400 μ Ilford C2 Nuclear Research Plates placed at 0°, 20°, 60° and 90° around the target. The distance between target and the scanned areas was 11 cm. The total deuteron charge on the target was 200 μc. The energies of the neutrons were determined by measurements of their recoil protons in the nuclear emulsions. An improved photographic method described by Gibson (1953) was used, thus simplifying the measurements and calculations.

§ 3. NEUTRON SPECTRA

Because of the short exposure, only a few tracks were found in the neutron groups corresponding to levels in ^{11}C up to 8 MeV. In the spectra observed, however, we found five higher levels in ^{11}C at 8·5, 9·0, 10·0, 10·5 and 10·85 MeV excitation energy. The last three levels could not be reached by Johnson because of the lower deuteron energy used by him. A broad level in ^{11}C at 10·0 MeV has previously been observed by measurements of resonances in the ^{10}B(p, α)^{7}Be reaction by Brown *et al.* (1951).

---

† Communicated by the Authors.

Our 20° spectrum is shown in fig. 1. The levels in ^{11}C at 10·0 and 10·5 MeV are only resolved in the 0° spectrum.

Fig. 1

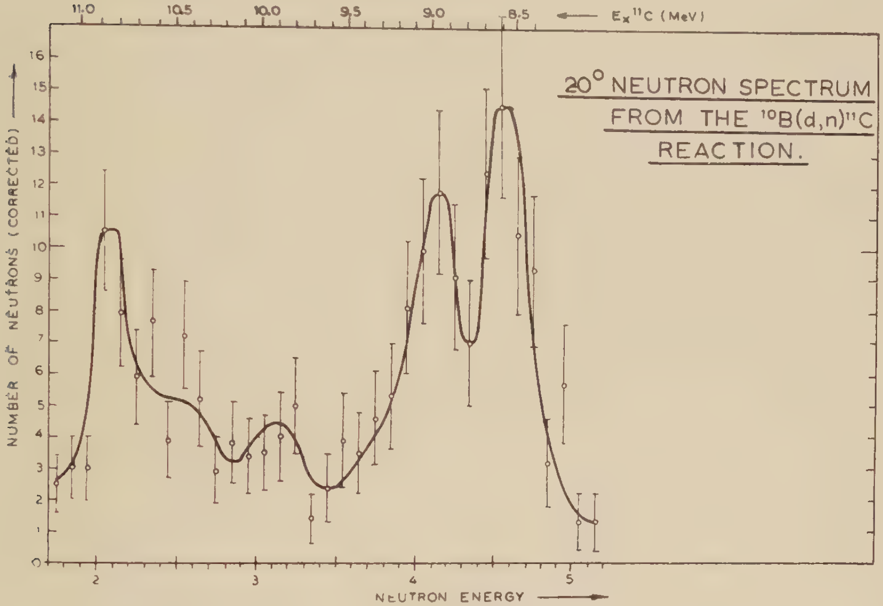

20° neutron spectrum from the ^{10}B(d, n)^{11}C reaction.

§ 4. ANGULAR DISTRIBUTION OF THE NEUTRONS

The angular distribution of the neutrons corresponding to the 8·5 MeV excited state in ^{11}C is shown in fig. 2. The experimental points are fitted with a pure $l=0$ stripping curve. This curve was calculated by means of a formula from the non-coulomb stripping theory by Friedman and Tobocman (1953). The formula has been rearranged in a form convenient for numerical calculations (Enge and Graue 1955). The nuclear radius of the target nucleus used in the calculations was $R=0{\cdot}43\times10^{-12}$cm, which was computed from the expression $R=(0{\cdot}17+0{\cdot}122\,A^{1/3})\times10^{-12}$cm.

Since the ground state of ^{10}B has spin 3 and even parity, the 8·5 MeV excited state of ^{11}C must have even parity and spin $\frac{5}{2}$ or $\frac{7}{2}$.

ACKNOWLEDGMENTS

The exposure and the development of the plates at 7 MeV were made during a visit of one of us (Trumpy) to Department of Physics, M.I.T., Cambridge, U.S.A. in May 1955. We want to express our most sincere

thanks to Professor W. W. Buechner for allowing us to make the exposures and for putting the facilities of his laboratory at our disposal.

We are also much indebted to Professor F. Ajzenberg and Dr. A. Sperduto for their kind helpfulness during the experiments.

Fig. 2

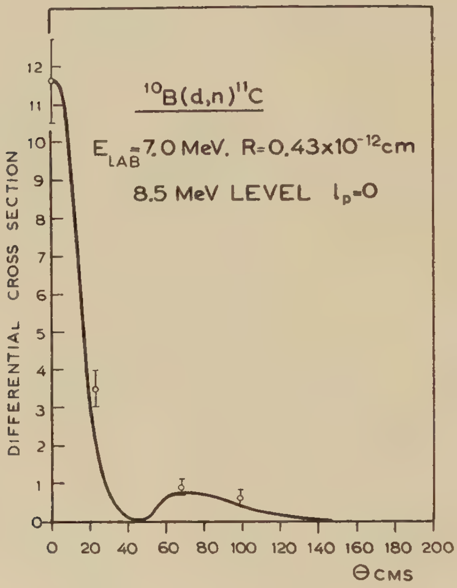

Angular distribution of the neutrons corresponding to the 8·5 mev excited state in ^{11}C.

References

Brown, Snyder, Fowler, and Lauritsen, 1951, *Phys. Rev.*, **82**, 159

Enge, H. A., and Graue, A., *Univ. Bergen, Årbok*, 1955, nr. 13.

Friedman, F. L., and Tobocman, W., 1953, *Phys. Rev.*, **92**, 93.

Gibson, W. M., 1953, *Phil. Mag.*, **44**, 297.

Graue, A., 1955, *Univ. Bergen, Årbok*, 1955, nr. 1 ; 1956, *Phil. Mag.* (to be published).

Johnson, V. R., 1952, *Phys. Rev.*, **86**, 302.

REVIEWS OF BOOKS

The Physics and Chemistry of Solids. Vol. 1, Nos. 1/2. (Pergamon Press: New York, London.) [Pp. (in this issue) 127.] Price per volume for private subscribers £3 10*s*.

The title of this new journal indicates its scope, which is now a major part of physics and chemistry. The first number contains both theoretical and experimental papers, the emphasis being 'fundamental' rather than 'applied'. The aim is to make it international, and the list of Editors and Advisors stretches from Massachusetts to Moscow. It is hoped that subsequent numbers will realize this aim, cutting across the present irrational collection into journals of papers whose only common factor is the nationality of their authors.

J. M. Z.

Applications of Spinor Invariants in Atomic Physics. By H. C. Brinkman. (Amsterdam: North-Holland Publishing Company, 1956.) [Pp. x+72.] Price 11 guilders.

In 1930 H. A. Kramers invented a simple technique for dealing with spinors and their transformation under the rotation group. Dr. Brinkman presents the details of this ingenious method and shows how it can readily be applied to many-electron atomic problems. It is an excellent introduction to spinors.

J. H.

Quantum Field Theory. By H. Umezawa. (Amsterdam: North-Holland Publishing Company, 1956.) [Pp. xiv+364.] Price 35 guilders.

The book starts with a thorough discussion of the relativistic theory of elementary particles; the theory for spins 0, $\frac{1}{2}$, 1, $\frac{3}{2}$ is given in detail. The chapters on quantum theory cover the same wide range of fields; in addition the powerful techniques developed in the last decade, and the renormalization theory are given in a careful treatment. This book should be of value to research workers wishing to learn the modern theory in its most general form.

J. H.

BOOK NOTICES

L'Origine des Planetes. By A. Dauvillier. (Presses Universitaires de France.) [Pp. 220.] Price 800 frs.

Atomic Physics. An Atomic Description of Physical Phenomena. By G. P. Harnwell and W. E. Stephens. (McGraw-Hill Book Company.) [Pp. x+401.] Price 60*s*.

Physical Techniques in Biological Research. Vol. I. Edited by G. Oster and A. W. Pollister. (Academic Books Ltd.) [Pp. xiii+564.]

The Mathematics of Diffusion. By J. Crank. (Oxford: Clarendon Press. London: Cumberlege.) [Pp. vi+347.] Price 50*s*.

The Structure of Turbulent Shear Flow. By A. A. Townsend. (Cambridge University Press. [Pp. ix+315.] Price 40*s*.

Thermodynamic Functions of Gases. Volume 1: Ammonia, Carbon Dioxide, Carbon Monoxide. Volume 2: Air, Argon, Acetylene, Ethylene, Propane. Edited by F. Din. [Pp. Vol. 1, viii+175. Vol. 2, vi+201.] Price 63*s*. per volume.

Order-disorder Phenomena. By E. W. Elcock. (Methuen & Co. Ltd.) [Pp. ix+164.] Price 11*s.* 6*d.*

Reports on Progress in Physics. Volume XIX. (London : Physical Society.) [Pp. 367.] Price to non-Fellows 50*s.* ; to Fellows 27*s.* 6*d.*

An Introduction to Cybernetics. By W. Ross Ashby. (Chapman and Hall.) [Pp. ix+295.] Price 36*s.*

Flow of Gases through Porous Media. By P. C. Carman. (Butterworths Scientific Publications.) [Pp. ix+182.] Price 30*s.*

Matrix Calculus. By E. Bodewig. (Amsterdam : North-Holland Publishing Company.) [Pp. xi+334.] Price 26.50 guilders.

Symposium on Monte Carlo Methods. By H. A. Meyer. (Chapman & Hall.) [Pp. xvi+382.] Price 60*s.*

Numerical Analysis: Proceedings of Symposia in Applied Mathematics. Volume VI. (Conference held at the Santa Monica City College, 26–28 August, 1953.) Edited by J. H. Curtiss. (McGraw-Hill Book Company.) [Pp. vi+303.] Price 73*s.*

Atoms and the Universe. By G. O. Jones, J. Rotblat and G. J. Whitrow. (Eyre & Spottiswoode.) [Pp. 254.] Price 25*s.*

Relaxation Methods in Theoretical Physics. Volume 2. By R. Southwell. (Clarendon Press : Oxford University Press.) [Pp. vi+273.] Price 55*s.*

Introduction to Mathematical Logic. Volume 1. By Alonzo Church. 2nd Edition. (Princeton University Press. London : Oxford University Press.) [Pp. ix.+376.] Price 60*s.*

Analysis of Deformation. Volume 3, Fluidity. By K. Swainger. (London : Chapman & Hall.) [Pp. xxvii+266.] Price 65*s.*

Tinplate Handbook. By W. E. Hoare. 3rd Edition. (Tin Research Institute.) [Pp. 44.] Free of charge.

Introduction to Electrical Applied Physics. By N. F. Astbury. (London : Chapman & Hall.) [Pp. xi+241.] Price 36*s.*

The Physics of Nuclear Reactors. A conference arranged by the Institute of Physics in London from 3 to 6 July, 1956. (London : Institute of Physics.) [Pp. iv+111.] Price 25*s.*

Arthur Stanley Eddington. By A. V. Douglas. (Edinburgh : Thomas Nelson and Sons Ltd.) [Pp. xi+207.) Price 25*s.*

Statistical Mechanics. By T. L. Hill. (London : McGraw-Hill.) [Pp. xiii+432.] Price 67*s.* 6*d.*

Remarks on the Foundations of Mathematics. By Ludwig Wittgenstein. Translated by G. E. M. Anscombe. (Oxford : Basil Blackwell.) [Pp. xix+204.] Price 37*s.* 6*d.*

The Theory of Functions of Real Variables. 2nd Edition. By L. M. Graves. (London : McGraw-Hill.) [Pp. xii+375.] Price 56*s.* 6*d.*

[*The Editors do not hold themselves responsible for the views expressed by their correspondents.*]

Photograph 1

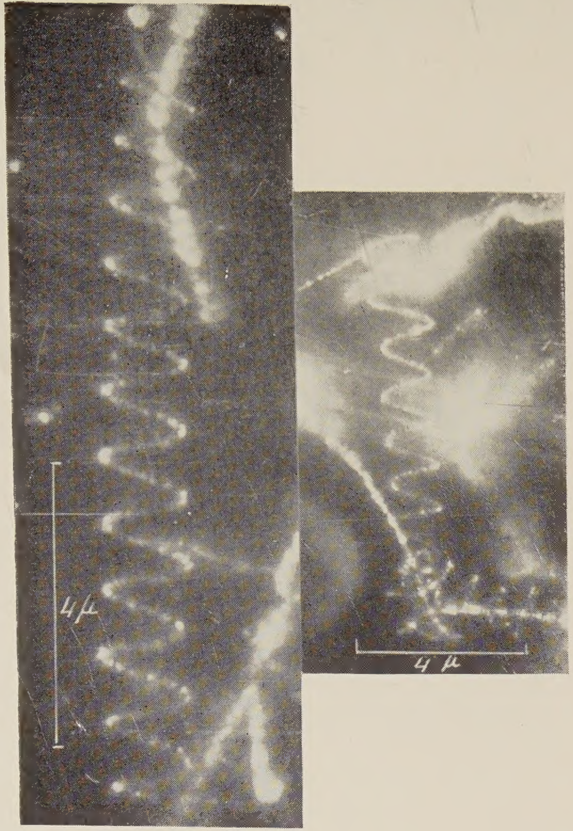

(a) (b)

Decorated helices observed in synthetic fluorite crystals.

Photograph 2

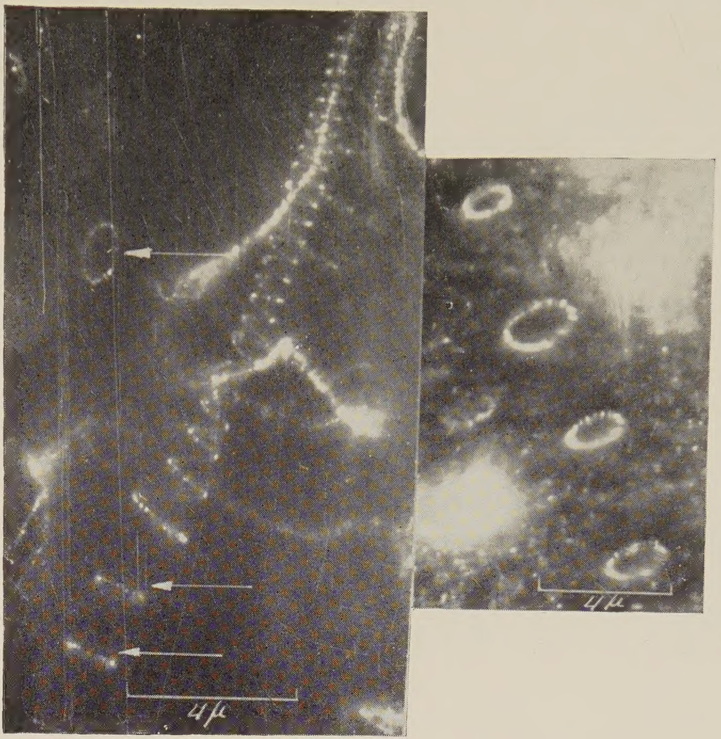

(a) (b)

Closed dislocation lines in synthetic fluorite crystals.

The magnification factor should be multiplied by a factor 10.

Fig. 1

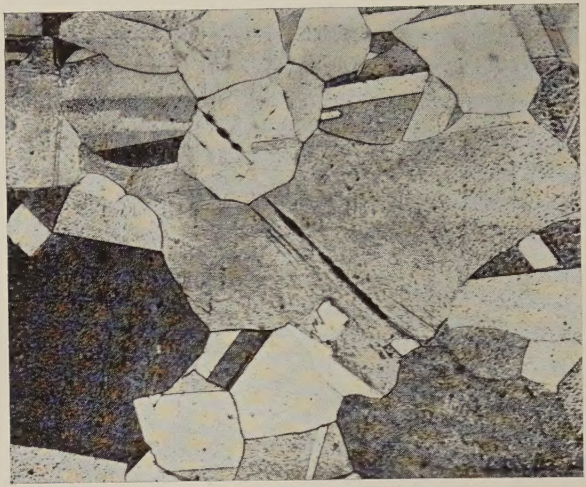

Rotating cantilever specimen run for approximately 10 % of its life (i.e. for $3{\cdot}7 \times 10^6$ cycles) at ±10 000 p.s.i. and 6000 c.p.m., then electrolytically polished and etched with dilute acid ferric chloride. Showing association of persistent slip bands with certain striations. ×150.

Fig. 2

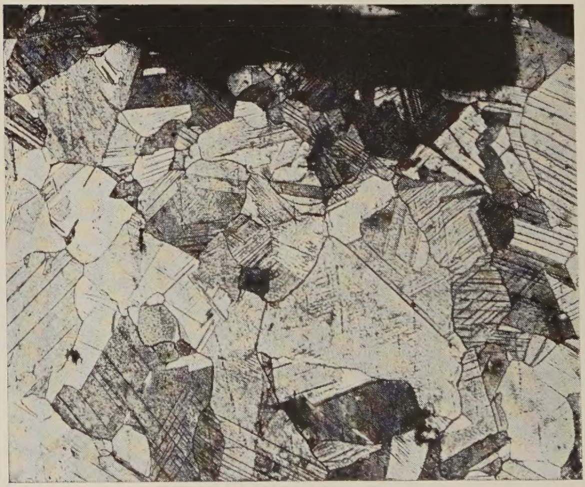

Similar specimen as in fig. 1, but run directly to failure without interruption. Numerous striations, but no persistent slip bands, are visible after electrolytic polishing and etching. × 150.